Epigenetic reprogramming and mitotic chromosome structure

by

Anne-Céline Kohler

A thesis submitted to Imperial College London for the degree of Doctor of Philosophy

Lymphocyte Development Group

MRC Clinical Science Center

Imperial College School of Medicine

October 2017

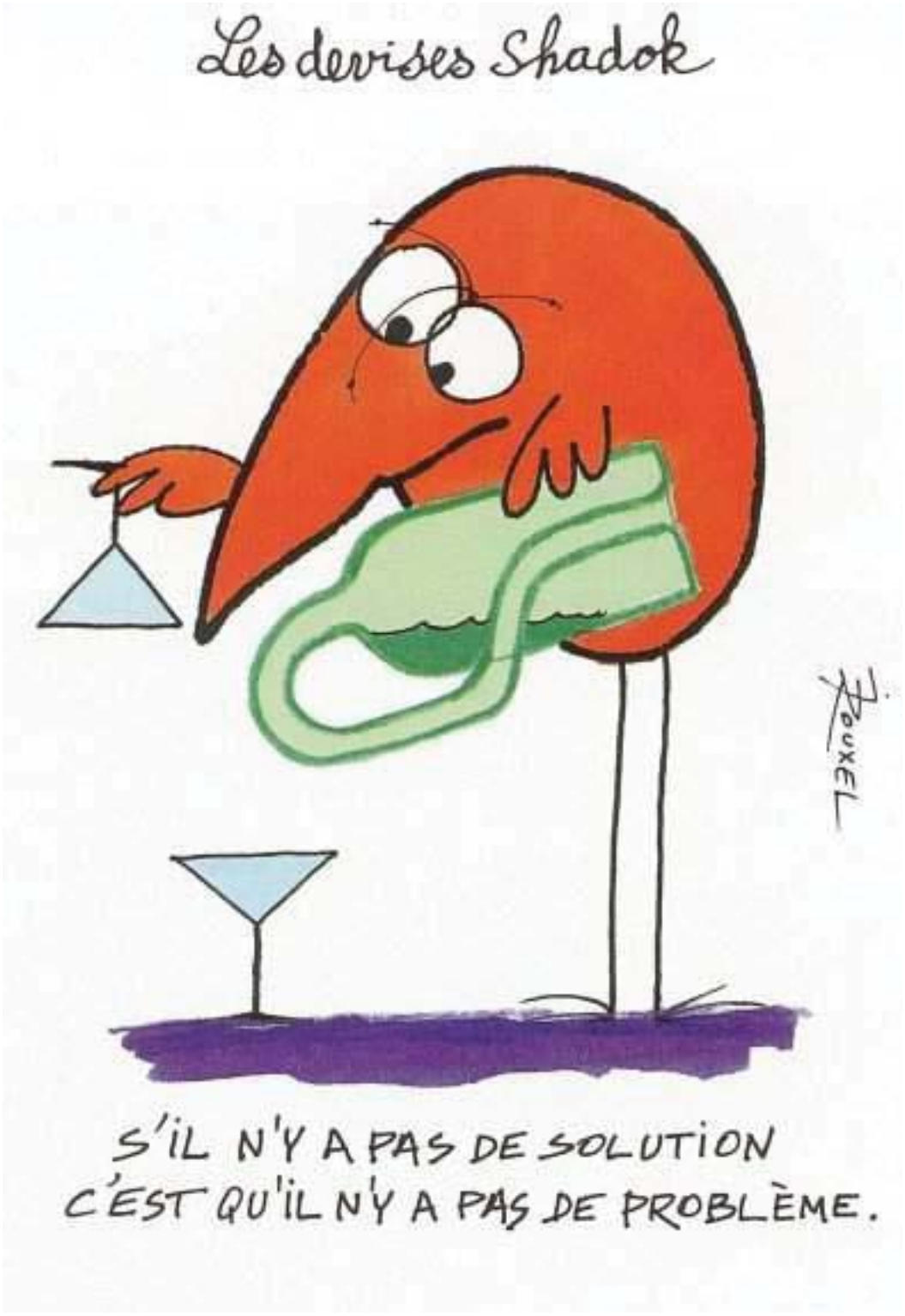

"if there is no solution there is no problem."

I, Anne-Céline Kohler, declare that this thesis is my own work and that work performed by others has been acknowledged and referenced accordingly

ABSTRACT:

The epigenetic memory of a cells defines its identity. Upon reprogramming towards pluripotency a somatic cell undergoes epigenetic remodeling in order to become pluripotent. The work I am presenting here is divided into two parts. In the first part, I am using cell fusion mediated reprogramming to investigate Xi reactivation, a typical example of epigenetic remodeling, as well as how ploidy affects reprogramming efficiency. Among all the technique established for *in vitro* reprogramming towards pluripotency, cell fusion has the advantage of allowing us to study early events of reprogramming as well as having a higher efficiency compared to induced Pluripotent Stem cells (iPS). Despites intensive research on the molecular mechanisms and the epigenetic changes leading a somatic cell towards pluripotency, a lot remain unanswered. In this thesis, I showed that somatic cells were able to reprogram towards pluripotency and that some X-linked genes were reactivated upon reprogramming. I also demonstrated that haploid Embryonic Stem cells (ES) cells are able to reprogram somatic cells with a lower potential compared to diploid ES cells. This low reprogramming potential can be partially rescued by overexpression of Nanog.

In the second part of my thesis, I focused on setting up a technique to visualize chromatin and aimed at studying the structure of mitotic chromosomes 19 using high resolution microscopy techniques such as Structured Illumination Microscopy (SIM) and cryo-Electron Microscopy (cryo-EM). Higher order chromatin structure remains unknown in mitosis. During mitosis, chromatin become highly compacted to form a mitotic chromosome. In order to isolate a specific chromosome (chromosome 19), first I re-established flow karyotyping technique to sort the chromosomes 19. I also showed that chromosomes after sorting retained a certain degree of compaction as well as protein important for centromeric integrity such as Centromere Protein A (CENPA). To validate the isolation of mitotic chromosomes and the use of cryo-EM in chromosomes structure analysis, I assessed the compaction of mitotic chromosomes 19 upon loss of cohesin. Chromosomes 19 lacking Rad21 cohesin subunit possess a larger area and their chromatin looked more decondensed compared to mitotic chromosomes 19 with cohesin. This promising tool could be used in the future to study how epigenetic modifications affect chromatin structure.

ACKNOWLEDGMENTS:

I would like to thanks Mandy and Matthias for hosting an engineer in their lab hoping that I would become a true molecular biologist. Thank you to past and present lab members for their expertise and help when I needed it. Special thanks to Kotryna and Amalia who were here for me since day 1 and until the very end! Thanks Preksha for being my rock when I needed one, Lesly for trying to teach how to dance Salsa even though I have two left feet, Lee for sharing my love for chocolate and Nutella, Andy for making fun of me a bit too much to my taste and Hakan for teaching me TC and how to make agarose gel.

Coco pour son soutien inconditionnel et d'avoir été là à chaque fois que j'avais besoin d'elle et pour m'apprendre des mots super bizarres comme 'vigousse'. Krikri pour faire des blagues qui me font rire et pour désamorcer des situations tendues. A ma famille pour toute son affection et soutien (en particulier la personne qui ne veut pas être cité dans mes remerciements).

TABLE OF CONTENTS

FIGURES AND TABLES

List of Figures

List of Tables

Abbreviations

2i	two inhibitors
5-AzaC	5 -deoxyazacytidine
AP	Alkaline Phosphatase
AR	Aspect Ratio
BSA	Bovine Serum Albumin
Cast	Mus musculus castaneous
CENPA	Centromere Protein A
chIP	chromatin ImmunoPrecipitation
CLEM	Correlative light Electron Microscopy
CRISPR	Clustered Regulatory Interspaced Short Palindromic Repeat
CryoEM	Cryo electron microscopy
DAPI	4', 6'-diamidino-2-Phenylindol
DMEM	Dubelcco's modified Eagle's medium
DMSO	Dimethyl sulfoxide
DNA	Desoxyribonucleic acid
DNA FISH	DNA Fluorescence in Situ Hybridization
Dom	Mus musculus domesticus
DOP-PCR	Degenerate oligonucleotide primed -PCR
dUTP	2'desoxyuridine,5'triphosphate

EBV	Epstein Barr Virus
EDTA	Ethylene Diamine Tetraacetic Acid
EM	Electron Microscopy
ES cell	Embryonic Stem cell
Esrrb	Estrogen-Related Receptor Beta
FACS	Fluorescence-Activated Cell Sorter
FCS	Foetal Calf Serum
gDNA	genomic DNA
GFP	Green Fluorescent Protein
HAT	Histone Acetyl Tranferase
HDAC	Histone deacetylase
Hi-C	High chromosome contact
ICM	Inner Cell Mass
iPS	Induced Pluripotent Stem cell
IRES	Internal Ribosome Entry Site
LIF	Leukemia Inhibitory Factor
MEF	Mouse Embryonic Fibroblast
miRNA	micro RNA
OSKM	Oct4, Sox2, Klf4, C-myc
PAB	Polyamide buffer
PB	Piggy Bac
PCR	Polymerase Chain Reaction

PEG	Poly Ethylene Glycol
PFA	Paraformaldehyde
PI	Propidium Iodine
piRNA	Piwi Interacting RNA
RNA	Ribonucleic acid
RT-PCR	Reverse Transcriptase PCR
RT-PCR	Reverse Transcriptase PCR
RT-qPCR	quantitative Reverse Transcription-PCR
SCNT	Somatic Cell Nuclear Transfer
SDS	SodiumDodecyl Sulphate
SIM	Structured Illumination Microscopy
siRNA	Small Interfering RNA
SNP	Single Nucleotide Polymorphism
TEV protease	Tobacco Etch Virus protease
TAD	Topologically Associated Domain
UTR	Untranslated region
WT	Wild Type
Xa	Active X chromosome
XCI	X Chromosome Inactivation
Xi	Inactive chromosome X
Xic	X inactivation center
Xm	maternal X

Xp	paternal X

Abbreviation of Units

Å	Ångström
kDa	KiloDalton
bp	base pair
Kp	Kilopair
L	Litre
M	Molar
nm	Nanometer
RPM	Rotation per Minute
µm	Micrometer

Chapter 1 : INTRODUCTION

1.1 Epigenetic mechanisms and inheritance

A multicellular organism is composed of a myriad of differentiated cells with specific roles, transcriptomes and proteomes, which ultimately the vast majority of them possess the same genome. Therefore, differences in gene expression between various cell types are caused by modifications on chromosomes without altering the DNA sequence. This phenomenon of epigenetics encompasses DNA methylation, histone modifications and variants, as well as non-coding RNA (Figure 1). In the following section I will attempt to give an account of these mechanisms.

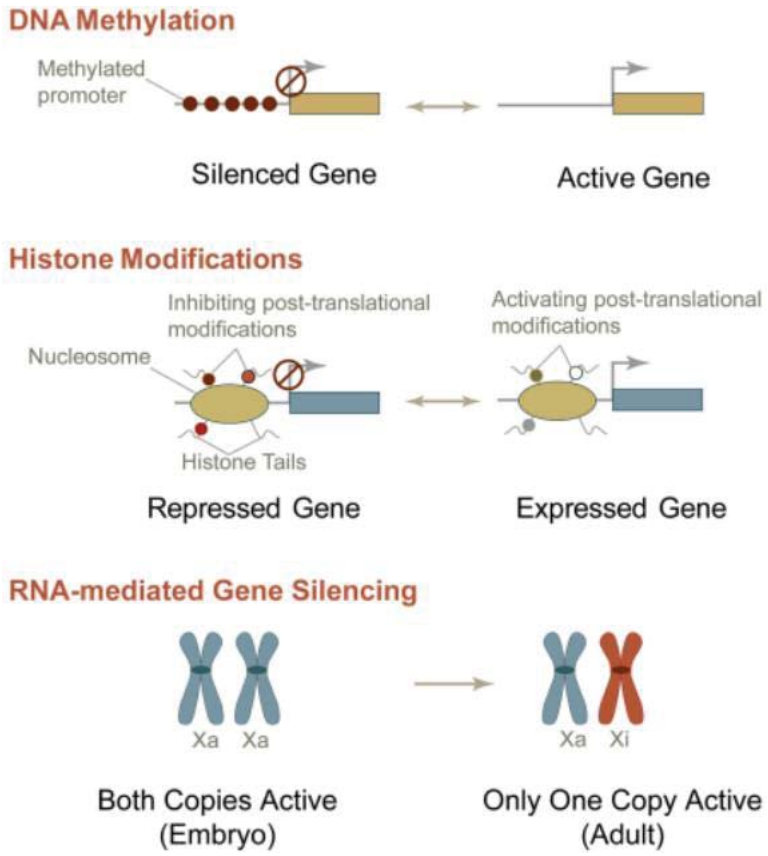

(Legend on the next page)

Figure 1-1: Epigenetic mechanisms involved in gene expression.

Methylation of DNA on specific promoters inhibit gene transcription. Histone modifications can either repress or activate gene expression depending on the residues present on the histone tails. Non-coding RNA such as Xist can trigger gene silencing, or in this particular case, the silencing of an entire genome. (Zaidi et al., 2010)

1.1.1 DNA METHYLATION

Of the three different types of epigenetic mechanisms known so far, DNA methylation has been the most extensively studied. DNA methylation was first described in the 1950 by Hotchkiss (Hotchkiss, 1948) but it wasn't until the 1970s that DNA methylation was associated with gene regulation (Holliday and Pugh, 1975). DNA methylation consists of the addition of a methyl group (-CH3) on DNA, preferentially at the 5-position of cytosine residues (5mC) at CpG dinucleotides (Robertson, 2005).

DNA methylation is a mechanism important for cell differentiation and gene expression. DNA methylation prevents the binding of transcription factors or the recruitment of proteins (Methyl-CpG-binding proteins) implicated in gene repression. Examples of gene silencing associated with DNA methylation include imprinting (Elhamamsy, 2017) and X chromosome inactivation (Kaslow and Migeon, 1987), the details of which I shall elaborate upon later on.

DNA methylation is catalyzed by the DNA methyltransferase (DNMTs) enzymatic family which can be separated into two distinct groups depending on the DNA substrate they use (Bestor, 2000; Bestor et al., 1988; Cheng and Blumenthal, 2008). The *de novo* methyltransferases, DNMT3a and DNMT3b, establish methylation on DNA soon after the embryo's implantation, whereas DNMT1 is associated with the maintenance of DNA methylation throughout cell mitosis. Indeed, DNMT1 binds on hemi-methylated DNA and methylates the newly synthesized DNA strand using the parental strand as a template (Figure 2) (Hermann et al., 2004). DNMT3L, a DNMT-related protein, associates with DNMT3a and DNMT3b to regulate their catalytic activity, though DNMT3L itself does not possess DNA-methyltransferase activity (Ooi et al., 2007). Previous work demonstrated that Dnmt1 knock-out mice are embryonically lethal, (Lei et al., 1996). Dnmt3a knockout mice die soon after birth, whereas Dnmt3b KO mice are not

viable (Okano et al., 1999). These studies illustrate the importance of DNA methylation in mammals.

Finally, the last member of the DMNTs family is DNMT2. Its biological role is not quite clear yet. One study however showed that DNMT2 methylates tRNA at cytosine 38 preventing tRNA segmentation (Goll et al., 2006).

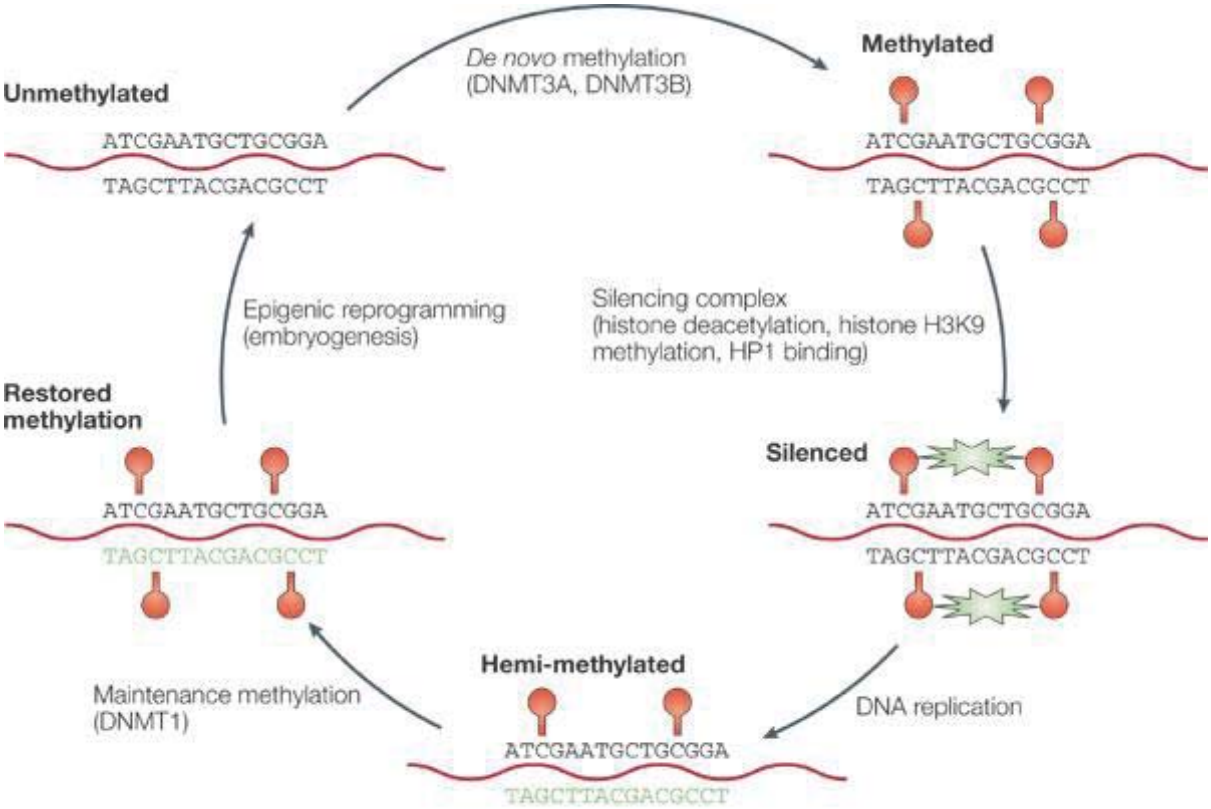

Figure 1-2: Mechanisms of DNA methylation.

Unmethylated DNA is methylated by de novo methyltransferases during embryogenesis post implantation. Other epigenetic mechanisms, such as histone modifications, are involved to successfully silence a gene. During DNA replication the newly synthesized strand is unmethylated leading to a DNA hemi-methylated. DNMT1 faithfully establishes the methylation mark on the unmethylated DNA strand using the methylated parental strand as a template. Methylation is erased during reprogramming towards pluripotency. (Issa,2004)

1.1.2 HISTONE MODIFICATIONS

Besides DNA methylation, another epigenetic modification important for gene regulation is histone modification. Gene expression is regulated through this mechanism by either altering chromatin structure or by recruiting histone modifiers. DNA methylation together with histone modifications have an intrinsic relation regarding the chromatin state (Cedar and Bergman, 2009).

Histones are proteins which are the building block of the first order of compaction of chromatin. Two copies of each core histone (H2A, H2B, H3 and H4) form an octamer, around which 147bp of DNA is wrapped to create nucleosome (Kornberg, 1974; Kornberg and Thonmas, 1974). The core histone possesses an N-terminal protrusion (histone tail) which can be modified according to the type of residue they have. Histone modifications are post translational modifications that happen on core histones on several residues (lysine, arginine serine and threonine). The long list of histone modifications encompasses, among others, methylation, acetylation, phosphorylation, ubiquitylation, and sumonylation (recapitulated in Table 1). Depending on the type of histone modifications and DNA methylation pattern, chromatin can either adopt an open or closed configuration. Open chromatin is associated with transcriptionally active regions named euchromatin, whereas closed chromatin is correlated with transcriptionally inactive regions that are referred to as heterochromatin (Figure 3).

Table 1-1: Different classes of modification in histones

Chromatin Modifications	**Residues Modified**	**Functions Regulated**
Acetylation	**K**-ac	Transcription, Repair, Replication, Condensation
Methylation (lysines)	**K**-me1 **K**-me2 **K**-me3	Transcription, Repair
Methylation (arginines)	**R**-me1 **R**-me2a **R**-me2s	Transcription
Phosphorylation	**S**-ph **T**-ph	Transcription, Repair, Condensation
Ubiquitylation	**K**-ub	Transcription, Repair
Sumoylation	**K**-su	Transcription
ADP ribosylation	**E**-ar	Transcription
Deimination	**R** > Cit	Transcription
Proline isometization	**P**-cis > **P**-trans	Transcription

The most well studied histone modifications are methylation and acetylation. Generally speaking, acetylation is associated with transcriptionally active chromatin whereas methylation is a feature of transcriptionally silenced chromatin. However, there are few exceptions where histones methylation is a transcriptionally active mark, such as H3K4me3, H3K36me2 and H3K36me3 (Schmitges et al., 2011).

Histone acetylation is catalyzed by histone acetyltransferase (HAT). Acetylation of histones neutralizes the positive histone charges, thus decreasing the interaction between DNA (negatively charged) and acetylated histones. This allows the unravelling of DNA making it accessible to proteins such as transcription factors to bind on the DNA and promote transcription of genes (Grunstein, 1997). Acetylation can be removed from histones by the Histone DeAcetylase (HDAC) enzymatic family.

Histone methylation consists of the addition of one, two or three methyl groups on the histone tail which occurs in the presence of histone methyltransferase (HMT) and will either repress or activate chromatin. Heterochromatin can either be facultative or constitutive. Facultative heterochromatin is enriched in H3K27me3, a histone modification strongly present on the inactive X chromosome (further details below). Constitutive heterochromatin is characterized by the presence of H3K9me3 and is localized at the centromeric and telomeric regions (Saksouk et al., 2015).

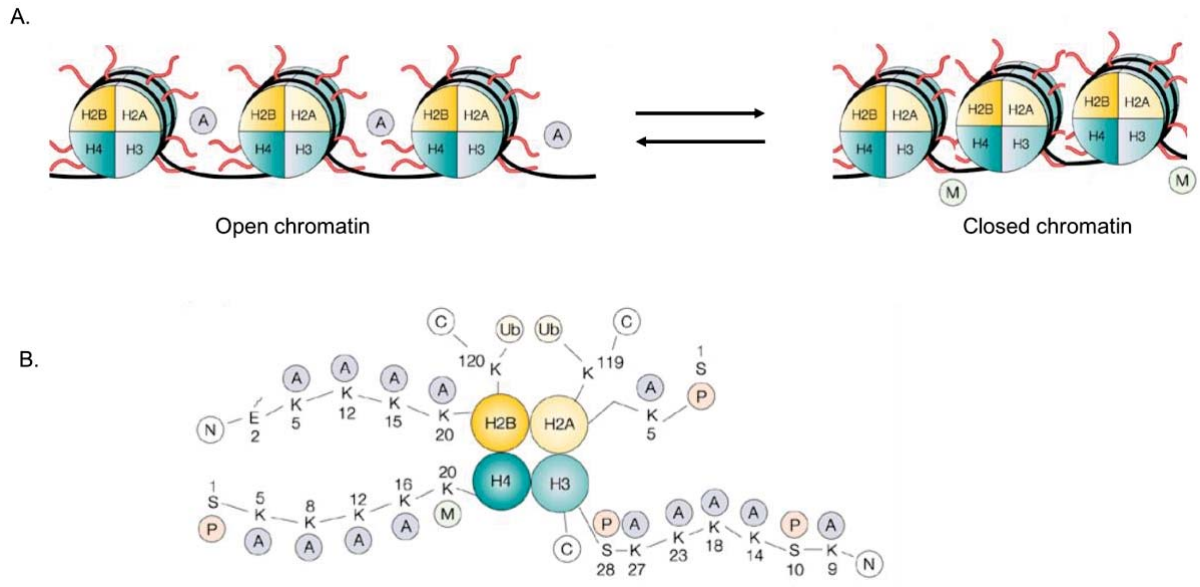

Figure 1-3: Histone modification and chromatin compaction.

(A) Schematic representation of open and closed chromatin according to histone modification. (B) Example of histone modification on different histone subunits and histone residues. Adapted from (Marks et al., 2001)

Little is known about the role of histone phosphorylation in gene expression. However, several studies have suggested that phosphorylation of histone is important during mitosis. Indeed, Fischle et al.,2005 have shown that phosphorylation of Serine 10 on histone H3 (H3S10) by Aurora B kinase during mitosis is important in chromatin condensation (Fischle et al.,2005). In this study, the authors indicate that H3S10 displace HP1 from H3K9me.The same year, Dai et al., demonstrated that phosphorylation of Threonine 3 on histone H3 is essential for alignment of metaphase chromosome.

Another histone, histone H1 (known as linker histone), plays also an important role in chromatin compaction and higher order structure (Thoma et al., 1979). H1 binds to the nucleosome and interacts with linker DNA, maintaining the DNA wrapped around the nucleosome (Thomas, 1999). H1 is the histone protein that possesses the most variants, however little is known about H1 modifications (Wiśniewski et al., 2007). An elegant study has demonstrated, using Fluorescent Recovery After Photobleaching (FRAP), the "stop and go" mechanism of H1 binding to nucleosomes highlighting the dynamics of chromatin structure (Catez et al., 2006). The "stop phase" occurs when H1 binds to the nucleosome, and its duration varies according to the modifications of the core histones. The duration of the stop phase is significantly longer than the "go phase", which occurs when H1 binds to another nucleosome.

1.1.3 NON-CODING RNA

Another element affecting chromatin states are long non coding RNAs (lnc-RNA), which are RNA transcribed from non-protein coding regions of the genome (Kapranov et al., 2007; Amaral and Mattick, 2008). Nc-RNA encompass several types of RNA which can be divided into two categories based on their size: Small nc-RNA and long nc-RNA. Small nc-RNA includes among others piRNA, miRNA, siRNA. Nc-RNA uses two mechanisms to regulate gene expression: small nc-RNA bind complementarily to mRNA and either inhibit their translation (miRNA) or degrade the RNA itself (siRNA) (Filipowicz et al., 2005). PiRNA is involved in gene silencing in germ cells in several organism(Siomi et al., 2011).The regulatory action of Small nc-RNA is transient, in contrast to the long term action of lnc-RNA.

Lnc-RNA have been shown to be crucial for cell pluripotency and differentiation as well as cell growth (Cesana et al., 2011; Wang et al., 2013). Lnc-RNA may be used as precursor for small nc-RNA, however recently it has been shown that lnc-RNA can also regulate gene silencing by direct interaction with DNA or chromatin modifiers (Marchese and Huarte, 2014). Indeed, the Hox locus (HOTAIR) lnc-RNA interacts with the PRC2 protein complex to silence a chromosomal domain (Rinn et al., 2007). Other lnc-RNA have been shown to recruit chromatin modifiers in the imprinting process to preferentially silence one allele. Another example of gene silencing mediated by lnc-RNA is the inactivation of the X chromosome triggered by the lnc-RNA Xist which acts in cis and adheres to specific loci on the Xi then spreads to inactivate an entire chromosome (see section 3.1 of the introduction for more details). These two examples demonstrate the variety of mechanisms used by Lnc-RNA to silence specific gene loci.

1.1.4 MITOTIC CHROMOSOMES AND EPIGENETIC MEMORY

1.1.4.1 Mitotic chromosomes

One of the most striking phenomenon that occurs during mitosis is the formation of mitotic chromosomes, which are a complex entity that arise from the compaction of chromatin. Mitotic chromosomes are condensed chromatin with the addition of proteins important for the compaction, structure and segregation of chromosomes. In this section, I will discuss the proteins important for mitotic chromosome structure.

Scaffolding proteins are important for the higher order structure of mitotic chromosomes. Two major members of this group of proteins are Topoisomerase II (Topo II) and condensin I and II (Earnshaw and Heck, 1985; Gasser et al., 1986; Saitoh and Laemmli, 1994). Topo II has different roles according to the cell cycle stage. During DNA replication, Topo II breaks and rejoins double-strand DNA in order to remove supercoiled or intertwined DNA, while during mitosis it acts as a scaffold. The other protein complex that acts as a scaffold during mitosis is the highly conserved condensin, composed of the five subunits. Two of these subunits are part of the Structural Maintenance of Chromosomes (SMC): SMC2, SMC4. The other non SMC-proteins

components called Condensin Associated Proteins (CAP) and are CAP-G/G2, CAP-D2/D3 and CAP-H/H2 (Ono et al., 2003). Maeshima and Laemmli demonstrated in an elegant study that Topo II and a condensin subunit (13S) localize on a vertical line in mitotic chromosomes. From these finding they proposed that Topo II and condensin intertwined to form a 'Barber Pole' pattern that acts as a scaffold in mitotic chromosomes (Maeshima and Laemmli, 2003). Condensin depletion generates mitotic chromosomes that appear to be larger and less condensed (Hudson et al., 2003) whereas lack of Topo II alpha diminishes chromatin condensation (Farr et al., 2014) but not the loading of condensin, suggesting two distinct pathways for Topo II alpha and condensin to act as a scaffold in mitotic chromosomes (Cuvier and Hirano, 2003).

Another protein important for mitotic chromosome structure is the cohesin protein complex. Cohesin is a tetrameric protein composed of 4 subunits: SMC1, SMC3, RAD21 and STAG. Its role is to hold the two sister chromatids, established during S phase, together during mitosis until the anaphase step of mitosis. The cohesin complex forms a ring-like structure within both sister chromatids are trapped. Cohesin counteracts the forces of the mitotic spindle, hence allowing the correct alignment and segregation of the sister chromatids (Nasmyth et al., 2000). Several studies using cohesin mutants showed that they were unable to hold sister chromatids together during metaphase (Guacci et al., 1997; Michaelis et al., 1997). At the onset of mitosis (prophase), cohesin is removed from mitotic chromosomes. Only a small percentage remain on mitotic chromosomes throughout the prophase-to-metaphase transition, where cohesin subunit's Rad21 can only be detected at the centromeric region (Waizenegger et al., 2000). To release the two sister chromatids in anaphase, cohesin needs to be cleaved by separin, leading to the release of cohesin from mitotic chromosomes and the separation of the chromosome arms. Rad21 links together all the other subunits of the cohesin complex. Destruction of Rad 21 results in the dissociation of the other subunits of cohesion from the chromosomes (Xu H et al, 2004).

Other proteins specific for mitotic chromosomes are centromere proteins (CENP-A, CENP-B and CENP-C) that are involved in kinetochore formation and centromere maintenance. CENPA is a histone variant of H3, that is specifically located at the centromere of mitotic chromosomes. CENP-A is required for the recruitment and assembly of kinetochore proteins

as well as the segregation of chromosomes (Kunitoku et al., 2003; Zeitlin et al., 2001). Human CENP-B proteins bind to a 17 bp region named the CENP-B box and may be involved in chromatin structure(Tanaka et al., 2001). CENP-C is a member of CENPA-nucleosomes associated complex that is a key factor in mitotic progression, chromosome segregation and kinetochore assembly (Gascoigne et al., 2011). DNMT3B is recruited by CENP-C to methylate centromeric and pericentromeric regions (Gopalakrishnan et al., 2009).

Another component of mitotic chromosomes which are also present in interphase chromosomes are the telomeres located at either end of each chromosome arm. Telomeres are made of kilo bases of nucleotides repeats and possess specific telomere proteins known as sheltering complex proteins. At each cell division, the nucleotides repeats are shortened until it reaches a critical point. When cells possess critically short telomeres they become senescent and stop proliferating. The shelterin complex is composed of five proteins TRF1, TRF2, Rap1, Pot1, Tin2 and TPP1. Shelterin proteins prevent shortening of the telomere and chromosomes end fusion by forming a T-loop DNA structure that avoids the end of a chromosomes from being identified as DNA damage (de Lange, 2005).

1.1.4.2 Epigenetic memory

Epigenetic mechanisms are maintained throughout cell division allowing, during symmetrical division, both daughter cells to possess the same phenotype as the parental cell. During mitosis, cells undergo drastic nuclear and cellular changes. One of the most evident changes is the compaction of chromatin into mitotic chromosomes and loss of the nuclear envelope. Another modification that happens during mitosis is the cessation of gene transcription and the removal of most proteins, including RNA polymerase and most transcription factors, from mitotic chromosomes (Spencer et al., 2000).

To maintain the epigenetic memory throughout the cell cycle, several mechanisms takes place. For instance, during S phase to retain methylation newly synthesized DNA is methylated by the DNMT1 enzyme. Eed protein, a component of PRC2 protein complex ensure the propagation of H3K27me3 during DNA replication (Margueron et al., 2009). These process ensure the stability of the epigenetic marks during cell cycle.

Following the transition between mitosis and G1 phase of the cell cycle, transcription is resumed in daughter cells in order to obtain a gene expression pattern similar to the parental cell in the case of symmetrical cell division. To allow the maintenance of the cell fate and proliferation throughout several cell cycles, a mechanism, named mitotic bookmarking, has been proposed. Mitotic bookmarking is a relatively recent concept and its details still remain to be fully elucidated. Mitotic bookmarking is the retention of specific transcription factors on the mitotic chromosomes to ensure an accurate and rapid transition from mitosis to G1 phase of the cell cycle. These bookmarking transcription factors are involved in cell fate or cell proliferation and even in oncogenesis (Zaidi et al., 2014). A recent study has shown using high-resolution microscopy techniques that in ES cells, the pluripotency associated factor Sox2 remains attached on mitotic chromosomes (Deluz et al., 2016) allowing the daughter cells to maintain their ES cell like state throughout rapid cell cycling. Another study demonstrated that Esrrb, another pluripotency-associated factors, remains bound to mitotic chromosomes (Festuccia et al., 2016). These findings corroborate the fact that mitotic bookmarking is important for the maintenance of cell fate.

1.2 Pluripotent Stem Cells and reprogramming towards pluripotency

1.2.1 Pluripotent Stem cells

Pluripotency is the ability of a cell to differentiate into the three primary germ cell type of the early embryo, therefore leading to the genesis of all the cells present in an adult body. Pluripotent Stem Cells are present in vivo specifically during embryogenesis. Pluripotent Stem Cells are defined by their ability to differentiate into the three primary germ layers (endoderm, ectoderm and mesoderm) and to self-renew with cell division. Other characteristics of pluripotent cells include the formation of teratomas (tumors that have the ability to form three different germ cell lines) in vivo and the formation of chimeras. In embryogenesis, pluripotent stem cells are found at the blastocyst developmental stage. Embryonic stem cells (ES cells) are derived from the Inner Cell Mass (ICM) of the blastocyst, and can be maintained in culture under specific conditions to retain their pluripotency state.

Two different types of culture conditions are used to maintain pluripotency in vitro: by the addition of Leukemia Inhibitory Factor (LIF) to the ES cell media, or alternatively by using two small molecules (Chir99021 and PD0325901) known as 2 inhibitors (2i) media. ES cells cultured in 2i media maintain their pluripotent state by inhibiting mitogen-activated protein kinase (MEK) and glycogen synthase kinase-3 (GSK3) (Ying et al., 2008). The gene expression profile of ES cells maintained in 2i media condition is different from ES cells maintained in LIF (Marks et al., 2012). ES cells cultured in 2i media express a stable level of Nanog contrary to ES cells in serum with LIF media that shows a periodicity in Nanog expression from Nanog-high to Nanog-low state. The Nanog low population is more prone to respond to differentiation (Singh et al., 2007).

Pluripotency is regulated by three main group of transcription factors, Oct4 (Pou5f1), Sox2 (SRY box2) and Nanog (Kim et al., 2008; Orkin et al., 2008). These three transcription factors represent the core factors of pluripotency. Oct4 is expressed in pluripotent ES cells both in vivo and in vitro (Nichols et al., 1998). Sox2 have been shown to be crucial for the generation of pluripotent epiblast stem cells and tightly regulates Oct4 expression in ES cells (Avilion et al., 2003). Nanog overexpression have been shown to promote ES cell self-renewal in the absence of Leukemia Inhibitory Factor (LIF) (Mitsui et al., 2003). The concentration of these three transcription factors is stringently controlled as their overexpression or loss leads to differentiation of ES cells. ES cells harboring a low level of Nanog are more prone to differentiate compared to ES cells with a high level of Nanog (Filipczyk et al., 2015). Small increases in Sox2 expression in ES cells leads to the differentiation of ES cells towards several lineages including neuroectoderm or mesoderm (Kopp et al., 2008). Slight overexpression of Oct4 in ES cells triggers differentiation towards mesoderm whereas knock-down of Oct4 enhances the differentiation towards trophectoderm (Hay et al., 2004).

ES cells have unique chromatin states that differ from differentiated cells. In ES cells histones can simultaneously possess both active (H3K4ac) and repressive histone modifications (H3K27me3). This status is called bivalency (Bernstein et al., 2006). Upon differentiation, one of the two histone modifications is lost while the other one remains. Furthermore, ES cells possess a global low level of DNA methylation and an enrichment of acetylation (Azuara et al., 2006).

1.2.2 Reprogramming

Reprogramming is the conversion of one cell type to another that can either be induced chemically or by ectopic expression of specific proteins. Reprogramming towards pluripotency is the process by which somatic cells are converted to ES cells. Reprogramming towards pluripotency can be achieved in vitro by three different ways: nuclear somatic cell transfer, cell fusion, and transcription-factor transduction induced pluripotent stem cells (iPS). The discovery of iPS cells has tremendous clinical applications, and more studies need to be conducted in order to fully understand the mechanisms regulating the reprogramming towards pluripotency process. Understanding the molecular mechanism can be done using the three in vitro reprogramming techniques. In this section I will briefly describe the three reprogramming methods.

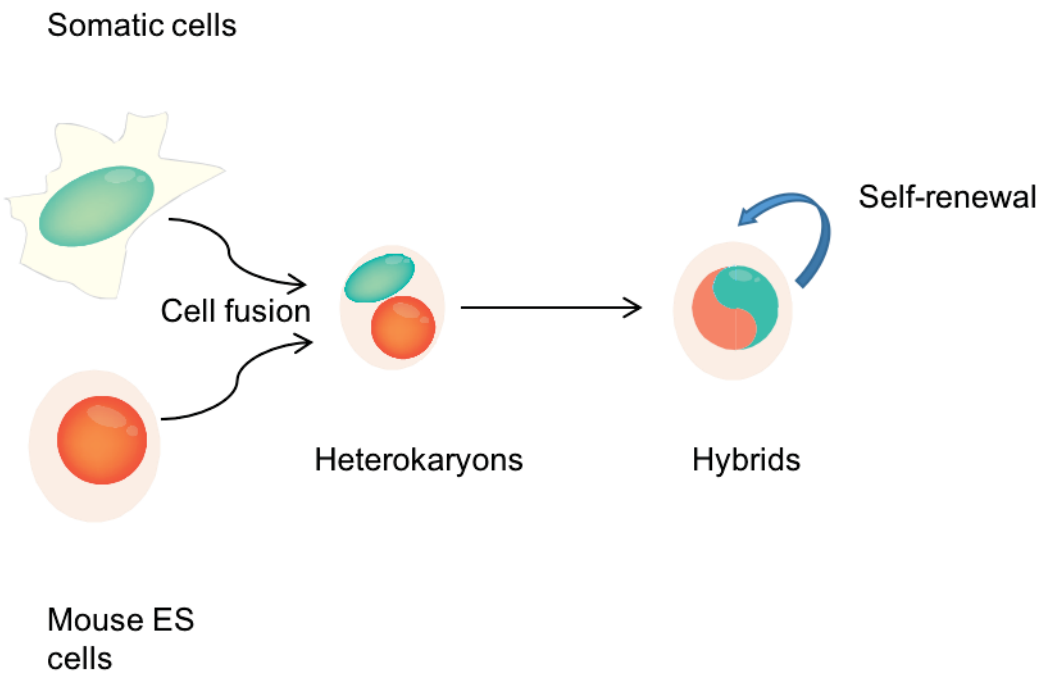

Figure 1-4: Cell fusion mediated nuclear reprogramming towards pluripotency.

Cell fusion mediated reprogramming is where a pluripotent cell (e.g ES cells) is fused with a somatic cell to form a single entity called a heterokaryon that share one cytoplasm and several nuclei. Heterokaryons can then give rise to hybrid cells that only have one cytoplasm as well as one nucleus and are tetraploid (i.e 4n). Those cells can undergo mitosis. Hybrid cells are generated when the fusion occurs between cells from the same species. If a fusion is performed with a human somatic cell and a mouse ES cell, the heterokaryon will die because of chromosomal instability. The chromosomal instability is due to the number of chromosomes in human and mouse cells which are different.

1.2.2.1 Nuclear Transfer

Nuclear transfer occurs when a nucleus from a somatic cell is transplanted inside an enucleated oocyte, followed by the nuclear reprogramming of the somatic cell nucleus leading to the creation of an entire individual possessing the exact same genome of the somatic cell nucleus. Briggs and Kings 1952 were the first to demonstrate the potential of nuclear reprogramming mediated by nuclear transfer. This experiment was carried out by inserting an early blastocyst cell nucleus into an oocyte from amphibians. This first study demonstrated the plasticity of somatic cells and their epigenetic mechanisms.

Later on, Gurdon performed the same experiment using a nucleus from fully differentiated tadpoles and successfully obtained normal adult frogs (Gurdon, 1962). These findings lead to the creation of Dolly the sheep (Wilmut et al., 1997) decades after. A year later, cloned mice were generated by nuclear transfer (Wakayama et al., 1998). In addition to the low efficiency of the somatic cell nuclear transfer (SCNT) process, cloned mice can have several abnormalities ranging from abnormal gene expression in embryos to shorter life span, suggesting that the erasure of the epigenetic memory, such as DNA methylation or histone modification, is not complete in cloned mice obtained by SCNT. Indeed, addition of a histone deacetylase inhibitor increases the efficiency of reprogramming by SCNT. Recently, a study was performed with enucleated human oocytes and human fibroblasts (Tachibana et al., 2013). This could be useful for future clinical application.

1.2.2.2 Transcription factor mediated reprogramming

In 1987, Gehring and colleagues showed in D.melanogaster that ectopic overexpression of a homeotic gene, antennapedia, led to a change in body plan by adding a pair of legs where the antenna should have been (Hiromi and Gehring, 1987). The same year, Weintraub and colleagues discovered that ectopic expression of myoD in fibroblasts in mice lead to their conversion to myogenic lineage (Davis et al., 1987). Another finding demonstrated that the deletion of Pax5 in B cells leads to their conversion to less specialized progenitors (Busslinger

et al., 1999). In 2006 the generation of pluripotent stem cells from mouse fibroblasts has been achieved by overexpressing Oct4, Sox2, Klf4 and c-Myc (OSKM) using retro-viral vectors and a DNA library of genes expressed in ES cells (Takahashi and Yamanaka, 2006).

The pluripotency status of those derived cells was assessed by their capacity to generate teratomas. Those cells were named iPS (induced Pluripotent Stem cells). iPS cell generation is a lengthy (up to three weeks) and low efficiency process (Hochedlinger and Plath, 2009). Its mechanism can be dissected into three phases: initiation, maturation and stabilization. In the initiation phase the cell cycle of somatic cells changes towards a more 'ES cell like' cell cycle profile, and a change in cellular morphology can be seen (e.g cells become smaller and round). A few days after transfection, Mesenchymal to epithelial transition (MET) occurs, indicated by the formation of small, round shape colonies. MET is the exact opposite of epithelial to mesenchymal transition (EMT) that happens during embryonic development. During the maturation/intermediate phase, cells start expressing pluripotency associated markers such as Alkaline Phosphatase, the cell surface marker SSEA1 and are self-renewable (Brambrink et al., 2008). Most of the cells transfected with OSKM remain stuck at the maturation stage indicating that there is an epigenetic barrier preventing them to move towards the fully pluripotent status. It has been shown that the choice of somatic cells is important, less differentiated somatic cells have a higher efficiency in reprogramming towards pluripotency (Raab et al., 2014). For example, neural stem cells already express Sox2 and a low level of Klf4, thus their reprogramming efficiency is higher compared to fibroblasts. Recently people have tried to increase the efficiency of iPS by various methods by either controlling the microenvironment of by changing the stoichiometry of the ectopic factors (Luni et al., 2016; Tiemann et al., 2011).

Overall these studies indicate that ectopic expression of specific proteins as well as deletion of proteins can change the cell fate of differentiated cells demonstrating the plasticity of somatic cells and their epigenetic memory.

1.2.2.3 Cell fusion mediated reprogramming

Experimental cell fusion was described by Henry Harris and Nils Ringertz in the 1960s (HARRIS et al., 1969). A few years later, production of monoclonal antibody was achieved with hybridomas generation by cell fusion between B cells and plasmacytomas NS1 (Köhler and Milstein, 1975). More recently cell fusion has been used to study the molecular mechanism of trans-acting elements from one genome to another one. Cell fusion studies showed that the fate of a somatic cell can be reversible and requires regulators such as proteins. Specifically the cell fusion technique demonstrated that when fusion occurs between ES cells and somatic cells, pluripotency associated factors from ES cells reprogram the nucleus of the somatic cells leading to chromatin remodeling and reactivation of previously silenced genes (Pereira et al., 2008). Cell fusion consists of the fusion of two or more cell types to generate one single entity which are heterokaryons or hybrid cells (Figure 1-4). The main difference between those two cells is that hybrid cells can undergo mitosis and possess one nucleus contrary to heterokaryons which have a short life-span and possess multiple nuclei. Upon cell fusion, RNA and protein are synthesized suggesting that cell fusion does not change fundamental cellular metabolism.

Cell fusion is useful to study events of reprograming such as DNA demethylation or X chromosome reactivation (Cantone et al., 2016; Piccolo et al., 2013). Surani and colleagues showed that when fusing embryonic germ cells with somatic thymocytes from mice, hybrid cells were generated (Tada et al., 1997). They demonstrated that the generated hybrid cells possessed pluripotent properties such as formation of chimera and self-renewal. Later on Tada et al took advantage of the hybrid system to show that hybrid cells created from the fusion between ES and somatic cells can acquire a pluripotent state (Tada et al., 2001). In this study they fused male ES cells with female somatic cells that contained a GFP reporter transgene driven by the promoter of Oct4. They found that some X-linked genes from the previously inactive X were reactivated and that GFP was expressed indicating the re-activation of Oct4. Subsequent studies with human ES cells showed the generation of tetraploid hybrid cells when fusing with human fibroblasts (Cowan et al., 2005). Those hybrid cells successfully express *Oct4* genes and can differentiate into the three different germ layers. Compared to iPS, pluripotency-associated factors can be detected 24 hours after fusion making this technique

useful to study early reprogramming events (Pereira et al., 2008). Changes in the chromatin environment are also detected, high level of acetylation and presence of histone modifications such as H3k4me3 can be detected (Kimura et al., 2004).

Cell fusion mediated reprogramming is highly dependent on the somatic cell partner. It has been shown that neural progenitors have a higher reprogramming efficiency compared to fibroblast (Silva et al., 2006). In this study, they also showed that overexpression of *Nanog* increases the efficiency of reprogramming towards pluripotency mediated by cell fusion (Silva et al., 2006). Increasing the reprogramming efficiency mediated by cell fusion is also achieved by treatment with the demethylating agent 5-AzaC, showing once more the importance of the chromatin environment to fully reprogram somatic cells towards pluripotency (De Carvalho et al., 2010).

1.3 Epigenetic mechanisms behind X chromosome inactivation and reactivation

1.3.1 X CHROMOSOME INACTIVATION

In placental female mammals one of the two X chromosomes is randomly inactivated (Lyon, 1962). This biological process ensures that both males and females express the same dosage of X-linked genes. In mammalian cells the inactive X chromosome (Xi) forms a Barr body that is characterized by an intense signal when cells are stained with DAPI (Barr, M.L. & Bertram, 1949). X chromosome inactivation happens only when there are more than one X chromosomes. As an example, individuals possessing only one X chromosomes and no other sex chromosomes (i.e X 0) have a female phenotype. This phenomenon is known as counting. Random Xi leads to mosaicism where some cells express genes from one X chromosome whereas other cells express X-linked genes from the other allele (Figure 1.2 A).

In mice, the first X chromosome inactivation occurs at the 4-cell stage, where the paternal X chromosome (Xp) is preferentially inactivated (Mak et al., 2004; Okamoto et al., 2004).This process is an example of imprinting as the maternal X chromosomes is prevented to not express Xist. Extraembryonic lineage such as trophectoderm and primitive endoderm will then maintain the inactive paternal X chromosome (Takagi and Sasaki, 1975). It is not fully understood why the Xp chromosome is preferentially inactivated, but it is hypothesized that the maternal X chromosome (Xm) possesses an epigenetic mark preventing it from being inactivated at the 4-cell stage. A Recent study suggests that H3K9me3 located at the Xist promoter on the Xm plays a role in preventing Xist expression from Xm (Fukuda et al., 2014). Xp inactivation is reversed at the blastocyst stage. At this stage random Xi occurs.

Random silencing of X-linked genes is initiated in epiblast cells of the blastocyst and is maintained thereafter throughout subsequent cell divisions (Rastan, 1982; Takagi et al., 1982). X chromosome inactivation (XCI) is an exemplar of epigenetic silencing that requires the presence of a specific region called the X Inactivation Center (Xic) located on both X chromosomes (Figure 1-5.B). In mice, XIC is a 100-500kb region (Lee et al., 1996). The core

region of XIC contains genes coding only for Ln-RNA such as Xist, RepA, Tsix, Xite and Jpx. A Recent study demonstrated that silencing of an autosome can be achieved by insertion of the core region of XIC on this autosome (Tang et al., 2010). Other element important for XCI are Ln-RNA Ftx, Tsx and the protein RNF12. XCI happens in a specific order that can be separated into an initiation phase and maintenance phase. These phases involving several long non-coding RNAs (Tian et al., 2010), histone modifications (Heard et al., 2001; Plath et al., 2003) and chromatin remodeling. Specifically, XCI is initiated by the transcription of Xist, a 17 kb long non-coding RNA localized on the Xic locus that is expressed and coats the future inactive X chromosome (Xi) in *cis* (Panning et al., 1997). Expression of Xist is tightly controlled by several lnc-RNA such as, *Jpx*, *ftx, Tsix* and proteins such as RNF12 (Sun et al., 2013). The most well-known lnc-RNA regulating Xist is Tsix, which when expressed prevents Xist expression (Lee et al.,2004). Another study revealed that RNF12 is essential of X inactivation by degrading Rex1 a pluripotency-associated factors that inhibits Xist transcription (Barakat et al., 2011; Jonkers et al., 2009).

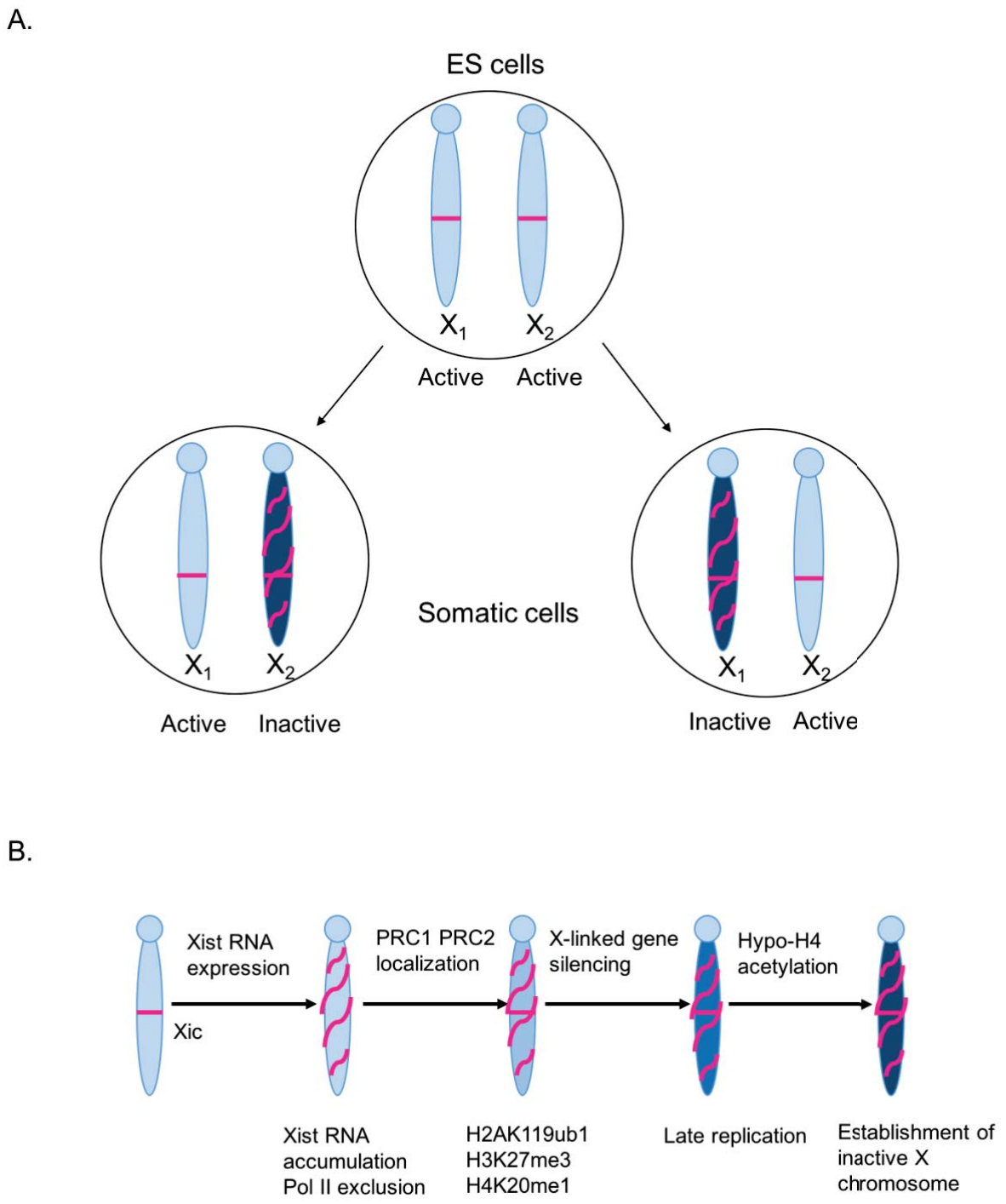

Figure 1-5: Random X inactivation mechanism.

(A) Upon differentiation somatic cells retain one X active and one inactive to ensure the same level of X-linked genes in male and female cells. This process occurs randomly. (B) Schematic representation of Xi. First Xist is expressed from the future inactive X closely followed by the exclusion of the transcription machinery such as RNA Pol II. PRC1 and PRC2 are recruited and catalyzed the histone marks H2AK119ub1 and H3K27me3, respectively. This lead to a late replication of the inactive X in S phase and a global hypo-H4 acetylation of the inactive X.

Xist expression triggers nuclear delocalization of Xi, closely followed by the exclusion of RNA polymerase II (Chaumeil, 2006) creating a repressive compartment on the Xi characterized by the lack of active histone modifications such as histone acetylation. Then chromatin modifiers such as polycomb repressive complex 1 and 2 (PRC1 and PRC2) are recruited to catalyze ubiquitination of H2A at lysine 119 (Fang et al., 2004) and histone H3 lysine27 tri-methylation (H3K27me3) (Csankovszki et al., 2001; Silva et al., 2003) respectively. Although it has been shown that Xist is necessary for the initiation of inactivation, it is not essential for maintaining the inactive state (Csankovszki et al., 1999). The maintenance phase involves DNA methylation and recruitment of heterochromatin proteins to the Xi. DNA (cytosine-5)-methyltransferase 1 (Dnmt1) has been shown to play a crucial role in the stabilization and maintenance of the Xi (Sado et al., 2000) by hypermethylating gene rich region on the Xi. Another key protein involved in the maintenance of the Xi is the structural-maintenance-of-chromosomes hinge domain containing 1 (Smchd1) protein. Its role is to hypermethylate CpG islands on the inactive X chromosome (Blewitt et al., 2008). Another factor affecting the stability of the Xi is macroH2A, a histone variant that is preferentially bound to Xist (Costanzi and Pehrson, 1998; Mermoud et al., 1999). The combination of different epigenetic factors is thought to make the Xi process highly stable.

1.3.2 X CHROMOSOME REACTIVATION

1.3.2.1 Xi reactivation *in vivo*

In mice, as well as in humans, reactivation of the Xi has been used as an indicator of the naïve pluripotent state (Plath and Lowry, 2011). Reactivation of the Xi chromosome happens both *in vivo* and *in vitro*. During mouse development, Xi reactivation takes place at three different stages of embryonic development. Xi reactivation first occurs at the two cell stage of the embryo, where the paternal X chromosome (Xp) is reactivated (green arrow figure 1-6). The second Xi reactivation occurs at the blastocyst stage, where cells from the Inner Cell Mass (ICM) reactivate the previously inactive paternal X chromosome (Lee et al., 2013). Xp reactivation is characterized by the loss of Xist expression, followed by loss of the repressive mark H3K27m3 and loss of PRC2. Surprisingly, the expression of some X-linked genes have been detected prior Xist and H3K27me3 loss indicating that Xpi reactivation occurs while Xist and H3K27me3 are present on the Xi (Williams et al., 2011).

The third Xi reactivation happens during the formation of primordial germ cells (PGCs), where the pluripotency gene network is re-expressed (de Napoles et al., 2007; Sugimoto and Abe, 2007). Embryonic stem cell lines can be derived from these Primordial Germ Cells (PGCs) (i.e. embryonic germ cells, EGCs). PGCs are derived from epiblasts where the Xi silencing has already occurred. Xi reactivation is initiated when PGC cells begins to migrate towards the genital ridge. The erasure of the epigenetic memory in PGCs occurs during this migration, and includes reactivation of Xi. Xi reactivation is a process that includes several steps. Loss of Xist expression and H3K27m3 are the first event to occur followed by reactivation of some X-linked genes. DNA demethylation and chromatin remodeling are required for the epigenetic reprogramming that happens during the formation of PGCs and this coincides with X-linked reactivation.

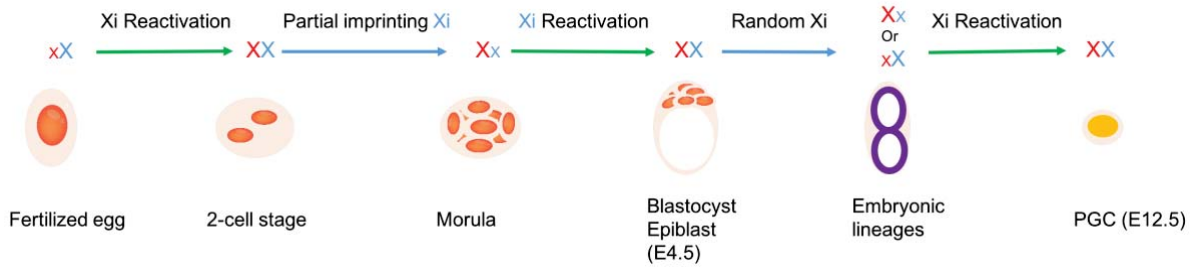

Figure 1-6: X inactivation and reactivation during mouse embryonic development.

After fertilization of the oocyte by the sperm and the first mitosis, both X chromosomes become active (First reactivation indicated by the green arrow). Then, the paternal X chromosome (Xp) become inactive and will remain inactive in the extraembryonic tissues. In contrast at the blastocyst stage Xp (blue) is reactivated (Second reactivation). Soon after this reactivation, random X inactivation happens (blue arrow). The last reactivation takes place in PGCs before oogenesis. Adapted from Ohhata and Wutz,2013.

1.3.2.2 Xi reactivation *in vitro*

In vitro the Xi re-acquires an active state during pluripotent reprogramming of a somatic cell, achieved by various approaches including exogenous factors (Maherali et al., 2007; Pasque et al., 2014), nuclear transfer (Eggan et al., 2000) or cell fusion (Tada et al., 2001; Takagi et al., 1983; Ying et al., 2002) (Recapitulated in Figure 1-7). Furthermore, some X-linked genes can be reactivated by chemicals such as 5-AzaC (Csankovszki et al., 2001). Xi reactivation is one of the last events during reprogramming and results in loss of expression of Xist RNA, displacement of polycomb-group repressor proteins and loss of chromatin-associated silencing marks such as H3K27me3.

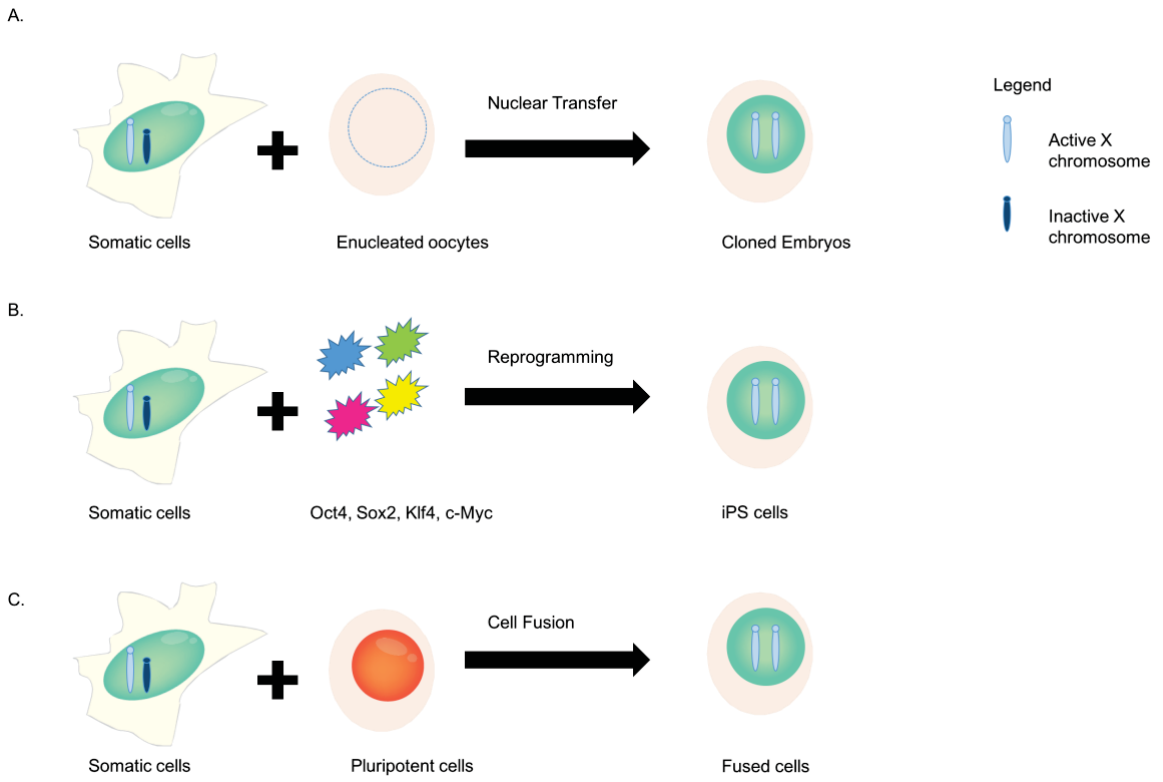

Figure 1-7: In vitro system for Xi reactivation.

(A) Using SNCT the female somatic cell nucleus is inserted inside and enucleated oocyte. This gives rise to an embryo with two active X chromosomes. (B) In iPS system, female somatic cells are transfected with four transcription factors upon which the somatic cells will become pluripotent, thus having two active X chromosomes. (C) Finally in cell fusion, the female reprogrammed cells will also possess two active X chromosomes. Adapted from Ohhata and Wutz 2013

Generation of cloned mice by SNCT, has shown that the Xi from the somatic donor cell is preferentially chosen for the inactivation in extraembryonic lineage (Figure 1-7.A). This process is similar to the inactivation of the paternal X chromosomes in extraembryonic tissues from fertilized eggs. If the donor cell is female random Xi occurs in extraembryonic tissues. However random inactivation is observed in cloned mice suggesting that the process of reactivation and inactivation of the X chromosomes is normal (Eggan et al., 2000). The SNCT technique has a lot of caveats, its efficiency is low and individuals generated from it carry genetic abnormalities due to failed erasure of epigenetic mark. In female embryos derived from nuclear transfer down-regulation of X-linked genes is observed due to improper XCI activation and Xist expression. Ectopic Xist expression has been shown to increase the efficiency of nuclear cloning (Inoue et al., 2010).

In iPS generation, Xi reactivation appears to be one of the last events in the epigenetic remodeling (Figure 1-7.B) (Stadtfeld et al., 2008). In this system, studies demonstrated that Xist repression is not sufficient to induce Xi reactivation they also found that DNA demethylation happens at a late stage during Xi reactivation and that DNA demethylation itself is also not sufficient enough to induce Xi reactivation (Pasque et al., 2014).

Cell fusion between mouse ES cells or Embryonic Carcinoma (EC) cells and female somatic cells showed Xi reactivation, demonstrating that mouse ES cells possess the chromatin environment necessary for Xi reactivation (Takagi et al., 1983). Xi reactivation is also achieved when fusing EG cells with female somatic cells. In this particular fusion system global DNA demethylation was detected (Tada et al., 1997). Cell fusion studies have been able to shed some light regarding the mechanism of reprogramming. Indeed, it has been shown that PRC2 components are required for cell fusion mediated reprogramming (Pereira et al., 2010). In contrast, DMNTs are not necessary for reprogramming mediated by cell fusion. This highlights the potential of cell fusion to understand the mechanism of Xi reactivation (Figure 1-7.C). Recent studies demonstrated that some X-linked genes are reactivated upon reprogramming towards pluripotency (Cantone et al., 2016).

X chromosome inactivation and reactivation has been associated with diseases. Despite recent advances in understanding molecular mechanism implicated in Xi reactivation, a lot still need to be discovered for potential clinical applications regarding the treatment of X-linked gene diseases. Females are less affected by X-linked genes diseases compared to male due to the silencing of one of the two X chromosomes. Rhett syndrome is an X-linked genes diseases that affects female and is due to a mutation on the MeCP2 gene (Lyst and Bird, 2015). Other studies have demonstrated that X chromosome could be involved in cancer. It has been shown that in breast cancer the Barr body which represents the inactive X chromosome disappear (Barr and Moore, 1957). This lead to the assumption that in cancer cell the Xi is reactivated. Understanding the mechanism of Xi reactivation could help future medical applications.

1.4 Chromosomes visualization

It was in the 19th century that mitotic chromosomes were observed for the first time. The process of how chromatin compacts into mitotic chromosomes still remains elusive. The vast majority of the discovery made on mitotic chromosome structures were done using microscopy techniques. Currently, four mitotic chromosome models exist. The first model consists of DNA wrapping around nucleosome which then will compact gradually into fibers (30 nm) to form chromatid (Belmont et al., 1987). The second well-known model hypothesizes that DNA form loops around a core unit of scaffold proteins (Earnshaw and Laemmli, 1983). In this elegant study, Earnshaw and Laemmli depleted purified human mitotic chromosomes of histones and imaged them by EM. They found that histone depleted human mitotic chromosome still harbor a metaphase chromosome shape (X shape) surrounded by a halo of DNA. The third proposed model suggests that DNA is stacked onto a 6nm layers perpendicular to chromosome axis (Daban et al, 2015). Finally, the last model propose that mitotic chromosomes are not based on scaffolding proteins but instead consist of chromatin cluster separated by proteins (Poirier and Marko, 2002). All of these models even though they have been scientifically demonstrated still remain debatable. These models were developed based on data obtained from microscopy. In this section I will review the recent advance of chromatin visualization by both high resolution light and electron microscopy.

1.4.1 Light microscopy chromosomes visualization

Several light microscopy methods have been used to study the chromatin compaction during mitosis. Light microscopy allow us to visualize mitotic chromosomes during the different stages of mitosis. However, little information could be extracted from it due to the resolution limits of standard light microscopy techniques (250nm). To obtain a better resolution, in the last couple of years, several new microscopy techniques were developed named high resolution microscopy techniques. The most performing technique, PhotoActivated Localization Microscopy (PALM) allowed us to achieve a resolution up to 10nm. Some of these techniques were used to decipher the substructures of mitotic chromosomes.

In 2010 Matsuda et al were able to image mitotic chromosomes from D.*melanogaster* at a resolution up to 20nm using PALM technique and H2A tagged with GFP. This study suggested that mitotic chromosomes from D.*melanogaster* are formed by an assembly od 70nm blocks (Matsuda et al., 2010). Two years later, 3D- Structured Illimunation Microscopy (SIM) technique was used to study the role of condensin in metaphase chromosomes (Green et al, 2012). They showed the importance of condensin in maintaining the structure and physical properties of mitotic chromosomes. In 2015, another group studied the role of condensin and topo II with super resolution microscopy and electron microscopy. This study suggests that both condensin and Topo II act as a scaffold for mitotic chromosomes by forming a helix. Condensin topo II and cohesion role in mitotic chromosome structure was further assessed a year later with high resolution microscopy. They discovered that blocking cohesin has little effect on mitotic chromosomes whereas inhibition of topo II prevent sister chromatid resolution (Nagasaka et al., 2016). Assessing the role of proteins involved in mitotic chromosomes structure is easier than assessing the compaction of DNA itself. Indeed, DNA has to be stained to be able to visualize it. The staining may generate artefacts regarding the structure of DNA. Dong et al, 2016 developed a new technique to image DNA. They used the autofluorescence property of the DNA and Stochastic Optical Reconstruction Microscopy (STORM) technique to image chromatin without staining DNA. In their study they were able to see the typical X shape of human mitotic chromosomes (Dong et al., 2016). The data collected on mitotic chromosomes suggest area were the DNA in more compacted than other areas.

1.4.2 Visualizing chromosomes and DNA by electron microscopy

Electron microscopy was first use as a tool to assess chromosomes structure in mitotic cells. In 1977 Paulson and Laemmli depleted chromosomes from histone H1, revealing a loop structure with scaffold using EM (Paulson and Laemmli, 1977). Later on, in 1983, Earnshaw and Laemmli developed a method to visualize intact mitotic chromosomes using EM and their findings corroborate with the results obtained from 1977. The same year X-ray scattering and EM was used to postulate the theory of a 30nm fiber as a substructure of interphase chromosomes (Langmore et al., 1983). More recently, reconstructed nucleosomes were analyzed by EM and showed also a redundant pattern identified as a 30nm fiber (Huynh et al., 2005). A new EM techniques visualized for the first time frozen intact mitotic chromosomes within the cells (Eltsov et al, 2008). Their data revealed that compacted DNA could be imaged using cryo-sectioning and EM. Another EM called FIB (Focused ion beam) combined with high resolution scanning electron microscopy technique was used to image mitotic chromosomes of plants (Schroeder-Reiter et al., 2009).

Another breakthrough regarding DNA imaging happened a couple of years later. In 2012, lambda DNA was imaged by Transmitted electron microscopy (TEM) showing for the first time an image of the double stranded DNA (Gentile et al., 2012). More recently, 3D-Clem was used to characterize chromosome volume of distinct chromosomes (Booth et al., 2016). They also were able to image Ki-67 a protein that surrounds mitotic chromosomes. 3D-CLEM is a hybrid technique that can image both fluorescence and electron microscopy. A year later, Ou et al used ChromEMT (ChromEM tomography), to study the structure of mitotic chromosomes and showed that the chromatin was not as ordered as one thought (Ou et al., 2017).

Aim of the study

Since iPS generation, the reprogramming of somatic cells towards pluripotency have been intensively studied in order to fully understand the molecular mechanisms behind the generation of pluripotent cells from differentiated cells. Despite great advances in the field many questions remain, such as the contribution of different transcription factors or the role of ploidy in reprogramming. Cell fusion is a rapid and efficient way to reprogram somatic cells towards pluripotency. It allows us to study early reprogramming events.

Here I am using cell fusion between pluripotent stem cells and somatic cells to generate heterokaryons and hybrid cells, which can be analyzed to understand the molecular mechanisms important for reprogramming somatic cells towards pluripotency and the reactivation of genes following successful reprogramming. Specifically, first I am first using hybrid cells originating from fusion between ES cells and fibroblasts to investigate the kinetics of Xi reactivation. I am then investigating the role of ploidy in reprogramming towards pluripotency. To do so I will use both heterokaryons and hybrid cells using human B lymphocytes and mouse B lymphocytes respectively. Both of these studies have potential clinical applications for X-linked diseases such as Rett syndrome or Duchennes muscular dystrophy as well as helping iPS to be safer for potential therapeutics.

I then focus my interest in using previously established techniques and adapting them for my purpose. In this section I used flow karyotyping to isolate a specific set of chromosomes to them image them by high-resolution microscopy techniques including cryo-EM. This newly established pipeline of techniques might then be used for biological applications to provide a better understanding of mitotic chromosomes structures and the role of specific proteins in maintaining chromosome structure.

Chapter 2 : MATERIALS AND METHODS

2.1 Cell culture:

Mouse ES cells were grown on 0.1% gelatin (Sigma) -coated surfaces. E14Tg2a cells were cultured in KO-DMEM medium (Gibco) plus 10% FCS, non-essential amino acids (NEAA) (Gibco), 2mM L-glutamine, 50 µM 2-mercaptoethanol, 10 µg/ml Penicillin and Streptomycin, and 1000 U/ml of homemade leukaemia inhibitory factor (LIF).

Immortalized Mouse embryonic fibroblasts (MEFs) were cultured in KO-DMEM medium (Gibco) plus 10% FCS, non-essential amino acids (NEAA) (Gibco), 2mM L-glutamine, 50 µM 2-mercaptoethanol, 10 µg/ml Penicillin. For the experiments the cells were used between passage P8-P12. The cells were obtained from the laboratory of Professor Brockdorff.

Immortalized Human embryonic fibroblasts were cultured in KO-DMEM medium (Gibco) plus 10% FCS, non-essential amino acids (NEAA) (Gibco), 2mM L-glutamine, 50 µM 2-mercaptoethanol, 10 µg/ml Penicillin. The cells were obtained from Lonza and immortalized using TERT.

Lymphoblastoid cells were cultured in RPMI medium (Gibco) supplemented with 10% delta FCS, 2mM L-glutamine, 50 µM 2-mercaptoethanol, 10 µg/ml Penicillin and Streptomycin. Kind gift of Dr Karen Cheung.

Abelson transformed Oct4-GFP (GOF18ΔPE) Puromycin-resistant mouse B cells were cultured in RPMI medium (Gibco) supplemented with 10% delta FCS, 2mM L-glutamine, 10 µg/ml Penicillin and Streptomycin. Those cells were a kind gift of Prof. A. Surani.

EBV-transformed Puromycin-resistant human B cells were cultured in RPMI medium (Gibco) supplemented with 10% delta FCS, 2mM L-glutamine, 50 µM 2-mercaptoethanol, 10 µg/ml Penicillin and Streptomycin.

Mouse haploid ES cells were grown on 0.1% gelatin (Sigma)-coated surfaces. H129 and AN3-12 cells were cultured in 2i + LIF medium containing N2B27 medium (NDiff 227; StemCells Inc), 3uM CHIR99021 (ReagentsDirect), 0.1mM PD0325901 (ReagentsDirect), 5ml of 7.5% BSA fraction V solution (Life technologies), 10 µg/ml Penicillin and Streptomycin and 1000 U/ml of homemade leukaemia inhibitory factor (LIF). The cells were obtained from Prof. A. Wutz.

Pre B cells Rad21$^{TEV/TEV}$ cells were cultured in IMDM medium (Gibco) supplemented with 10% delta FCS, 2mM L-glutamine, 50 µM 2-mercaptoethanol, 10 µg/ml Penicillin and Streptomycin. Those cells were derived and immortalized in my host laboratory.

2.2 Hybrids experiment:

Hybrids were generated by fusing mouse pluripotent cells (mESCs E14tg2a mcherry puromycin resistant) and mouse embryonic fibroblast in 1:1 ratio using 50% polyethylene glycol (PEG 1500) (Roche Diagnostics) as described in Pereira and Fisher, 2009. Briefly, cells were harvested, mixed in an appropriate ratio and washed twice in serum-free DMEM. The supernatant was completely removed and typically 1ml of PEG (37°C) was added to the pellet of cells over 60 seconds and incubated at 37°C for 90 seconds with constant stirring. Then, 1.4 ml of serum-free DMEM were carefully added over a period of 4 minutes, followed by 10 ml of serum-free DMEM and incubation at 37°C for 3 minutes. After centrifugation (1350 rpm, 5 minutes), the pellet was allowed to swell in complete mES medium for 3 minutes. Cell mixtures were then resuspended and cultured under conditions promoting the maintenance of undifferentiated mESC.18h after fusion, puromycin (1.5µg/ml) and HAT were added to the media to remove the unfused cells.

2.3 Taqman assay:

RNA was extracted using the RNeasy mini Kit (Qiagen). Residual DNA was removed with DNA-free Kit (Ambion). 1µg of extracted RNA was used for cDNA synthesis with the Superscript First-Strand Synthesis system (Qiagen).

DNA extraction was done by phenol chlorophorm procedure. Briefly, cells were incubated overnight at 55 degree Celsius with proteinase K (200 µg/ml) and lysis buffer containing Sodium chloride, Tris, EDTA, Sarcosyl. Same volume of Phenol solution (Sigma) was added after the overnight incubation. Samples were spun for 5 min at maximum speed. The aqueous phase was collected. The same procedure was done with phenol chlorophorm solution (Sigma) and chlorophorm alone.

DNA was used to confirm the presence of both alleles within the genome by Taqman assay. RNA was used to check the biallelic expression of X-linked genes. Allele-specific Taqman probes were used and custom design for the following SNPs (table1). Taqman PCR was done with

Taqman Universal Master Mix (Applied Biosystem). The assay was done according to the manufacturer instruction. Data analysis was performed using the following formula (NRFU1)/(NRFU1+NRFU2) where NRFU1 and 2 stands for Normalized Relative Fluorescent Unit. Fluorescence 1 corresponds to the FAM fluorescent dye and the second fluorescent correspond to the VIC fluorochrome. Each fluorescent dye corresponds to a specific allele.

2.4 RT-PCR analysis:

RNA extraction and cDNA synthesis was done as before. RT-PCR was performed using Phusion enzyme (ThermoFisher) according to the manufacturer instruction with different sets of primers (Table 2).

2.5 Purifying the haploid G1 cell population by Fluorescence-Activated Cell Sorter (FACS):

Prior to staining, the cells were harvested and collected in a tube to perform the Hoechst staining. After centrifugation the cells were resuspended in 2i media containing 15ug/ml of Hoechst 33342. The tube containing the cells was then place inside an incubator for 20 minutes at 37 degre in the dark. Before sorting, cells were filtered and placed on ice. The haploid G1 cell population and the diploid G2 cell population were collected in 15ml falcon tube containing 2i media complemented with Gentamycin to avoid contamination. After sorting cells were, centrifuged and resuspended in 2i media and plated on gelatin-coated plates. The sorts were performed on a BD Fusion containing a 355 nm laser.

2.6 Haploid ES cells fusion: hybrids

Hybrids were generated by fusing mouse Haploid pluripotent stem cells (H129) and Oct4-GFP puromycin-resistant mouse B cells in 1:1 ratio using 50% polyethylene glycol (PEG 1500) (Roche

Diagnostics) as described in Pereira and Fisher, 2008. Briefly, cells were harvested, mixed in an appropriate ratio and washed twice in serum-free DMEM. The supernatant was completely removed and typically 350ul of PEG (37°C) was added to the pellet of cells over 60 seconds and incubated at 37°C for 90 seconds with constant stirring. Then, 4ml of serum-free DMEM were added drop by drop over a period of 4 minutes, followed by 10 ml of serum-free DMEM and incubation at 37°C for 3 minutes. After centrifugation (1350 rpm, 5 minutes), the pellet was allowed to swell in complete mouse haploid ES cells media. Cell mixtures were then resuspended and cultured in 2i media condition. 18hours after fusion puromycin (1.5µg/ml) was added to the media to select for fused cells.

2.7 Haploid ES cells fusion: heterokaryons

Heterokaryon were generated by fusing mouse Haploid pluripotent stem cells (H129) and puromycin-resistant human B cells in 1:1 ratio using 50% polyethylene glycol (PEG 1500) (Roche Diagnostics) as described in Pereira and Fisher, 2009. Briefly, cells were harvested, mixed in an appropriate ratio and washed twice in serum-free DMEM. The supernatant was completely removed and typically 350ul of PEG (37°C) was added to the pellet of cells over 60 seconds and incubated at 37°C for 90 seconds with constant stirring. Then, 4ml of serum-free DMEM were added drop by drop over a period of 4 minutes, followed by 10 ml of serum-free DMEM and incubation at 37°C for 3 minutes. After centrifugation (1350 rpm, 5 minutes), the pellet was allowed to swell in complete mouse haploid ES cells media. Cell mixtures were then resuspended and cultured in 2i media condition. 18hours after fusion puromycin (1.5µg/ml) and Ouabain (10^{-5} M) was added to the media to select for fused cells. 3 days after fusion the remaining cells were collected for gene expression analysis.

2.8 Western Blot:

Protein quantification:

Fluorescent Western blots analysis was performed on proteins extracted from the whole cells. Briefly, cells were incubated at 95^0C in Laemmli sample buffer for 5 minutes and stopped on ice afterwards. For the total protein quantification, Pierce BCA protein assay kit (ThermoFisher) was used according to the manufacturer's instruction. The reading was performed using a spectrometer with a 548nm wavelength. Serial dilution of bovine serum albumin was used as a calibration curve to calculate the final concentration of proteins.

Western blot analysis:

Sodium dodecyl sulfate-polyacrylamide gel electrophoresis (SDS-PAGE) was composed of 4% stacking gel (4% (w/v) acrylamide, 0.125M Tris pH=6.8, 0.1% (w/v) SDS, 0.1% ammonium persulphate and 0.1% (v/v) N,N,N',N'-tetramethylenediamide) and 12% of running gel (12% (w/w) acrylamide, 0.4M Tris pH=8.8, 0.1 %(w/v) SDS, 0.1% ammonium persulphate and 0.1% (v/v) N,N,N',N'-tetramethylenediamide). For Western blot of sorted chromosomes, pre-cast gels (Biorad) were used. The running buffer was composed of 1.5% (w/v) Tris, 7.2% glycine, 0.5% (w/v) SDS. 8ul of the total protein extract was loaded in the gel and run for 1hour at 20 Volt and 180 Amper. The blotting was performed by semi-dry using PVDF membrane (Millipore) and ransfer buffer (Trizma base 48mM, 0.037% of SDS, Methanol 20% (v/v), Glycine 39mM) to transfer the proteins onto the membrane. Membranes were blocked for an hour at room temperature with gentle shaking in blocking buffer (5% (w/v) milk powder (Marvel), 1.2g/L Tris pH= 7.4, 7.5g/L NaCl) directly followed by an overnight primary antibody incubation (diluted in blocking buffer) at 4^0C. 3 washes were done the next day at room temperature for 5 minutes with TBS-Tween (1.2g/L Tris bas pH=7.4, 8.75g/L NaCl, 1ml/L Tween 20). Secondary fluorescent antibodies (1:10000, Life Science) were incubated for 1hour at room temperature to visualize the proteins with Odyssey imaging system (LI-COR).

2.9 Quantitative RT-PCR analysis:

Cells were pellet and the dry pellet was snap frozen in liquid nitrogen and kept at -80^{o}C until RNA extraction. The RNA extraction was carried using RNeasy plus mini kit (Qiagen), according to the manufacturer's instruction. cDNA synthesis was done using Superscript III Reverse Transcriptase (invitrogen). Briefly, to the RNA was added 1ul of oligo(dT) (50uM), 1ul of random primer (0.5ul/ul) 1ul of dNTP mix (10mM each dATP, dGTP, dCTP, dTTP). The reaction was completed with RNAse free water to obtain a final volume of 13ul. The solution was incubated for 5 minutes at 65^{o}C in a thermo cycler followed by 1 minute of incubation on ice. 5X First strand buffer (4ul), 1ul of DTT (1M), 1ul of RNAseOUT (40 units/ul) and 1ul of Superscript III RT (200 units/ul) was added to the RNA solution. The reaction was performed by incubating the RNA at 25^{0}C for 5 minutes followed by 50 minutes at 50^{0}C. The reaction was stopped by incubating it at 70^{0}C for 15 minutes.

The qPCR reaction was performed using the SybrMix (Qiagen) and primers (10uM) that are specific for the RNA of interest (see Table 2-3). The amplification was achieved using the following program: 95^{0}C for 15 minutes, 94^{0}C for 15 seconds, 60^{0}C for 30 seconds, followed by 72^{0}C for 30 seconds. The last three steps were repeated 39 times. The genes expression analysis was done using the deltaCt formula.

2.10 Cell cycle Profile:

Cells were collected and fixed with ice cold 70% ethanol. Prior to staining the cells were washed twice in PBS and resuspended in staining buffer (0.05mg/mg of Propidium Iodine, 0.05% of NP-40, 1mg/ml of RNAse A completed with PBS). The samples were then incubated at room temperature for 10 minutes in the dark and then for 20 minutes on ice in the dark. The cell cycle profile was then done using an LSR II. Data analysis was done using the FlowJo software.

.

2.11 Alkaline phosphatase staining:

Alkine phosphatase (AP) staining was performed on hybrids cells according to the manufacturer's instruction. To compare the number of AP positive colonies in the haploids ES cells experiments the same number of cells was initially plated after fusion (2 millions of cells per plates). The staining was performed 10 days after fusion and the colonies were counted by hand.

2.12 Generation of haploid ES overexpressing Nanog:

Nanog overexpressing haploid ES cell line was generated by transfecting 1ug of PB-CAG-mNanog-pAPGK- hygromycin plasmid and 2ug of PBase-expresssion pCAG-PBase plasmid using electroporation (Amaxa, Lonza). Transfected cells were selected for 10 days by adding hygromycin (200ug/ml) to the 2i media.

2.13 DNA FISH:

The cells were incubated for 4 to 6 hours with demecolcine (Sigma) at 0.01ug/ml. The cells were collected using trypsin under close monitoring then pelleted and washed once with PBS. Cells were then fixed with cold fixative solution (methanol acetic acid with a ratio of 3:1) and dropped on a glass slide previously incubated with the fixative solution. The slides were then aged for 3 to 4 days in a vacuum sealed desiccator. The slides were treated with RNAseA (Invitrogen) DNAse-free for 1h30 min at 37 C, washed and dehydrated at room temperature then air dried for 10 minutes. Then the slides were denaturated using 70% of formamide for 3 minutes at 70 C. The reaction is then quenched on ice with various concentration of ethanol (70%, 90%, 95%, 100%) and dry for 10 minutes. The probe was prepared according to the manufacturer's instruction for the nick translation. The slides were hybridized overnight at 37

C by using 5ul of the probes with 5ul of hybridization buffer. The day after the slides were washed and mounted with Vectashield containing DAPI.

2.14 Chromosomes Isolation:

The cells were treated with demecolcine (Sigma) at 10ug/ml when they reached 70 to 80% confluent. Depending on the cell type cells were incubated for a period of time ranging from 4 hours to 16hrs (see table XX). For cells growing in suspension, cells were harvested and centrifuge at 1500 RPM for 5 minutes at room temperature. For adherent cells, mitotic cells were collected by mitotic shake off and spun down at 1500 RPM. After centrifugation, cells were incubated with 10 ml of hypotonic solution (75mM KCl, 0.5mM spermidine, 0.2mM spermine and 0.01M $MgSO_4$, pH=8) for 15 minutes at room temperature. The cells were then resuspended in 3 ml PolyAmine Buffer (PAB) (containing 15 mM T ris, 2 mMEDTA,0.5mMEGTA,80mMKCl,3mMdithiothreitol,0.25%Triton X-100, 0.2 mM spermine, 0.5 mM spermidine, pH=7.5) and incubated for 15 minutes on ice. The chromosomes were released from the cells by vortexing them for 40 seconds at maximum speed. To verify the efficiency of the chromosomes extraction, the preparation was mixed with Propidium Iodine (PI) and checked under an epifluorescence microscope for isolated mitotic chromosomes. If the amount of chromosome obtained is not sufficient enough cells can be vortex again. To remove the debris and the non-mitotic cells, the preparation was spin down at 1200 rpm for 3 minutes at 4 degrees. The supernatant was collected and filtered using a 20 um mesh size filter. The chromosomes were then stained overnight at 4 degre with chromomycin A3 (50ug/ml), Hoechst (5ug/ml) and 10mM of $MgSO_4$, Sodium citrate (10mM) and Sodium sulphite (25mM) were also added to the solution at least 2 hours before sorting. Sorted chromosomes were collected in Eppendorf tube in PAB buffer for further image analysis or in fixative solution (methanol: acetic acid) for FISH or in empty tubes to use them as a DNA template. FAC sorting was performed on a BD influx with 200mW 447nm laser and 100mW 355nm laser with a 75um nozzle.

2.15 DOP-PCR:

Generation of chromosome painting was done by Degenerated Oligonucleotide PCR (DOP-PCR). This technique consists of using sorted chromosomes as a template to create chromosomes paint. Chromosomes were sorted in empty tubes. The sorted chromosomes were then used as DNA template for a first PCR. The PCR mix contained 1X buffer, MgCl2 (2mM), 2ul dNTP (0.2mM), mouse random primers (2uM), 2.5 U Taq-polymerase (Biogen), 1ul of Chromosomes-specific DNA completed to 50ul with nuclease-free water and the following program was used 5 minutes at 95^0C as the initial step followed by 4 cycles of 1 minute at 95^0C, 1.5 minutes at 95^0C, 1.5 minutes at 30^0C, 3 minutes transition from 30^0C to 72^0C and 3 minutes extension at 72^0C, then 34 cycles of 95^0C, 1.5 minutes at 62^0C and 3 minutes at 72^0C with an addition of 1 second per cycle to the extension step and finally 10 minutes at 72^0C. To verify whether the PCR amplification worked 5ul of the PCR was run on an agarose gel (1%).

Another DOP-PCR was used to incorporate fluorescent dUTP to the chromosome template. The reaction mix contained the following reagents: 1X PCR buffer $MgCl_2$ (2mM), AGC (0.2mM), dTTP (0.15mM), fluorescently labelled dUTP (0.05mM), mouse random primer (2uM), 1U of Taq-Polymerase (Biotaq). The second PCR run is more stringent compared to the first one and uses the following program: an initial step of 5 minutes at 94^0C followed by 35 cycles containing 1 minute at 94^0C, 1 minute at 56^0C and 4 minutes at 72^0C and the final step of 5 minutes at 72^0C. the PCR amplification was then verified on an agarose gel (1% w/v).

Ethanol precipitation and preparation of chromosome paint:

To purify fluorescently labelled DNA from the PCR reaction, ethanol precipitation was used. For 3 ul of the PCR reaction, 10ul of mouse DNA cot-1, 5ul of salmon sperm, 2ul of NaOAc and 50 ul of 100% ethanol was added to the reaction. The ethanol precipitation tube was left overnight at -20^0C and centrifuged at 4^0C for 30 minutes at 18.890g. The supernatant was discarded and the pellet was washed with 400ul of 70% (v/v) ethanol. Another centrifugation step was done for 10 minutes at 4^0C at 18.890g. The chromosome paints were then dried at 42^0C and resuspended in 100% (v/v) deionized formamide and left at 37^0C in a thermoshaker for 45 minutes. The same volume of hybridization buffer was added to the probes. The prepared chromosome paint was then mixed with the commercially available one and that

mixed was incubated overnight at 37^0C on prepared slides (see DNA FISH in materials and methods).

2.16 Immunofluorescence:

Immunofluorescence on isolated chromosome:

After sorting the mouse chromosome 19 in PAB, chromosomes were cytospined (Shandon Cytospin 3) onto a glass slide at 1300 rpm for 10 minutes. The chromosomes were then fixed with 1% PFA (paraformaldehyde) for 15 minutes at room temperature and washed 3 times in PBS. Blocking was then performed at room temperature in a humid chamber for 30 min using blocking buffer (3% (v/v) goat serum, BSA), and incubated in a humid chamber overnight at 4^0C with primary antibody diluted in blocking buffer. The next day, the slides were washed 3 times for 5 minutes in washing buffer (PBS, 0.2 % (w/v) BSA, 0.05% (v/v) Tween). After the washes, the chromosomes were incubated with secondary fluorescent antibody (Molecular probes) diluted in blocking buffer (1:400) for 30 to 45 minutes in a humid chamber at room temperature. After 3 washed in washing buffer, the slides were mounted using mounting media containing DAPI (Vectashield, Vectorlabs). Pictures were acquired using Leica SP5 system or Structured Illumination Microscopy (SIM) Zeiss Elyra microscope.

2.17 TEV-Protease cleavage:

Mitotic chromosomes were incubated overnight after sorting in PAB buffer supplemented with Ac TEV protease (10U/µl), 20X TEV Buffer and 0.1M DTT. Briefly to 140ul of sorted chromosomes 19 was added 7.5ul of 20X TEV buffer, 1.5ul of DTT and 1ul of TEV-protease. The samples were left overnight at 4 degree rotating. The samples were then collected from western Blot (denaturation of protein by boiling) or for cryo-EM (plunge freezing).

2.18 Cryo- Electron Microscopy:

This part has been performed by a collaborator Tanmay Bharat.

Sample preparation:

Chromosomes samples for cryo-EM were prepared by pipetting 2.5 µl of chromosomes in solution onto a Quantifoil Cu/Rh 200 mesh grids (R3.5/1 for chromosomal tomography). After removing the excess of liquid, the grid was then plunge frozen into liquid ethane in a Vitrobot Mark IV (FEI). The frozen grids were then stored in liquid nitrogen.

Image acquisition:

Data collection for two dimension images was performed using FEI Krios microscope and operated at 300 kV. Data were collected using EPU software on a Falcon II direct electron detector. Exposure time was 1 s and the total dose of electrons per square ångström for each exposure was between 25 to 32. An underfocus of 1 to 6 µm was used to collect images. For tomography, FEI Krios was used with the addition of a Quantum energy filter (Gatan) using SerialEM software27. The detector used was K2 direct electron detector used in counting mode. Tilt series were performed with a rotation of ±60° with 1° tilt increment at 4-12 µm underfocus. The electron dose applied for over the full series was 120 electrons per square ångström.

Image processing and data analysis:

For the reconstruction of tomogram, the images were aligned with IMOD software. The three dimensional reconstruction was done with the SIRT algorithm in Tomo3D software. UCSF Chimera was used to visualize the reconstructed chromosomes. Additional analysis was performed using FIJI software. Heatmap was generated by PRISM.

Table 2-1: list of SNPs used for allele specific assay

Hprt
rs30419453

Table 2-2: Human gene-specific primers

Human gene	sequence 5'- 3'
GAPDH F	TCTGCTCCTCCTGTTCGACA
GAPDH R	AAAAGCAGCCCTGGTGACC
OCT4 F	TCGAGAACCGAGTGAGAGGC
OCT4 R	CACACTCGGACCACATCCTTC
NANOG F	CCAACATCCTGAACCTCAGCTAC
NANOG R	GCCTTCTGCGTCACACCATT
CRIPTO F	AGAAGTGTTCCCTGTGTAAATGCTG
CRIPTO R	CACGAGGTGCTCATCCATCA

Table 2-3: List of antibodies

Primary Antibody	Manufacturer	Dilution
Oct4	Goat, Santa Cruz, WB, sc-8635	1:2000
Nanog	Rabbit, Cosmo Bio, WB, RCAB001P	1:1000
Lamin B	Goat, Santa Cruz, WB, sc 6217	1:10000
CENP-A	Goat, Cell signaling technology,IF, 2186	1:800
ESRRB	Mouse, Perseus protein, WB	1:1000
c-Myc	Mouse, Santa Cruz, WB	1:1000
Histone H3	Rabbit, Abcam, WB	1:10000

Table 2-4: Mouse gene-specific primers

Mouse gene	Sequence 5'-3'
Oct4 F	GGCGTTCTCTTTGGAAAGGTGTTC
Oct4 R	CTCGAACCACATCCTTCTCT
Nanog F	AGGGTCTGCTACTGAGATGCTCTG
Nanog R	CAACCACTGGTTTTTCTGCCACCG
Rex1 F	GCCCTCGACAGACTGACCCTAA
Rex1 R	CTTCCTCAGGGCGGTTTTACCC
Brachyury F	TGCTGCCTGTGAGTCATA
Brachyury R	ACAAGAGGCTGTAGAACATG
Oct4 F	CGTGGAGACTTTGCAGCCTG
Oct4 R	GCTTGGCAAACTGTTCTAGCTCCT
Nanog F	GAACTATTCTTGCTTACAAGGGTCTGC
Nanog R	GCATCTTCTGCTTCCTGGCAA

Chapter 3 : REACTIVATION OF THE INACTIVE X CHROMOSOMES BY CELL FUSION MEDIATED REPROGRAMMING TOWARDS PLURIPOTENCY

3.1 Introduction

X chromosome inactivation (XCI) is a long non-coding RNA-mediated process that encompasses synchronous epigenetic mechanisms including DNA methylation and histone modifications (Chow and Heard, 2009; Panning et al., 1997). XCI ensures dosage compensation in mammals, and has been widely studied to decipher the roles of epigenetic mechanisms that lead to chromosomal silencing. With the emergence of iPS reprogramming, several studies have recently focused on the mechanisms and kinetics that underlie Xi reactivation (Maherali et al., 2007; Pasque et al., 2014). A deep understanding of the Xi reactivation process may lead to potential clinical applications of X-linked gene diseases.

In my host laboratory, a study of X-chromosome reactivation in human somatic cells during interspecies cell-fusion mediated reprogramming has shown re-expression of human pluripotency factors and loss of XIST and H3K27me3 from the Xi (Cantone et al., 2016). Allele-specific expression analysis has demonstrated that only some X-linked genes were reactivated during reprogramming and current studies in my host laboratory are focused on elucidating the reasons behind this selective X-linked gene reactivation. In both humans and mice, genes with low levels of repressive H3K9me3 and H3K27me3 have a higher probability of escaping XCI (Marks et al., 2009). Cantone et al., 2017, showed that treatment with 5-deoxy azacytidine (5-AzaC), a DNA demethylating agent, does not affect Xi reactivation prior to reprogramming towards pluripotency. However, a subset of X-linked genes previously resistant to Xi reactivation, was reactivated upon 5-azaC treatment combined with cell-fusion mediated reprogramming (Figure 3-1.B, orange) (Cantone et al., 2017). ChIP data revealed that this subset of genes was predominantly found in a H3K27me3 depleted chromatin region enriched for H3K9m3 (Figure 3-1.C, orange).

Due to their short life span, interspecies heterokaryons are useful to study early events of reprogramming and Xi reactivation. At day 6 after fusion some X-linked genes are reactivated upon reprogramming towards pluripotency. At the later time point, more X-linked genes could be reactivated. As an alternative, I will study the kinetics of Xi reactivation during reprogramming of female mouse fibroblasts upon fusion with mouse ES cells. This type of fusion generates stable tetraploid hybrids that can be monitored and expanded for a longer period of time (> 31 days after fusion). This will allow me to determine whether some X-linked genes are reactivated earlier than other X-linked genes and determine the epigenetics marks such as histone modifications or DNA methylation associated with early and late X-linked genes reactivation.

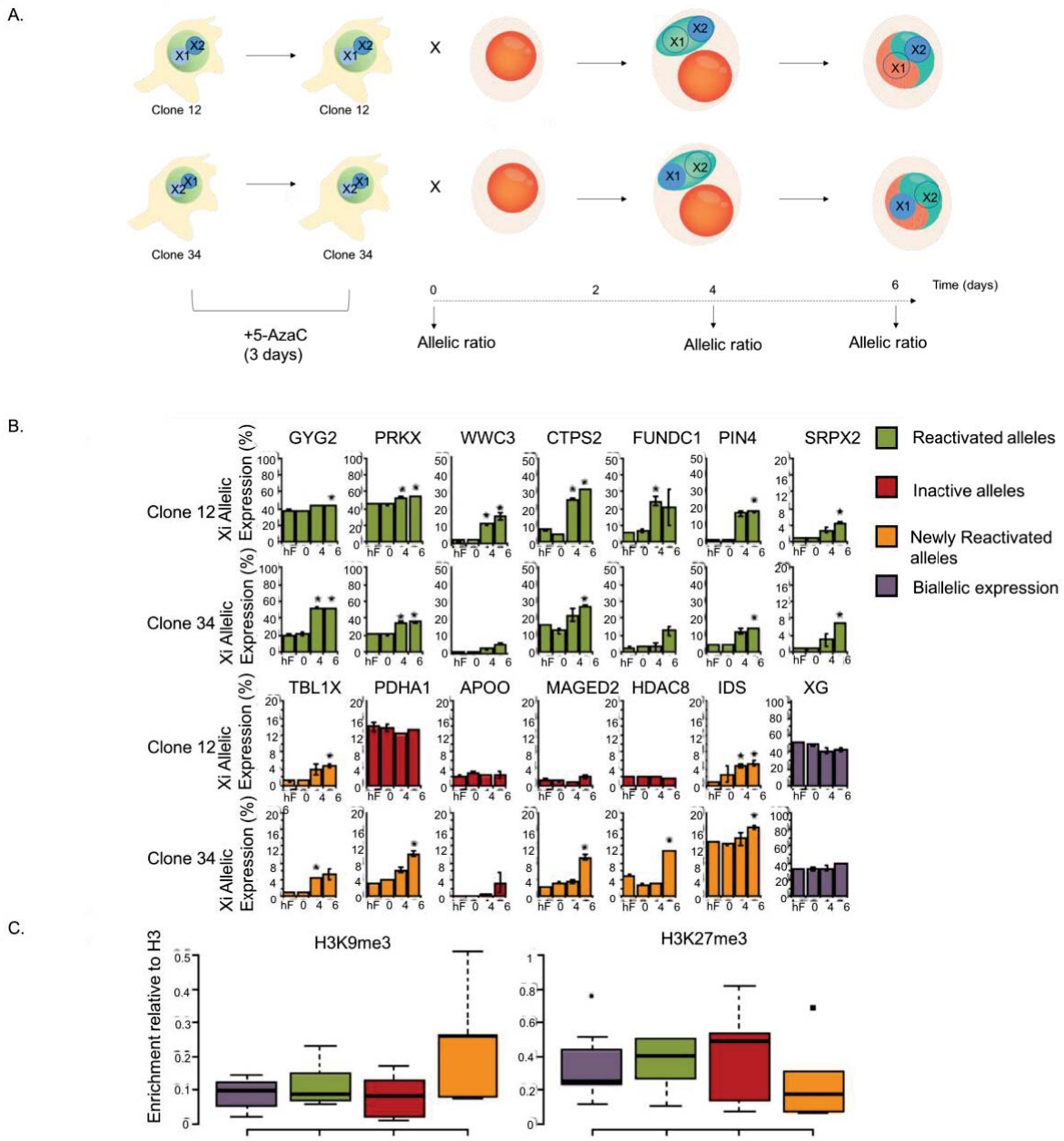

Figure 3-1:Demethylation of DNA induces Xi reactivation upon reprogramming towards pluripotency at loci within high H3K9me3 and low H3K27me3.

(A) Schematic representation of the experimental system. Human Fibroblasts (hF) (Clone 12 and 34) were cultured in the presence of 5-AzaC for three days prior to fusion with mES cells. Both clones were derived from the same original population and where picked because each of them has a different inactive X chromosome. The drug was removed after fusion and allelic expression of several X-linked genes was assessed at day 0, 4 and 6 after fusion. (B) Histograms representing X-linked genes allelic expression during reprogramming after 5-AzaC treatment at different time points. Allelic expressions are color coded relative to their expression pattern. Green plots represent the X-linked genes that were reactivated only after reprogramming whereas the orange graphs correspond to reactivation of allele that were induced by 5-AzaC combined with reprogramming. Red histograms represent allele refractive to both reprogramming and drug treatment. Violet are the biallelically expressed X-linked genes. Asterix mark significant changes vs day 0 ($p \leq 0.05$, two-sided t-test). Taqman probes was used to measure allelic expression. Data represent the mean of two independent experiments ± SD. (C) Box plots showing enrichment of H3K9me3 and H3K27me3 for clone 12 and clone 34. ChIP was performed in two independent experiments. Figure adapted from Cantone et al., 2017

3.2 Generation of pluripotent hybrid cells from cell fusion between MEFs and mouse ES cells

As described in the general introduction, Xi reactivation can take place *in vitro* via various epigenetic reprogramming systems (iPS, nuclear transfer and cell fusion). Cell fusion mediated reprogramming is faster and more efficient than iPS generation (Hasegawa et al., 2010). To study the extent of Xi reactivation, particularly at later time points, I am using intra-species cell fusion. Accordingly, I am fusing male mouse ES cells (XY) with female Mouse Embryonic Fibroblasts (MEFs) (XiXa) in the presence of Poly Ethylene Glycol (PEG) with a 1 to 1 ratio to generate pluripotent cells that will then allow me to study the kinetics of Xi reactivation. Fusing two cells from the same species give rise to intra-species heterokaryons, which are cells that possess two nuclei; one from mouse ES cell and one from the fibroblast. Between day 3 and day 6 after fusion, intra-species heterokaryons fuse their nuclei, giving rise to a tetraploid nucleus, which, in my system, contains three X chromosomes: two from the female MEFs and one from male ES cells. Hybrid cells are able to undergo mitosis, and therefore can be maintained in culture for a long period of time. Upon fusion, hybrid cells are enriched upon drug selection (HAT and puromycin). The mouse ES cell line (E14tg2A) is sensitive to HAT and resistant to puromycin whereas MEFs do not possess any antibiotic resistance and are not sensitive to HAT. Several hybrid clones are isolated 10 days after fusion and expanded for the analysis of Xi reactivation (Figure 3-2).

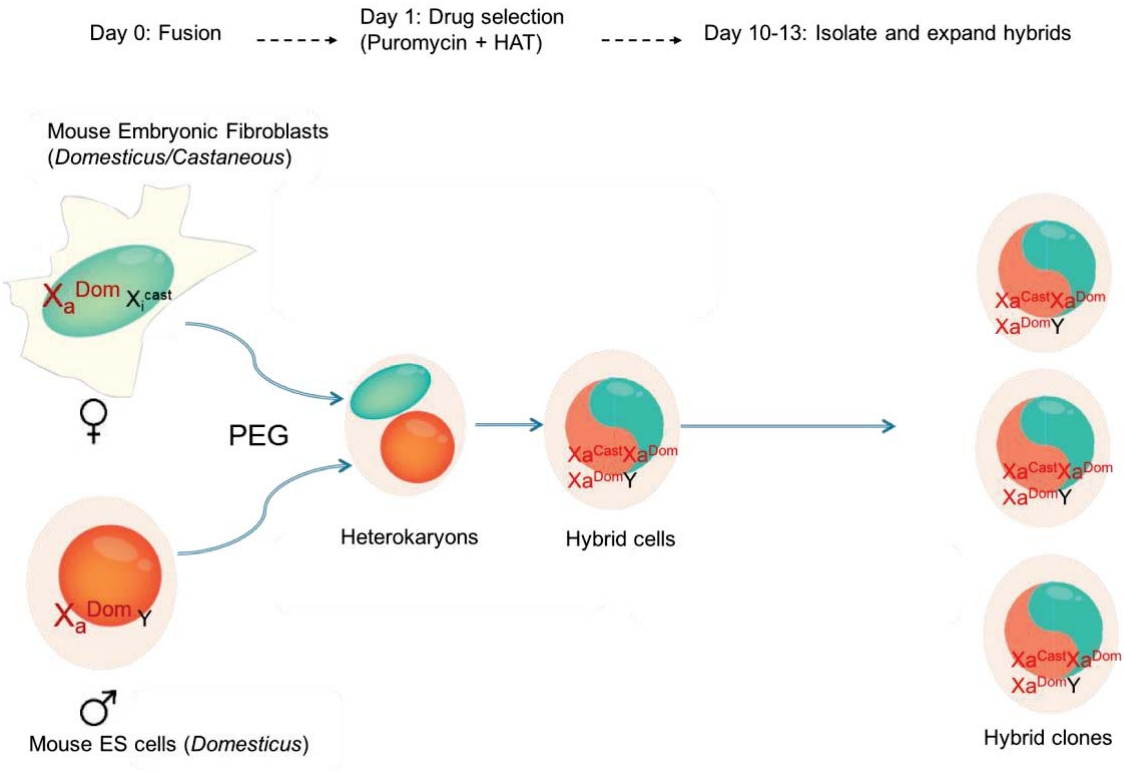

Figure 3-2: Generation of pluripotent hybrids cells between male ES cells and MEFs mediated by cell fusion.

Schematic representation of cell fusion between male mES cells (XY) and female MEFs (XX). Cell fusion is promoted by PEG, the day after fusion drugs were added to enrich for fused cells. Between day 10 and day 13 after fusion, hybrid clones were hand-picked based on their ES cell-like morphology.

To visualize X chromosomes in the parental male ES cells (XY), MEFs (XX) and in fused hybrid clones (hybrid one and two), a labeled probe for the X-linked gene *Hprt* was used and mitotic chromosomes preparations were analyzed using DNA FISH. Samples of male ES cells showed a normal karyotype with 39 chromosomes in which a single *Hprt* signal (red) was evident (as exemplified in Figure 3-3.A). In both hybrid clones we anticipated that each cell should contain three *Hprt* signals corresponding to the X chromosomes inherited from male and female parents. However, in most hybrid cells from clone 1 (70 %) I detected two *Hprt* signals (red, Figure 3-3.B) suggesting that these cells may not have preserved their chromosomal content and had lost one of their X chromosomes. Consistent with this, a close inspection of the karyotype of hybrid cells revealed a sub-tetraploid chromosome content (average chromosome number = 65±10) as compared with, for example, diploid ES cells (average chromosomes number= 39 ±1) (Figure 3-3.C). As in only 10% of hybrid cells the anticipated

three X-chromosome signals seen (Figure 3-3.D) these data suggest that hybrid cells are not karyotypically stable in culture, as compared to ES cells.

To further confirm the karytopic instabilities of hybrid clones, another hybrid clones (hybrid #2) was analyzed. In hybrid clone #2, the total number of chromosomes indicate a near tetraploid karyotype (average chromosomes number = 87 ± 20) (Figure 3-3.B and C), a number similar to the expected number of chromosomes in tetraploid hybrids (80 chromosomes). However approximately two third of cells (57%) had four X chromosome signals, and one third (31%) had three X chromosomes according to the *hprt* signal (Figure3-3.D). One possible explanation for this result is that one of the two parental cell lines is subject to aneuploidy with an increase in the number of chromosomes. Previous studies have shown that fusion between two cells with different number of chromosomes may generate karyotypically instable hybrids. As previously mentioned, male ES cells have 39 chromosomes and one X chromosome, indicating a normal karyotype. A close examination of the female MEFs revealed a total number of 65±10 chromosomes indicating that MEFs are triploid (Figure 3-3.A and C). Detailed analysis of the Hprt DNA signal in MEFs revealed five X chromosomes in 42 % of the cells (Figure 3-3.D). Taken together these data indicates that hybrid clones derived from near triploid MEFs are karyotypically instable and prone to chromosome loss.

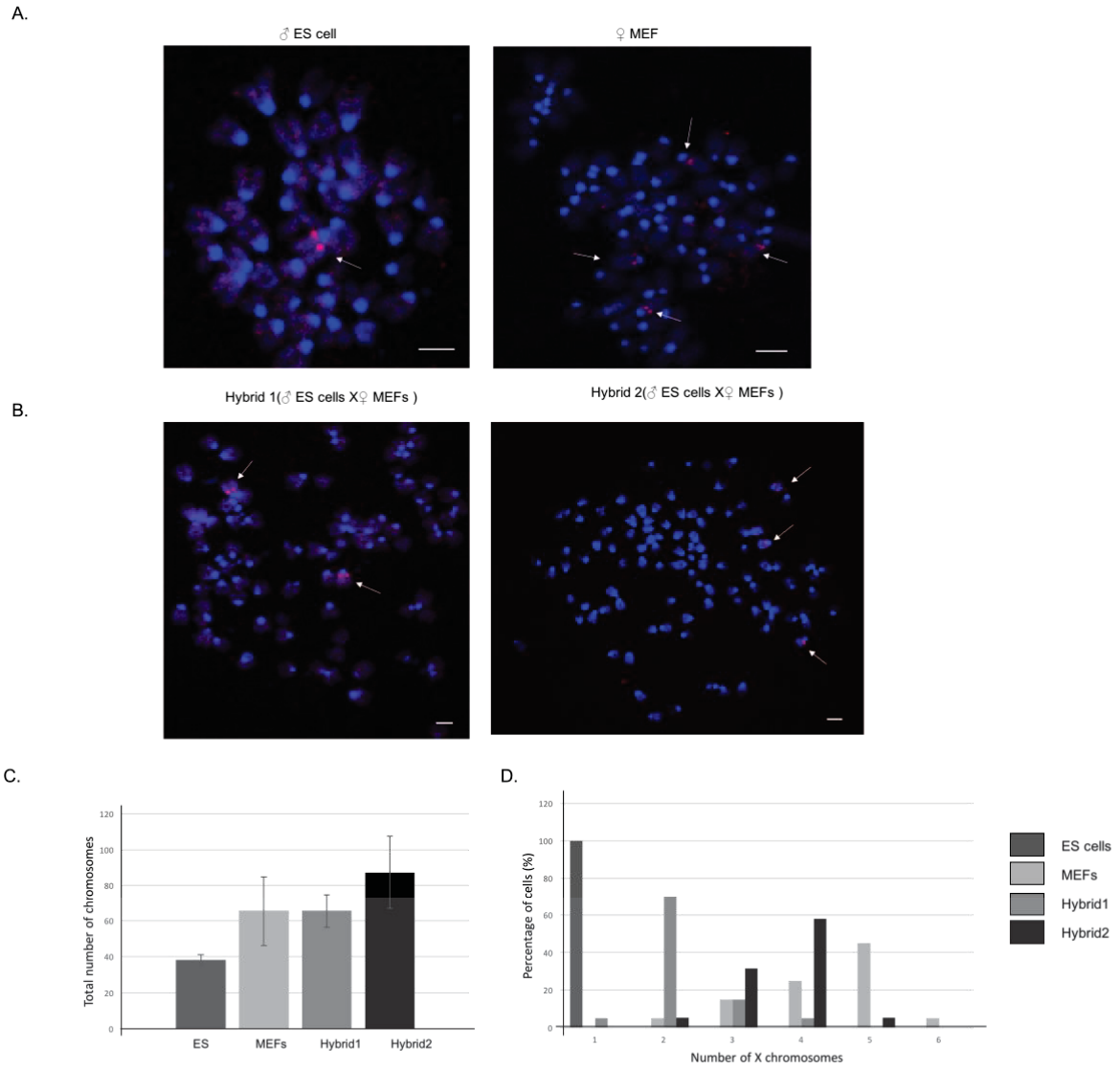

Figure 3-3: Comparison of chromosomes number in ES cells, MEFs and hybrid clones.

(A) Representative images of DNA FISH for Hprt (red signal) on metaphase spread chromosomes for ES cells, MEFs, and both hybrid clones. Scale bar is 10µm. White arrows indicate the localization of Hprt DNA FISH probe. The total number of chromosomes for each cell type was counted (DAPI staining) (B) in the metaphase spread cells and the number of X chromosomes (C) was calculated based on the Hprt probe signal in the DNA FISH. Error bar represents the standard variation with n=30.

Despite their karyotipic instabilities, hybrid clones still possess multiple X chromosomes. Therefore, the Xi from the somatic cells is still susceptible to Xi reactivation upon reprogramming towards pluripotency. Xi reactivation takes place during the transition from differentiated cells towards pluripotency. After cell fusion, hybrid cells are maintained in culture for more than 30 days. To assess their pluripotency state, staining for Alkaline Phosphatase (AP), a cell surface marker associated with pluripotency, was performed. As expected, after fusion hybrid cells are positive for AP and are able to form colonies with a morphology typical of ES cell colonies (Figure 3-4.A, right). To further characterize the pluripotent state of hybrid clones, RT-PCR was performed on ES cells, MEFs and on two hybrid clones to assess the expression of pluripotency-associated factors. Both hybrid clones expressed *Oct4*, *Nanog* and *Rex1* transcripts, detected by RT-PCR (Figure 3-4.B). As expected, male ES cells express also *Oct4*, *Nanog* and *Rex1*, whereas no expression is observed in MEFs. *Oct4*, *Nanog* and *Rex1 expression by hybrids was* at similar levels to ES cells, consistent with the acquisition of pluripotent. Taken together, these data suggest that MEFs are able to generate pluripotent hybrids upon fusion with mES cells.

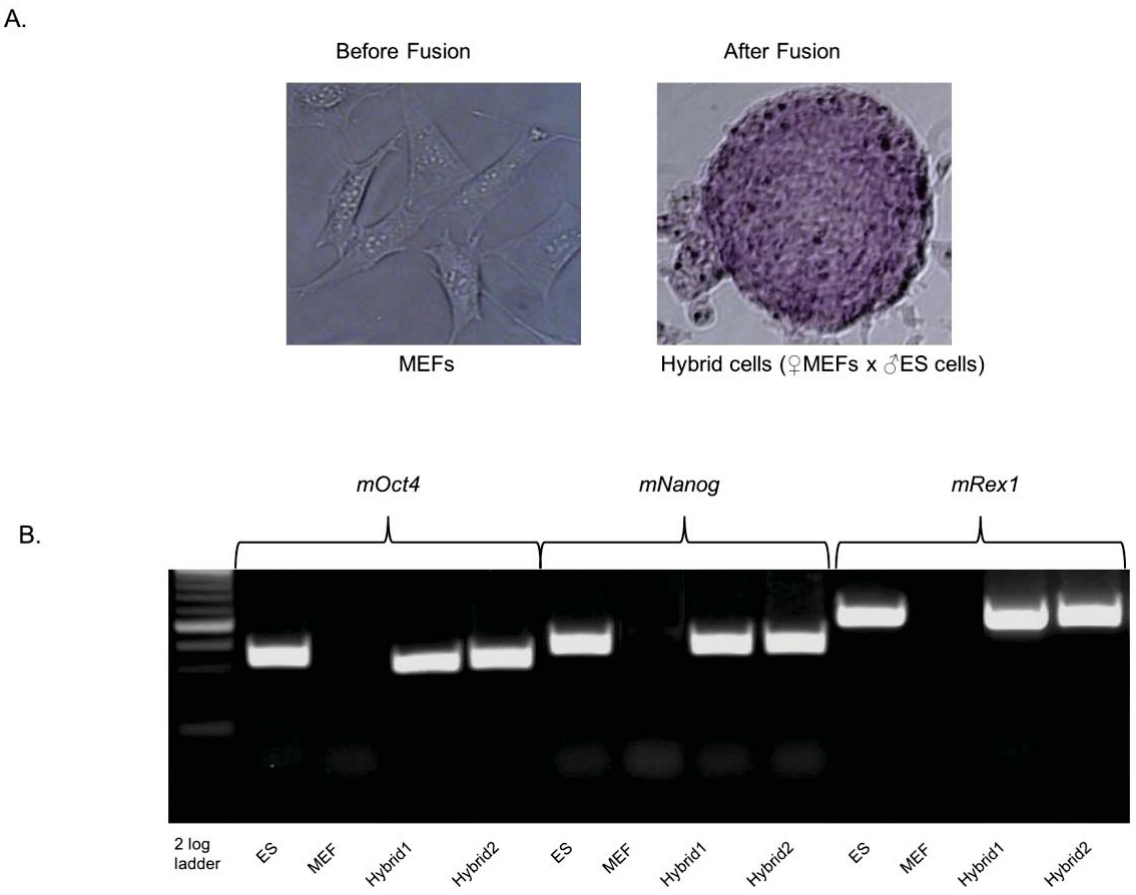

Figure 3-4: Gene expression analysis of Hybrid cells compared to parental cells.

(A) Representative image of MEFs before fusion and hybrid cells after fusion stained with Alkaline Phosphatase (AP) staining (magnification: 40X). (B) Gel electrophoresis of RT-PCR analysis indicating the detection of transcripts of several pluripotency associated genes, including mOct4, mNanog and mRex1 in ES cells, MEFs and hybrid clones.

3.3 Xi reactivation in hybrid clones

To study the origin and activity of the X chromosomes within hybrid cells obtained from a fusion between same species (mouse), Single Nucleotide Polymorphism (SNP) was used to discriminate Xa^{Dom} and Xi^{cast}. MEFs were derived from a cross between *Mus musculus casteneous (cast)* and *Mus musculus domesticus (dom)* (Figure3-5.A). A clonal population that has the inactive X chromosome originated from the *castaneous* allele and the active X chromosome from the *domesticus* allele was selected. The genomic background of those two subspecies has been extensively studied and characterized in the past few years, thus allowing us to use a previously identified allele specific SNP as a marker to detect the origin and expression of X-linked genes (Frazer et al., 2007). In this study, I am focusing on the *Hprt* gene that was reported to be susceptible to Xi reactivation (Grant and Worton, 1989). Male ES cells, used as fusion partners, were derived from the *domesticus* strain. Therefore, in hybrids, expression of X-linked genes from *castaneous* alleles could infer reactivation of a previously silenced MEF originated Xi^{cast} chromosomes.

Using SNP analysis of genomic DNA (gDNA) isolated from cells ahead of fusion, I confirmed that female MEFs contain both *castaneous* (Figure 3-5.B, dark grey) and *domesticus* (Figure 3-3.B, light grey) alleles with an almost one to one ratio (0.4 for the *domesticus* allele and 0.6 for the *castaneous* allele) whereas male ES cells have only the *domesticus* allele for *Hprt*. After fusion, hybrid cells should possess three X chromosomes: one from the *castaneous* allele and two from the *domesticus* allele shifting the allelic ratio to two to one (two domesticus allele and one *castaneous* allele). Here, Hybrid #1 contains both *castaneous* (Figure 3-5.B, dark grey) and *domesticus* (Figure 3-5.B, light grey) alleles. However, the ratio is approximately one to one (0.45 for the *domesticus* allele and 0.55 for the *castaneous* allele) instead of the expected two to three, suggesting that the X chromosome lost was Xa^{Dom}. Surprisingly, Hybrid #2 only has one *domesticus* allele (Figure 3-5.B, dark grey) indicating the loss of Xi^{cast}.

As expected before fusion, the expression of *Hprt* is exclusively from the *domesticus* allele in female MEFs (Figure 3-5.C, dark grey). Expression of *Hprt* in hybrid #2 is from *domesticus* allele,

consistent with the presence of only the *domesticus* allele in hybrid #2, whereas surprisingly hybrid #1 expresses *Hprt* from the *castaneous* allele only (Figure 3-5.C, light grey).

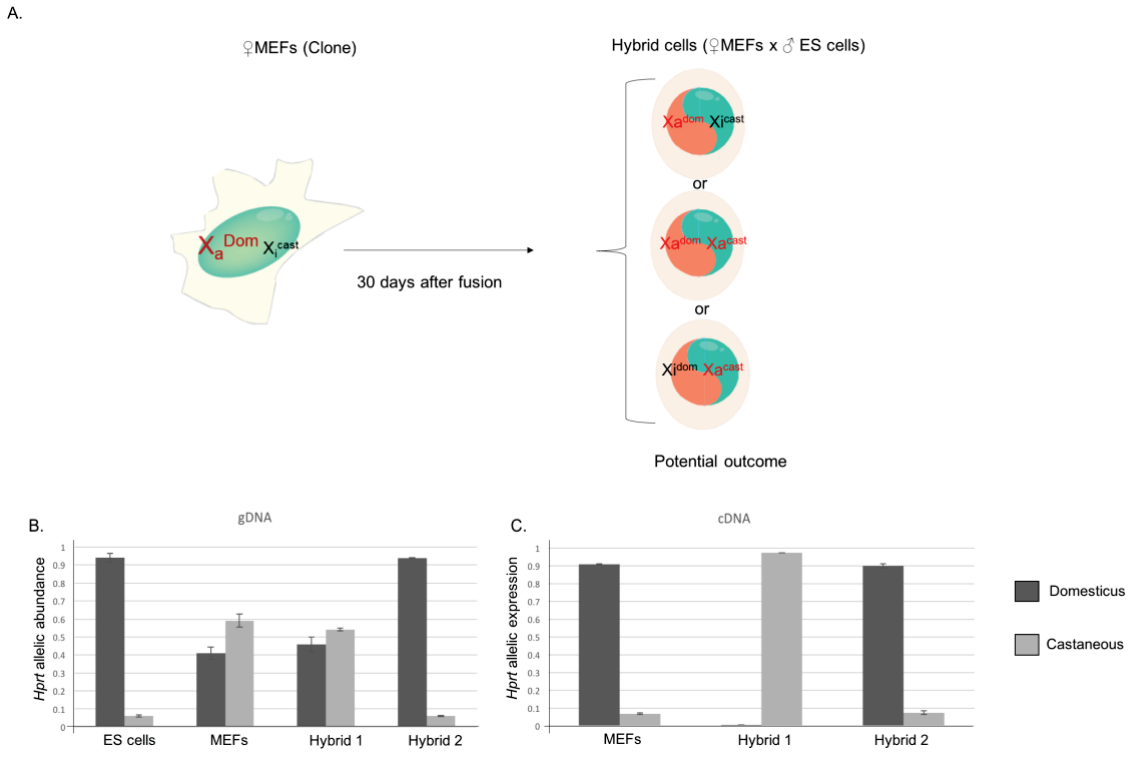

Figure 3-5: Comparison of *Hprt* allelic expression and allelic abundance in female MEFs and hybrid cells.

(A) Schematic representation of the potential allelic expression of Hprt in hybrid clones. Either both X chromosomes are active leading to biallelic expression (*castaneous* in black and *domesticus* in red) of Hprt or one of the two X chromosomes is active leading to monoallelic expression of Hprt from the previously inactive allele (*castaneous* expression) or the already active allele (*domesticus* expression). (B) Genomic analysis of the allelic abundance of *Hprt* in mouse ES cells and MEFs, and hybrid cells. This was performed on genomic DNA to assess the presence of both alleles in hybrid cells. (C) Allele-dependent Hprt expression in hybrid cells and MEFs. Allelic expression and abundance were assessed by Taqman probes specific for SNP detection. The Allelic expression and abundance were calculated based on the following formula: fluorescence from allele of interest/ (fluorescent allele 1+ fluorescent allele 2). Error Bars represent standard deviation with n=2.

Both hybrid clones showed expression of pluripotency associated genes, therefore both X chromosomes should be active, thus the expression of *Hprt* should be biallelic (Xa^{Dom} Xa^{Cast}) (Figure 3-5.A). Hybrid clone #1 results suggests a reactivation of Xi^{Cast} followed by an inactivation of Xa^{Dom}. Since Xi phenomenon happens during differentiation, one hypothesis is that even though hybrid one showed expression of *Oct4*, *Nanog* and *Rex1*, it may have started to differentiate. To confirm this hypothesis, gene expression analysis was performed on both hybrid clones for the early mesodermal differentiation marker *Brachyury*. As expected, ES cells

do not express *Brachyury* whereas MEFs express a low level of *Brachyury*. Quite surprisingly, both hybrid clones expressed *Brachyury* indicating that both hybrid clones started to differentiate (Figure 3-6).

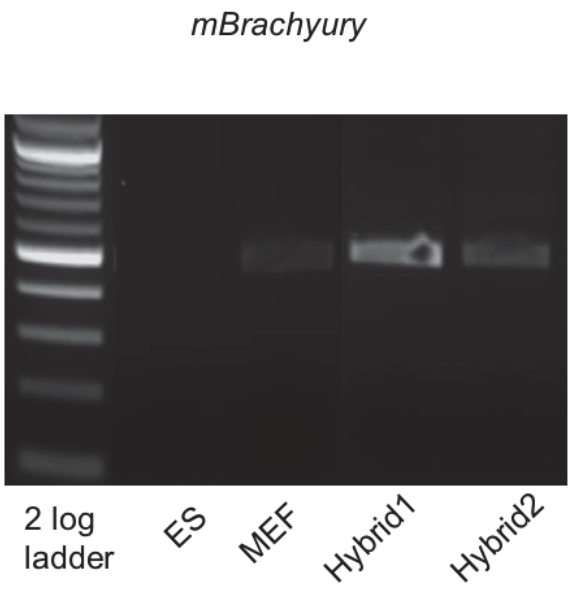

Figure 3-6: Gene expression analysis hybrid clones revealed expression of mesodermal differentiation marker Brachuyry.

Gel electrophoresis of RT-PCR samples from ES cells MEFs and both hybrid clones.

3.4 Discussion and Future Works

Xi reactivation in human fibroblasts revealed that some but not all X-linked genes were able to become reactivated after reprogramming towards pluripotency mediated by cell fusion (Cantone et al., 2016). In this study, I investigated whether female MEFs fused with male ES cells could generate pluripotent hybrid cells in which Xi reactivation could be systematically examine.

First I assessed whether hybrid clones were tetraploid upon cell fusion with mES cells and MEFs. A careful examination of the karyotypes of two hybrid clones (Figure 3-3) revealed karyotypic abnormalities including chromosome loss by both hybrid clones. Previous studies described similar phenomena illustrating that hybrid cells are not karyotypically stable when they are maintained in culture for a more than 30 days (Castillo et al., 1994; Croce, 1976). Chromosome loss happens preferentially in interspecies hybrids this is due to the difference in chromosome number between both species (Yamanaka and Blau, 2010). In my case chromosome loss could be explained with this reason since MEFs possess more chromosomes compared to ES cells that are diploid (Figure 3-3). Indeed, I have shown that both hybrid clones suffered from chromosome loss (Figure 3-3). Hybrid clone #1, possesses two X chromosomes, one from the *castaneous* allele and one from the *domesticus* allele. However, there is no biallelic *Hprt* expression in this hybrid. The *Hprt* is only expressed from the *castaneous* allele. This could be explained by the fact that hybrid clone # 1 has undergone differentiation. Both hybrid clones express low levels of early mesodermal marker *Brachyury* (Figure 3-6). Cell differentiation is linked to X chromosome inactivation (Ohhata and Wutz, 2013), therefore if hybrid clones started differentiated the process of random X inactivation will occur (Figure 3-7).

Hybrid #2 possesses 87 chromosomes making it near tetraploid. However, the number of X chromosomes varies between 4 and 5 and do not have the *castaneous* X chromosome which indicates chromosomal loss. This is explained by the fact that female MEFs possess a near triploid karyotype (65 ± 10) with 4 to 5 X chromosomes. Therefore, fusing 40 chromosomes from male ES cells with 65 chromosomes from female MEFS would generate hybrid cells with 105 chromosomes in total. Also with one X chromosome from the male ES cells and 4 to 5

others from female MEFs, their hybrids should possess between 5 and 6 chromosomes, which is less than what hybrid clone #2 contains.

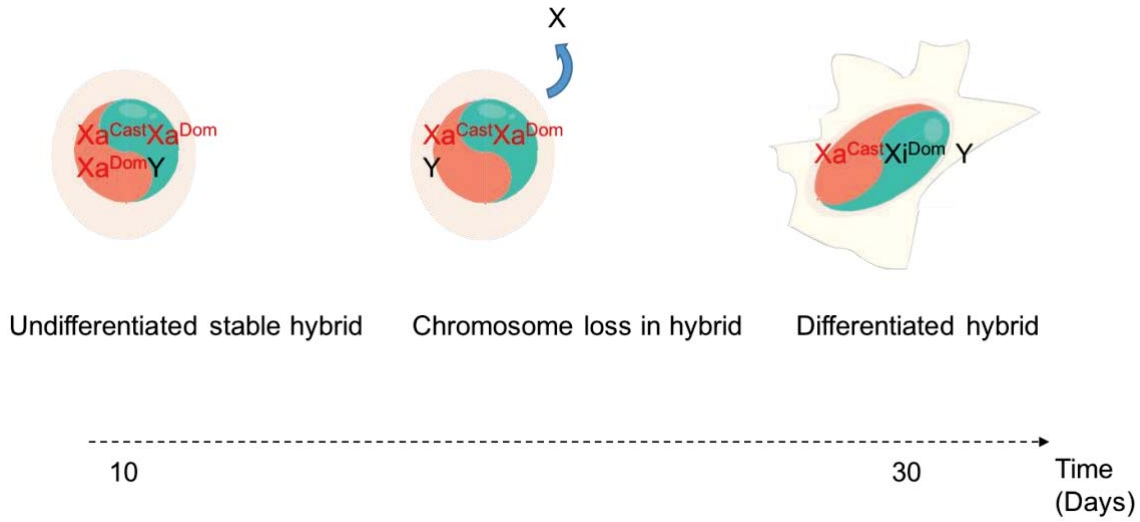

Figure 3-7: Hybrid clones chromosomes loss and differentiation.

Schematic representation of hybrid clone behavior. At first, the generated hybrid cells are karyotypically stable and are pluripotent. Then chromosomes loss and cell differentiation occurs.

Despite their karyotypic abnormalities, I showed that MEFs are able to generate hybrid cells which express pluripotency associated genes such as Nanog, Oct4 and Rex1 upon cell fusion, but only two hybrid clones were isolated from these cell fusion experiments (Figure 3-4). This may reflect the fact that MEFs have a low reprogramming potential towards pluripotency (Gridina and Serov, 2010). To further confirm the pluripotency state of hybrid cells derived from MEFs, additional experiments should be performed. One way of assessing pluripotency would be to differentiate them using embryoid bodies. Embryoid bodies allow spontaneous differentiation into the three primary germ layers. A gene expression analysis would then be performed to assess differentiation.

3.4.1 Future works

To overcome a prolonged time in culture, a specialized targeted cell line carrying a silent reporter inserted at the endogenous Oct4 locus could be generated (Figure 3-8). The activation of *Oct4* expression from this cell line would provide an indicator for pluripotent reprogramming. A similar system has previously been used by isolating mouse B cells from

Oct4-GFP transgenic male mice (Yeom et al., 1996) to detect pluripotent hybrid cells after cell fusion. Here I am planning to use CRISPR (Clustered Regulatory Interspaced Short Palindromic Repeat) Cas9 (CRISPR associated) system to insert GFP at the 3'UTR of the endogenous *Oct4* locus (Yang et al., 2013).

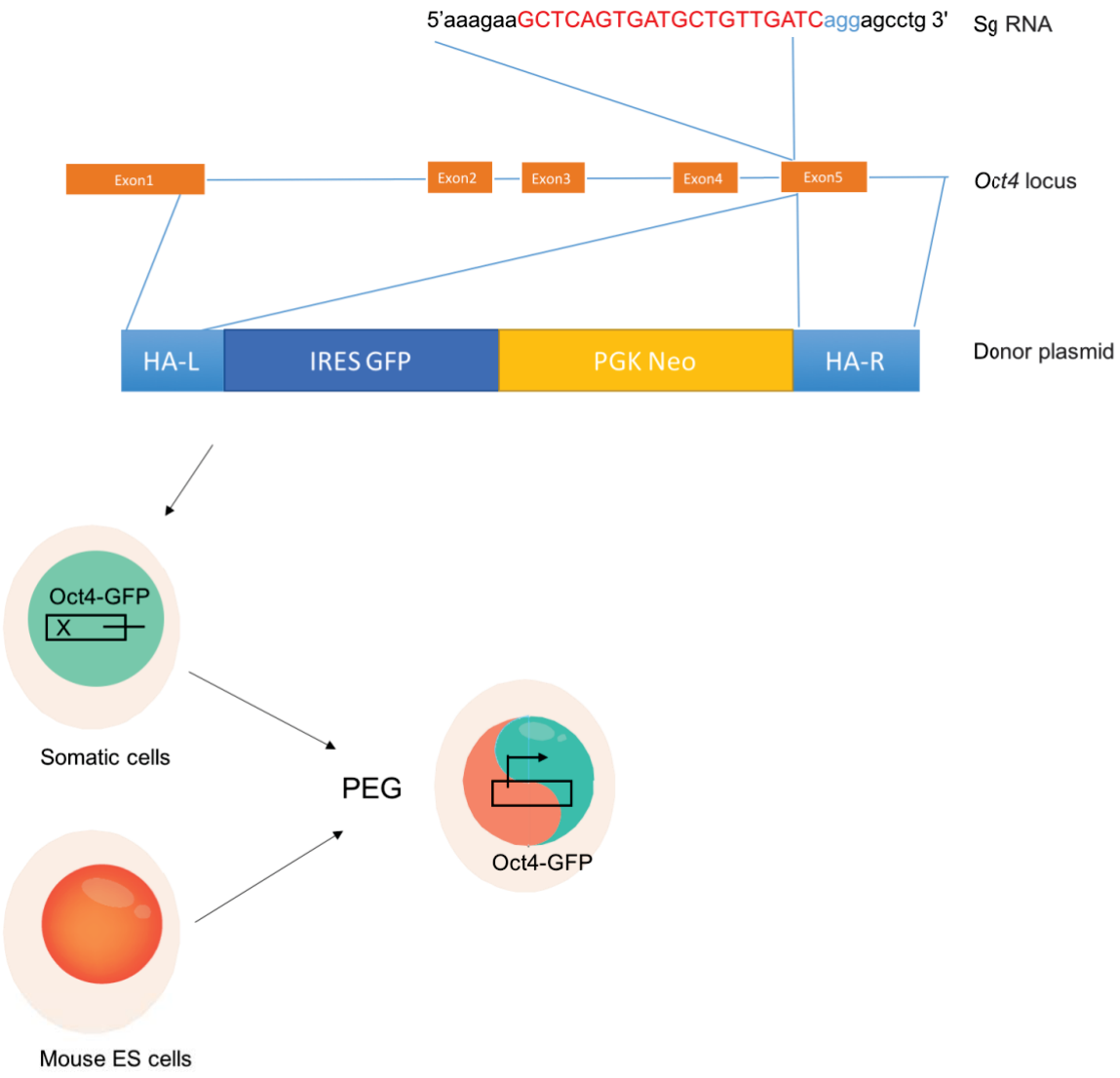

Figure 3-8: Generation of Oct4-GFP cell line using CRISPR/Cas9.

Top: Schematic of homologous recombination mediated by CRISPR/cas9 on the Oct4 gene, Sg RNA represents the single guide RNA; in red is the guide sequence and in blue is the Protospacer Adjacent Motif (PAM) sequence. The donor plasmid contains 2 Homology Arms (HA) left (HA-L) and right (HA-R), an Inter Ribosome Entry Site (IRES)-GFP as well as a selection cassette to select for the transfected cells under a strong promoter (PGK Neomycin). Bottom: Once the Oct4-GFP is successfully inserted inside somatic cells, cell fusion can be performed between the Oct4-GFP somatic cells with mouse ES cells. The GFP protein will only be expressed if the fused cells are expressing Oct4.

To overcome a low reprogramming potential, male ES cells were adapted to 2i media conditions and cell fusion was performed in 2i. ES cells maintained in 2i reached the ground-state of pluripotency, thus their reprogramming potential should be better than ES cells cultured in serum with LIF (Ying et al., 2008). Unfortunately, the fusion yielded to an unusual amount of cell death, thus no hybrid cells were detected at day 10 after fusion. An alternative way to increase the number of hybrid cells generated in cell fusion would be to use a semi-automated platform to perform high-throughput cell fusion. Recent studied described high-throughput and single cell cell fusion platforms as tools for increased cell fusion efficiency (Hu et al., 2013). Single cell high-throughput cell fusion would also allow me to collect fused cells at different time points and study the kinetics of Xi reactivation.

Chapter 4 : ROLE OF PLOIDY IN CELL FUSION MEDIATED REPROGRAMMING

4.1 Introduction

The last decade has seen remarkable progress in understanding pluripotency and reprogramming. Cell fusion have previously been used to identify factors essential to reprogram somatic cells towards pluripotency. For example, Pereira et al, 2008 showed that Oct4 is required for reprogramming somatic cell whereas Sox2 is not (Pereira et al., 2008). Another study demonstrated that PRC2 was important to successfully reprogram somatic cell suggesting the importance of chromatin remodeling in reprogramming (Pereira et al., 2010). In a recent study, my host laboratory showed that the reprogramming efficiency of mouse ES cells varied according to the cell cycle stage. Tsubouchi et al., (Tsubouchi et al., 2013) demonstrated that mouse ES cells during S and G2/M phase of the cell cycle are more efficient at reprogramming somatic cells in G1 towards pluripotency, as compared to interphase mouse ES cells, or ES cells in G1. They provided evidence that it is due to the precocious DNA synthesis soon after cell fusion in the somatic cell nucleus in the G1 stage of the cell cycle. This finding is consistent with previous studies of cell cycle progression in fused cells which showed that early DNA synthesis was induced in cells that are in G1 upon fusion with cells at the S or G2/M stage of the cell cycle (JOHNSON and RAO, 1970; RAO and JOHNSON, 1970). Despite all the work done in understanding the molecular mechanisms crucial for reprogramming towards pluripotency, a lot remain unanswered.

Haploid ES cells were first described by *Leeb et al.,* (Leeb and Wutz, 2011) (Figure 4-1). The karyotype of haploid ES cells consists of 20 mitotic chromosomes instead of 40 mitotic chromosomes in mouse diploid cells (Figure 4-1.B). Several groups have taken advantages of this specific haploid feature to generate knock out cell line more efficiently. Monfort et al, designed a screen to detect factors that are important for X chromosomes inactivation (Monfort et al., 2015). Penninger and colleagues used their own haploid ES cells for a drug screen (Elling et al., 2011).

The generation of haploid ES cells is achieved by activating oocytes with either Strontium Chloride ($SrCl_2$) or ethanol. The activated oocytes are then implanted inside a surrogate mouse. At the blastocyst stage (days E 3.5-E 4.5), cells from the Inner Cell Mass (ICM) are isolated and sorted, based on their DNA content, in order to enrich for haploid ES cells (Figure 4-1.A). The authors of this paper further characterized haploid ES cells and showed that they form colonies with a morphology characteristic of diploid ES cells in 2i condition (Figure 4-1.B).

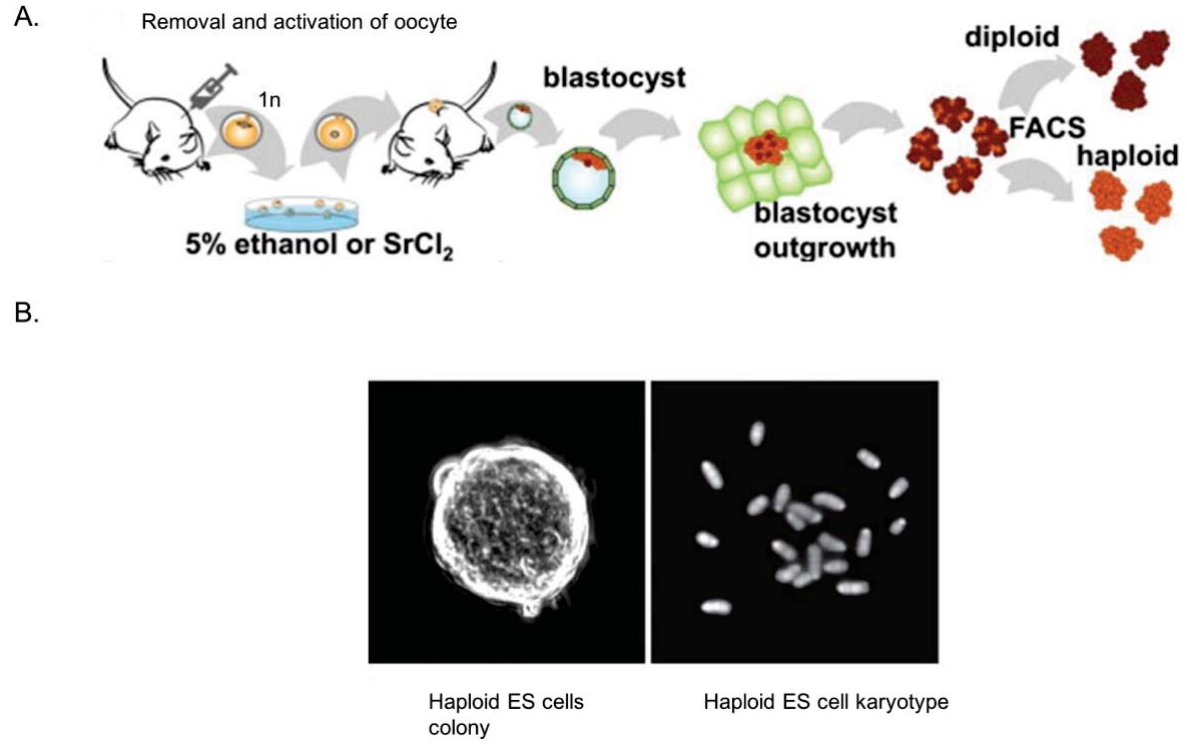

Figure 4-1: Generation and characterization of haploid ES cells.

(A) Schematic representation of the generation and isolation of the haploid ES cells. (B) Bright Field image and fluorescent confocal microscopy image of a typical haploid ES cells colony in 2i condition (B, left) and haploid karyotype (20 metaphase chromosomes instead of 40) (B, right) the chromosomes were stained with Hoechst. Figure adapted from Leeb et al, 2011.

In this study, I am assessing the reprogramming potential of haploid ES cells and compare it with diploid ES cells. Fluorescent Activated Cell Sorting (FACS) was used to enrich for haploid and diploid ES cells originating from the same cell population. Cell fusion was used to test the reprogramming potential of haploid ES cells. These experiments were performed to verify if

the haploid ES cells have a similar reprogramming potential as diploid ES cells. If the reprogramming potential is similar in haploid and diploid ES cells, a microfluidic based high-throughput screen could be implemented to determine which pluripotent factors are essential for cell fusion reprogramming. Due to the presence of one allele only in haploid ES cells the KO efficiency would be better.

4.2 Enrichment of haploid mouse ES cells

Haploid ES cells are not stable in vitro and gradually revert to a diploid state upon continuous culture, resulting in a mixed population (Guo et al., 2017). This means that haploid ES cells must be re-purified by flow cytometry using Fluorescent Activated Cell Sorting (FACS sorting), periodically in order to maintain the ratio of haploid to diploid cells at or above 85% of haploid ES cells. To do this, FACS was used to enrich for haploid ES cells, revealed by staining for DNA using Hoechst for sorted for G1 haploid ES cells (1n) (blue, Figure 4-2.B) and G2/M diploid ES cells (4n) as a control for the reprogramming assays (green, Figure 4-2.B). Briefly, DNA was stained with Hoechst, a cell-permeable DNA dye preferentially binding to AT-rich regions, to obtain a DNA content profile. For my purpose, G1 haploid ES cells (1n) (blue, Figure 4-2.B) and G2/M diploid ES cells (4n) (green, Figure 4-2.B) were sorted.

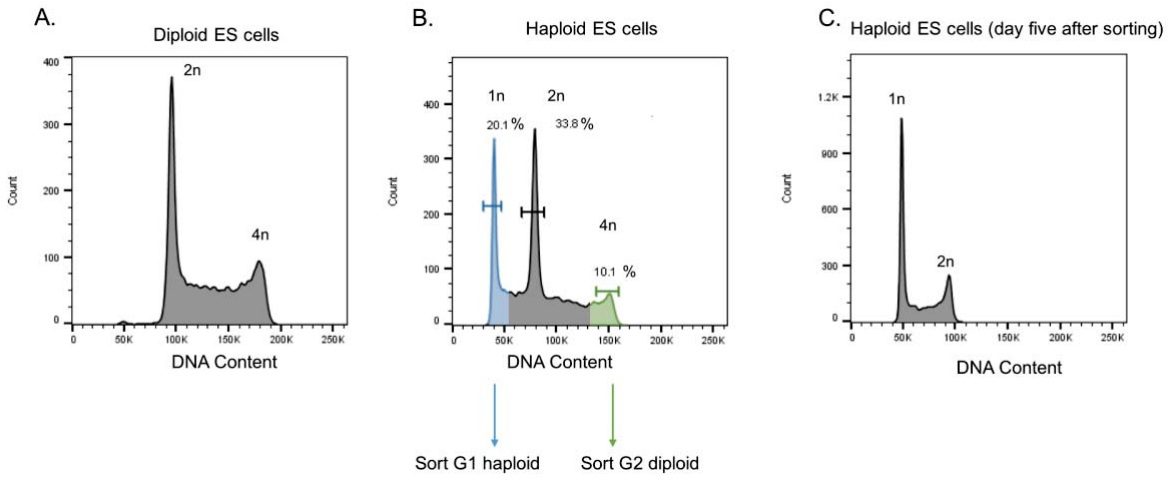

Figure 4-2: Enrichment of haploid ES cells from in vitro culture .

(A) Representative Propidium Iodine (PI) profile of diploid ES cells. (B) Cell cycle profile of haploid ES cells. Green and blue highlight the population that are sorted for cell fusion experiments. The first peak harbors the cells with one set of DNA (1n)

and corresponds to G1 haploid ES cells (20% of the cell cycle profile), the second peak contains the 2n cells which represents a mixed population of G2 haploid and G1 diploid ES cells (34% of the cell cycle) and the last peak corresponds to the 4n cells which constitute pure population of diploid ES cells in G2/M (10 % of the cells cycle). (C) Representative PI profile of haploid ES cells at day 5 after sorting. 1n (haploid), 2n (diploid) and 4n (tetraploid) represents the number of chromosomes present in haploid and diploid ES cells.

Figure 4-2 summarizes the cell cycle profile of diploid ES cells (Figure 4-2.A), haploid ES cells that remained in culture for more than 10 days (Figure 4-2.B) and haploid ES cells five days after sorting (Figure 4-2.C). Figure 4-2.A represents a typical cell cycle profile of diploid ES cells with a diploid peak (2n) and a tetraploid peak (4n) corresponding to cells in G1 and G2/M phase of the cell cycle, respectively. In the haploid ES cells sample (Figure 4-2.B) an additional peak representing sub-G1 peak (1n) corresponds to haploid ES cells in G1. In this profile, peaks at 2n probably comprise a mixture of haploid ES cells in G2/M, and diploid ES cells in G1,
To minimize diploid ES cell contamination, and to enrich for haploid ES cells for reprogramming assays, haploid ES cells were gated an enrichment >85% was achieved before the ES cells were used to fuse. Figure 4-2.C shows a typical haploid ES cell population, where a minimal contamination of diploid ES cells can be inferred by the lack of a 4n peak. In each experiment the cell cycle profile was verified before cell fusion experiment to minimize and control diploid ES cells contamination.

4.3 Haploid ES cells have a lower reprogramming potential compared to the diploid ES Cells

To my knowledge, cell fusion-mediated reprogramming has never been attempted using haploid ES cells. To study the impact of ploidy in cell fusion-mediated reprogramming towards pluripotency, I fused haploid ES cells (1N) with asynchronous EBV-transformed human B cell line (hB) and compared the reprogramming potential to fusions between diploid ES cells and hB. Both haploid and diploid ES cell fusions were conducted with the same initial number of cells. Briefly, ES cells and hB cells were mixed in the presence of polyethylene Glycol (PEG) at a ratio of 1:1. Fusions between mouse ES cells and human somatic cells formed interspecies heterokaryons, which were cells that possess two nuclei: one nucleus from mouse ES cells and the other one from hB cells, and share one cytoplasm. To enrich for heterokaryons, drug selection (puromycin and ouabain) was applied on the day after fusion (Figure 4-3.A). The hB

cell line was puromycin resistant and sensitive to ouabain treatment whereas haploid ES were eliminated by puromycin and not sensitive to ouabain. Heterokaryons that achieved reprogramming towards pluripotency, expressed human pluripotency-associated genes such as *OCT4*, *NANOG* or *CRIPTO* three days after fusion. I took advantage of the difference in their DNA sequences between mouse pluripotency associated factors and human pluripotency associated factors to design human specific primers. Then, I used these primers to detect human pluripotency associated genes using RT-qPCR where GAPDH was used a positive control.

Relative gene expression analysis of *OCT4*, *NANOG* and *CRIPTO* showed that, as expected, day 3 heterokaryons generated with diploid ES cells, upregulate human pluripotency markers (Figure 4-3.B). However, the expression level these factors was consistently lower in haploid ES cells compared to diploid ES cells. For example, the expression of *CRIPTO* was seven-fold lower in haploid ES cells heterokaryons as compared to diploid ES cells heterokaryons. This result suggested that haploid ES cells were able to reprogram somatic cells towards pluripotency but at a much reduced level as compared to diploid ES cells.

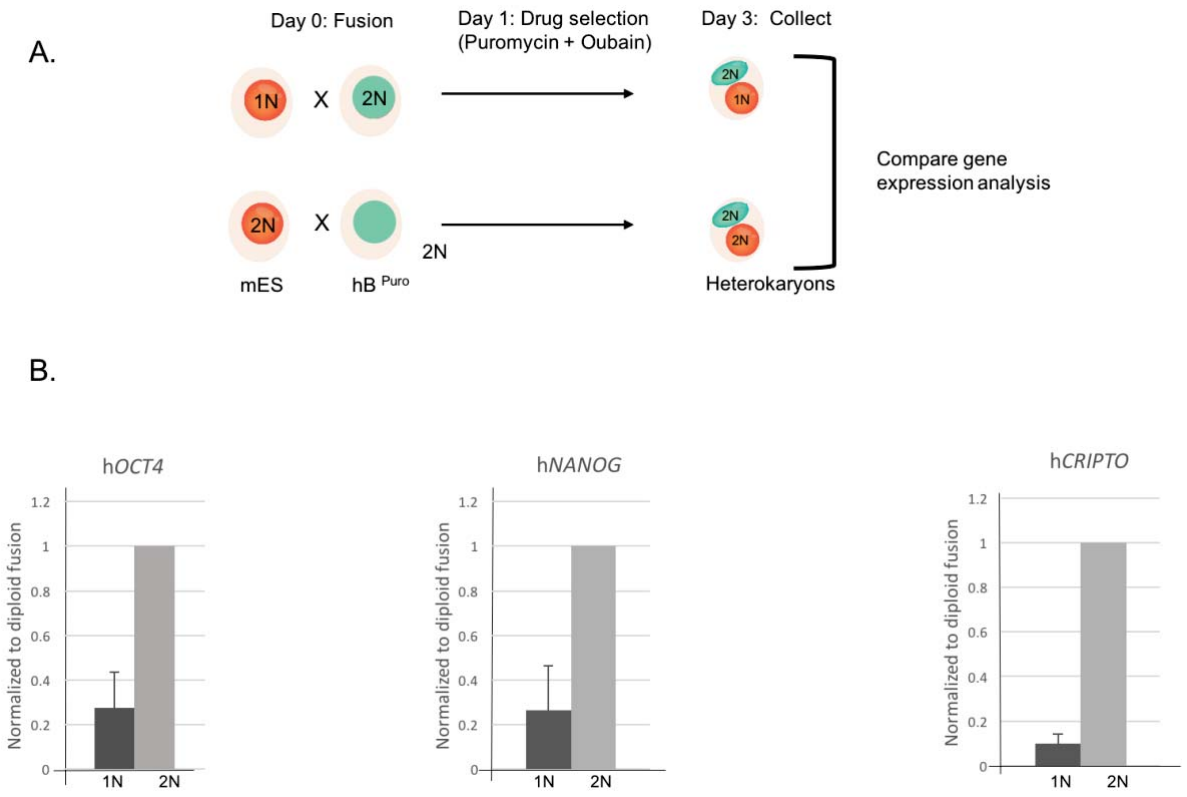

Figure 4-3: Haploid ES cells reprogramming potential is lower than diploid ES cells.

(A) Schematic representing the experimental system to generate heterokaryons. Drug selection was applied to enriched for fused cells. At day 3 after fusion, heterokaryons were collected. (B) Human transcripts of pluripotency associated genes were analyzed using RT-qPCR and normalized to GAPDH. Data represent the mean of three independent experiments and error bar represent standard deviation with n=3. Asterix shows statistically significance between the means of 1N and 2N fusions. Non-parametric statistical test (Man-Withney) was performed and showed no statistical differences.

One explanation for the lower reprogramming potential of haploid ES cells could be that the kinetics of pluripotency induction may be slower in haploid ES cells as compared to diploid ES cells; haploid ES cells might require more time to reprogram somatic cells towards pluripotency. Therefore, I decided to assess reprogramming at a later time point, by performing hybrid analysis. Fusion between haploid ES cells and mouse somatic cells was performed as previously described in this thesis in order to generate intraspecies heterokaryons that subsequently give rise to tetraploid hybrid cells. Diploid ES cells fusions were used at a control. Hybrid cells proliferate therefore they can be maintained in culture for a longer period of time compared to interspecies heterokaryons. This allows me to study, at a later time point, the reprogramming potential of haploid ES cells.

To facilitate the analysis, I used mouse B cells as somatic targets. These cells carry puromycin resistant mouse B cells carrying an Oct4GOF18ΔPE-GFP ($mB^{Oct4\text{-}GFP}$) reporter (Do and Schöler, 2004). GFP will only be expressed if mouse B cells start expressing Oct4, which is a pluripotency associated factor present in ES cells and successfully reprogrammed cells (Figure 4-4.A). Thus, expression of GFP in mB cells would indicate that those cells undergo reprogramming towards pluripotency. To eliminate unfused mouse ES cells, puromycin is added to the media and several washing is performed to remove unfused mB cells.

Reprogramming potential was also assessed by Alkaline Phosphatase (AP) staining of hybrid cells at day 10 after fusion. AP is a marker associated with pluripotency, and was used to score "pluripotent" conversion. The number of AP positive colonies was counted for hybrid from both haploid and diploid ES cells fusions. As expected, diploid ES cells were able to generate hybrid colonies positive for AP staining (Figure 4-4.B). AP positive hybrid colonies were obtained from haploid ES cells fusions (Figure 4-4.B). However, the number of AP positive hybrid colonies from haploid ES cells fusions was 10-fold less (292 ± 125 AP positive colonies) than the number of AP positive hybrid colonies from diploid ES cells fusions (2292 ± 250 AP positive colonies) (Figure 4-4.C).

To further confirm the low reprogramming potential of haploid ES cells, I took advantage of the Oct4-GFP reporter and counted GFP positive hybrid colonies generated by haploid ES cells and diploid ES cells fusion. As expected, diploid ES cells fusions generated hybrid colonies that were GFP positives (Figure 4-4.D). GFP positive hybrid colonies were also visible in haploid ES cells fusions. Hybrid cells from haploid and diploid fusions were able to form compact colonies (Figure 4-4.D). Consistent with the previous result, the number of GFP positive colonies generated was ten-fold less using haploid ES cells (48 ± 20 GFP positive colonies) than diploid ES cells fusion (512 ± 50 GFP positive colonies) (Figure 4-4.E). These data were in agreement with obtained result from the heterokaryons assay and suggests that haploid ES cells fused with $mB^{Oct4\text{-}GFP}$ cells were able to reprogram mB $^{Oct4\text{-}GFP}$ cells towards pluripotency but with a lower efficiency than diploid ES cells fused with $mB^{Oct4\text{-}GFP}$ cells. It also indicates that this is not likely to be due to slower kinetics of haploid ES cells mediated reprogramming.

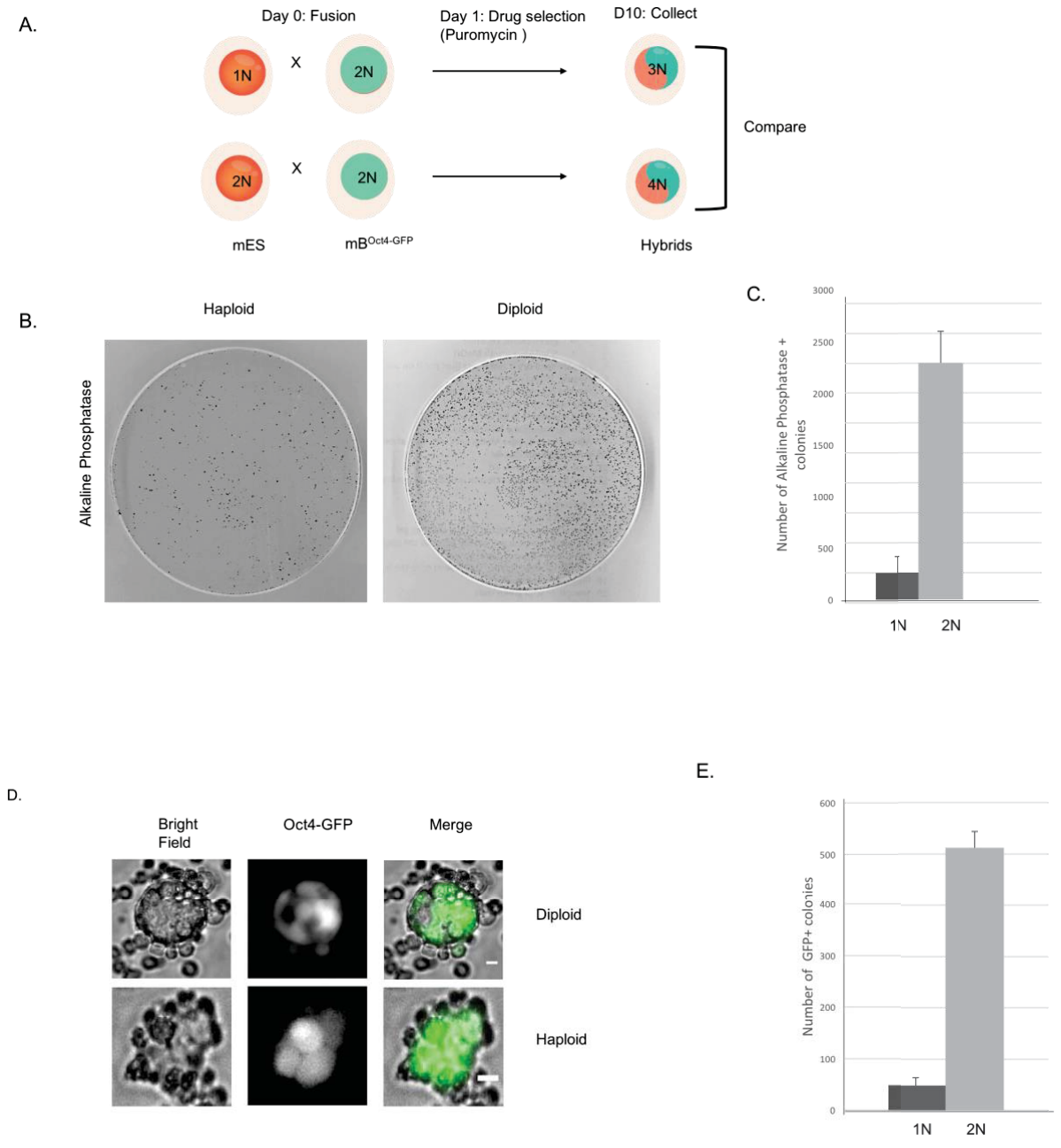

Figure 4-4: Generation of hybrid cells by cell fusion mediated reprogramming is lower when generated with haploid ES cells than with diploid ES cells.

(A) Schematic representation of the experimental setup. (B and D) Representative pictures of Alkaline phosphatase positive hybrid cells (B) and GFP positive hybrid colonies in both haploid and diploid ES cells fusion (D) plated at a density of 2 millions of cells, scale bar=10 µm. (C, E) Number of AP (C) and GFP positive (E) colonies. Error bars represent standard deviation with two biological replicates. Non-parametric statistical test (Mann-Withney) was performed and were non-significant.

4.4 Haploid ES cells possess less transcripts and proteins compared to the diploid ES cells

Previous studies that some pluripotency associated factors, such as Oct4. are essential for reprogramming towards pluripotency (Pereira et al., 2008). Work done in iPS cells demonstrated that high level of ectopic Oct4 in somatic cells increases the reprogramming efficiency (Rongeat et al., 2011). It is possible that due to their decrease in ploidy, haploid ES cells have less pluripotency-associated proteins such as Oct4. Therefore, the low level of pluripotency-associated proteins could prevent haploid ES cells to reprogram somatic cells towards pluripotency with the same efficiency as diploid ES cells. Indeed, several studies have shown that an increase in DNA content increased the transcript level (Padovan-Merhar et al., 2015; Weiss et al., 1975). Transcript level and protein level usually correlate suggesting that haploid ES cells have less transcript and thus protein level than diploid ES cells.

To assess whether low level of pluripotency associated factors might explain the low reprogramming potential of haploid ES cells, I first assessed whether total transcript and protein level were lower in haploid ES cells as compared to diploid ES cells. To do this, I measured the concentration of total RNA by spectrometry in haploid and diploid ES cells. The same number of cells was used for both haploid and diploid ES cells samples. Figure 4-5.A showed that there was approximately a 50% reduction in total RNA in haploid ES cells compared to diploid ES cells. Consistent with this, measurement of total protein concentration, by spectrometry analysis (bicinchoninic acid (BCA assay)), revealed that the total protein concentration in haploid ES cells was two-fold lower (1.6 µg/µl ± 0.4) compared to diploid ES cells (0.8 µg/µl ± 0.5) (Figure 4-5.B).

I then determined whether the level of specific proteins that were important for reprogramming towards pluripotency such as Oct4 and Nanog varied between haploid and diploid ES cells. Quantification of Oct4 and Nanog proteins by fluorescent Western blot was performed on equal cell number of haploid vs diploid ES cells. As expected, both haploid and diploid ES cells expressed Oct4 and Nanog proteins (Figure 4-5. C and E). Quantification of the Western blot revealed a higher Oct4 protein level (1.3 fold) in diploid ES cells compared to

haploid ES cells (Figure 4-5.D). Quantification of Nanog protein also showed an increase in Nanog protein level in diploid (1.75 fold) ES cells compared to haploid ES cells.

The difference in protein level between haploid and diploid ES cells was as expected. Haploid ES cells have 50 % of total RNA and total protein with a similar trend for Oct4 and Nanog protein level. This data suggests that to reprogram somatic cells, a threshold needs to be reached for pluripotency factors rather than a linear correlation between the amount of pluripotency factors and the reprogramming potential of ES cells. This hypothesis could explain the 10-fold difference between haploid and diploid ES cells reprogramming potential with the 50% less Oct4 and Nanog proteins.

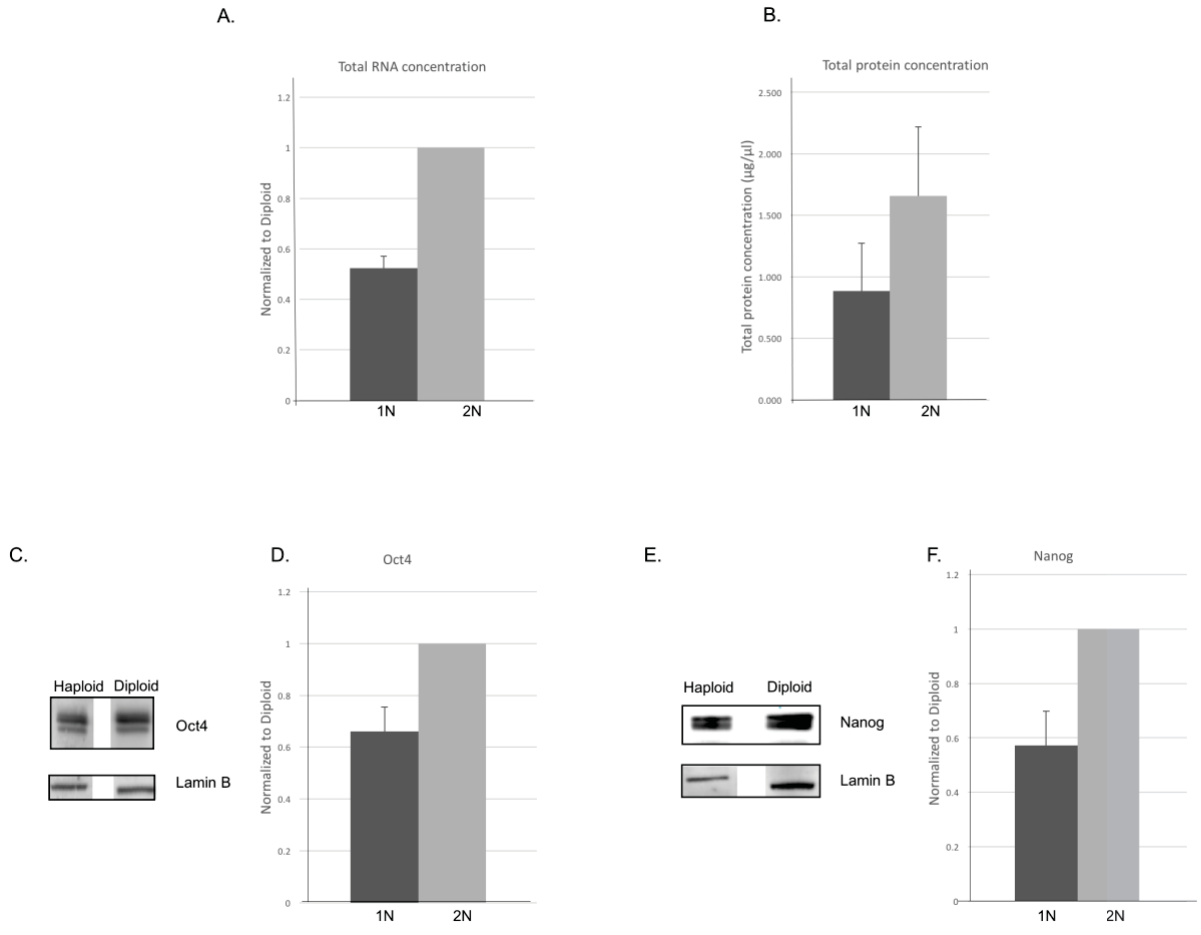

Figure 4-5: The protein level in haploid ES cells is lower than diploid ES cells.

(A) Total amount of RNA normalized to Diploid ES cells. (B) Total amount of proteins in haploid and diploid ES cells. Data represent mean of three independent experiments. Error bars denote the standard deviation with n=3. (D, F) Quantification of Oct4 and Nanog proteins was performed by fluorescent Western blots. The Oct4 and Nanog protein level was normalized to the amount of proteins in the diploid ES cells, Error bars represent the S.D with n=3. (C, E). Representative Western blots of Nanog and Oct4 proteins detected in haploid and diploid ES cells. Lamin B was used as a loading control. The same number of cells for haploid and diploid ES cells was used.

4.5 *Nanog* overexpression increases the reprogramming potential of haploid ES cells

Nanog has been shown to increase reprogramming efficiency in cell fusion system (Silva et al., 2006) and in other reprogramming towards pluripotency system (iPS) (Theunissen et al., 2011). To assess whether overexpression of Nanog could rescue reprogramming potential of haploid ES cells, I overexpressed Nanog in haploid ES cells and compared the reprogramming with wild type haploid and diploid ES cells. To generate stable haploid ES cell line overexpressing Nanog, I used the approach previously described in Theunissen et al., 2011 which took advantage of PiggyBac (PB) transposon to increase the efficiency of stable integration of plasmid. Briefly, the PB plasmid was cotransfected with the Nanog overexpressing plasmid. Transfected cells were selected using hygromycin for 10 days to select for cells that incorporated Nanog plasmid. After the drug selection, both non-transfected (wild type) and transfected haploid ES cells were sorted to enrich for haploid ES cells (Figure 6.A). Nanog overexpressing haploid ES cells showed a cell cycle profile similar to wild type haploid ES cells (Figure 4-6.A, right).

To validate Nanog overexpression, I performed Western blot analysis for Nanog protein in transfected cells (Nanog OE) haploid ES cells after the selection, and compared it to wild type (WT) haploid ES cells. Figure 4-6.B showed an increase in Nanog protein level in Nanog OE cells compared to the WT haploid ES cells indicating a successful overexpression of Nanog in haploid ES cells.

To verify if overexpression of Nanog does not affect other pluripoptency associated factors, I assessed the protein levels of Oct4 and Estrogen-Related Receptor Beta (Esrrb) A study revealed that Esrrb was a direct target of Nanog (Festuccia et al., 2012). Previous studies have demonstrated that Esrrb activated the transcription of Oct4 (van den Berg et al., 2008; Zhang et al., 2008). As expected, both Nanog OE and WT haploid ES cells express Oct4 and Esrrb (Figure 4-6. B). Western blot analysis of Oct4 showed a similar level in both wt and Nanog OE haploid ES cells. Western blot of Esrrb also indicated an increase in Nanog OE compared to WT haploid ES cells.

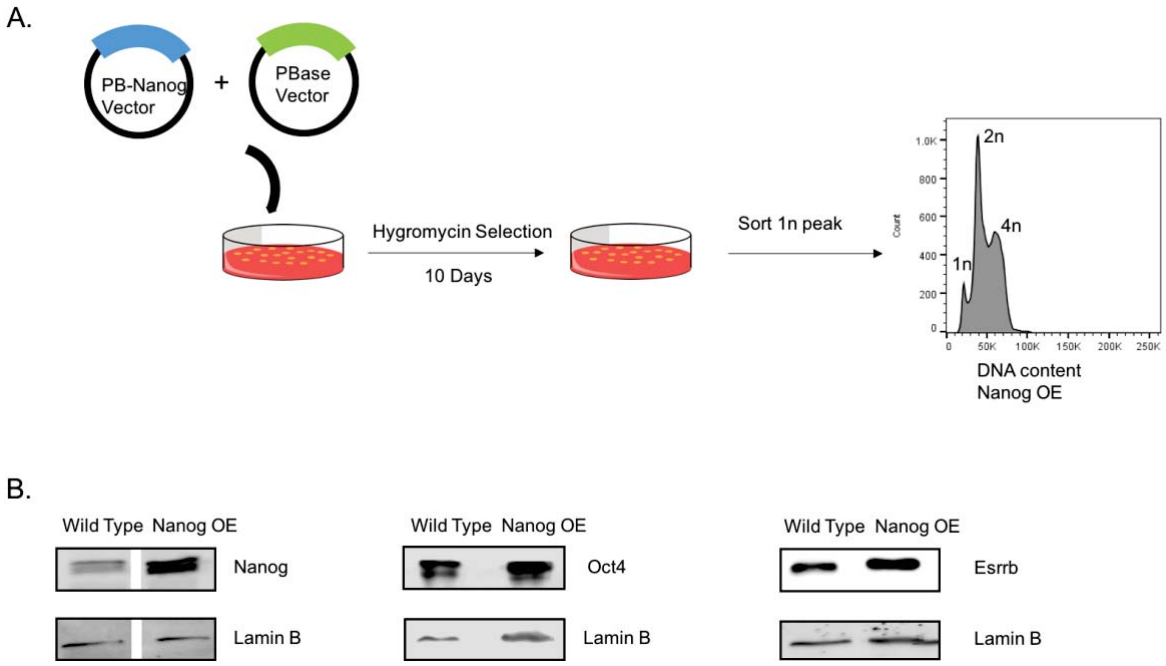

Figure 4-6: Generation and characterization of haploid ES cells overexpressing Nanog.

(A) Schematic representation of the generation of stable Nanog overexpressing cell line. Haploid ES cells were cotransfected with PB Nanog and PBase. Hygromycin selection was applied after transfection to select for cells that incorporated the plasmid. To enrich for haploid ES cells, the 1n peak was gated for sorting this population. (B) Western blot of Nanog, Oct4 and Esrrb proteins in haploid (WT) and Nanog OE haploid ES cells. Lamin B was used as loading control.

To determine whether Nanog overexpression increased the reprogramming potential of haploid ES cells, I fused in parallel wild-type haploid ES cells, Nanog OE haploid ES cells and wt diploid ES cells with hB cells using the same experimental protocol described in 4.2. The interspecies heterokaryons cells were collected at day 3 after fusion and transcript level of human pluripotent genes was analyzed using RT-qPCR (Figure 4-7.A). Figure 4-7.B showed an up-regulation of human pluripotency factors including *OCT4*, *NANOG* and *CRIPTO* in both the heterokaryons originating from diploid and haploid ES cells fusions. Nanog OE haploid ES cells are able to create heterokaryons that induce human *OCT4*, *NANOG* and *CRIPTO*. Nanog OE haploid ES cells consistently express more pluripotency-associated factors compared to WT haploid ES cells. This result was in accordance with previously published data where overexpressing Nanog resulted in an increased reprogramming potential of ES cells in cell fusion system (Silva et al., 2009). Heterokaryons from Nanog OE haploid ES cells consistently expressed more human *OCT4* and *CRIPTO* compared to heterokaryons from diploid ES cells.

However, *NANOG* up-regulation was higher in diploid ES cells compared to Nanog OE haploid ES cells fusions. Taken together, these data suggested that Nanog overexpression increased the reprogramming potential of haploid ES cells and partially rescues haploid ES cells reprogramming potential. Additional experiments should be performed to assess the pluripotency status of heterokaryons obtained. As an examples, differentiating heterokaryons or hybrid cells by the generation of embryo body could be one possibility to further characterize their pluripotency.

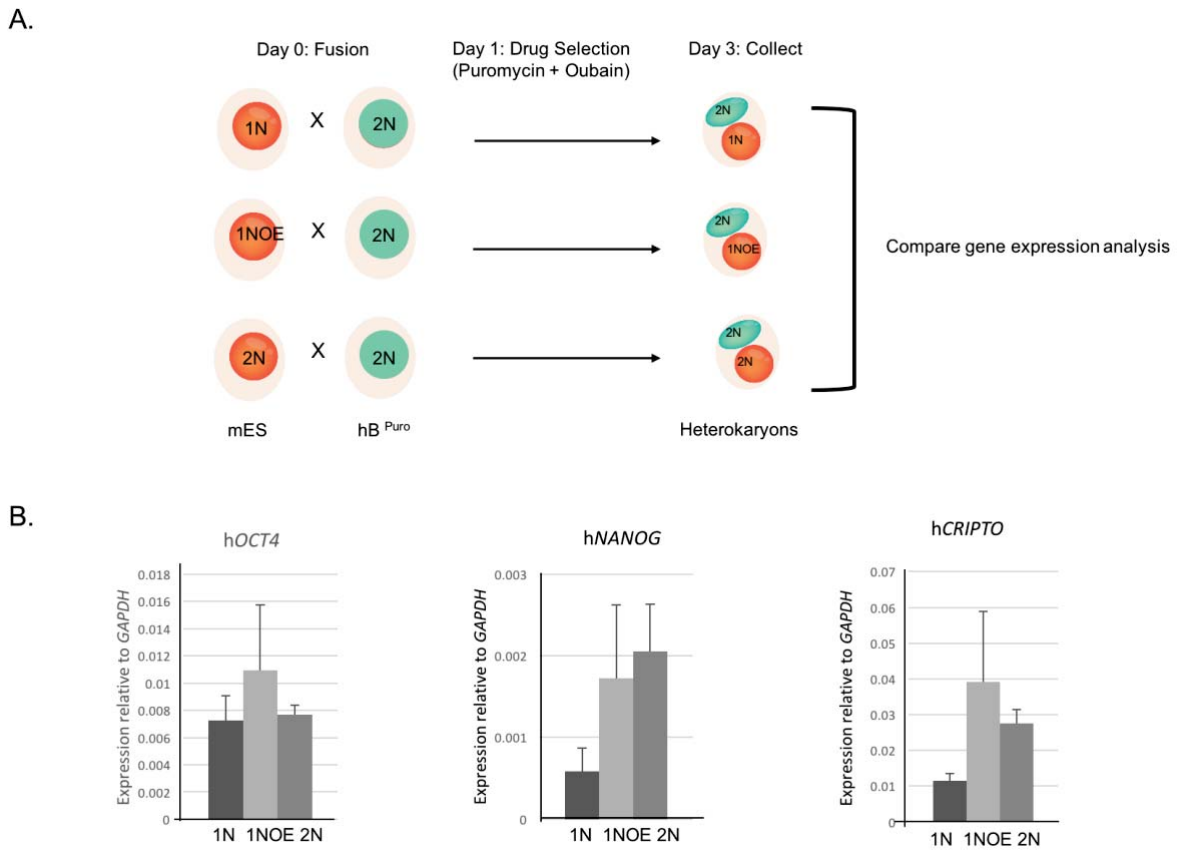

Figure 4-7: Nanog overexpression increases haploid ES cells reprogramming potential.

(A) Schematic representing the experimental system to generate interspecies heterokaryons in order to study the reprogramming potential of haploid ES cells. (B) Human transcripts were analyzed using RT-qPCR at day 3 after fusion and normalized to human GAPDH. Error bars represent standard deviation with n=3.

4.6 Discussion and future works

Here, I have examined the capacity of haploid ES cells to reprogram somatic cells towards pluripotency using cell fusion. Previously my host laboratory showed that diploid ES cells are capable of reprogramming diploid somatic cells using cell fusion system (Pereira et al., 2008; Piccolo et al., 2011a). Other studies have demonstrated that tetraploid fibroblast fused with diploid ES cells do not undergo reprogramming towards pluripotency but instead reprogram ES cells towards fibroblast (Kruglova et al., 2010). This suggests that ploidy may be important for the direction of reprogramming outcomes. To understand the mechanism behind these observations I examined how ploidy may affect reprogramming.

Here, I have demonstrated that haploid ES cells can reprogram somatic cells towards pluripotency with a lower efficiency as compared to diploid ES cells (Figure 4-3). This confirmed the assumption that ploidy may be important for reprogramming towards pluripotency mediated by cell fusion. Single cell analysis has revealed that transcript level within a cell population varies in between cells. Transcript and protein level may vary within the haploid ES cells population leading to a population of haploid ES cells more prone to reprogram somatic cells towards pluripotency. In order to ascertain this, several clones could be derived from the original haploid ES cell population and cell fusion could be performed with each of them to assess the range of cellular reprogramming potential of haploid ES cells. Another cause of the low reprogramming potential of haploid ES cells could be that the kinetics of reprogramming towards pluripotency is slower in haploid ES cells. This was assessed with the generation of hybrid cells from haploid ES cells fusions and compared with hybrid cells from diploid ES cells fusions. The result revealed that even at a later time point haploid ES cells still have a lower reprogramming potential than diploid ES cells (Figure 4-4). Low reprogramming of haploid ES cells could also be due to their sizes. Haploid ES cells are much smaller than diploid ES cells. their volume is 2.5 time smaller compared to diploid ES cells. The same observation was done on their nucleus (Anton Wutz, personal communication).

Finally, I assessed whether low ploidy could also lead to low protein level in haploid ES cells compared to diploid ES cells. I showed that that haploid ES cells have less total RNA and protein than diploid ES cells. This result is in agreement with previous work reviewed in (Marguerat and Bähler, 2012). Specifically, the level of crucial pluripotency associated factors, such as Oct4 and Nanog is reduced in haploid ES cells compared to diploid ES cells (Figure 4-5). Previous study in iPS showed evidence that reprogramming efficiency was regulated by the ectopic level of Oct4, Sox2, Klf4 and c-Myc (OSKM) (Sridharan et al., 2009). Polo et al. 2012 (Polo et al., 2012) corroborated this hypothesis by genetically engineering fibroblast to express a higher dose of transcription factors (OSKM), which led to an increase in the efficiency/kinetics of pluripotent reprogramming. They also noticed that the protein levels of those four factors were reduced in cells blocked at an intermediate states compared to cells which were able to be reprogrammed towards pluripotency. A similar process could explain the low reprogramming potential of haploid ES cells, where a minimum amount of pluripotency-associated proteins is required to reprogram somatic cells towards pluripotency. To assess this, I overexpressed Nanog in haploid ES cells and showed that the low reprogramming potential of haploid ES cells can be rescued by overexpression of Nanog in haploid ES cells (Figure 4-7). This result is in agreement with previous studies which stated that Nanog overexpression enhances the efficiency of reprogramming (Silva et al., 2009; Theunissen et al., 2011). As previously mentioned in the results, Nanog directly targets Esrrb which activates the regulation of Oct4. Besides Nanog and Oct4 are part of the core transcription factors network that regulates pluripotency (Rodda et al., 2005). Therefore, the increase in reprogramming potential in haploid ES cells overexpressing Nanog could be due to the increase in protein level of Oct4 and Esrrb as well. To assess whether Nanog overexpression partially rescue the low reprogramming of haploid ES cell at a single cell level, clonal population of haploid ES cells overexpressing Nanog should be derived. Those clone would then be fused with somatic cells to determine the reprogramming potential of each NanogOE clonal population. This will allow me to determine whether the frequency of reprogramming is equivalent between clones. Further studies will be required to explore whether overexpression of other transcription factors such as Oct4 have the same effect as supplementing with Nanog. It would be interesting to overexpress Nanog in haploid ES cells at the same level as it is expressed in diploid ES cells.

It would be important to investigate whether this low level of proteins is also present in other haploid ES cells line and is not just a specificity of this particular cell line. At the moment, there is only one other haploid ES cell line available (Elling et al., 2011). Preliminary data performed on this new cell line shows that the total protein level as well as the protein level of Oct4 and Nanog is also lower in this cell line suggesting that the low amount of proteins is a feature of haploid ES cells in general. More cell fusion experiments need to be done on this new haploid ES cell line to see whether the reprogramming efficiency is also low compared to diploid ES cells.

Chapter 5 : VISUALIZING MITOTIC CHROMATIN BY HIGH-RESOLUTION MICROSCOPY

5.1 Introduction

During mitosis, chromatin drastically condenses to form a mitotic chromosome. The hierarchical model of mitotic chromosome stipulates that DNA wraps itself around a histone octamer to form the basic structure of chromosomes: the nucleosome. Nucleosomes then fold into 30nm fiber which then form chromonema and chromatids (Figure 5-1). However, previous work has challenged the existence of the 30nm fiber (Eltsov et al., 2008; Nishino et al., 2012). Indeed, Eltsov et al., performed cryo-electron microscopy (cryo-EM) on mitotic cells after vitrification of the samples, the results obtained suggested that the chromatin in mitotic chromosomes forms a "molten" mass where no 30nm structures could be detected. These studies do not corroborate the hierarchical model of mitotic chromosomes suggesting that higher order structure of mitotic chromosome still remains unknown.

Several proteins are involved in mitotic chromosomes structure, such as topoisomerase II or condensin who act as a scaffold (Green et al, 2012.). Another protein complex playing a role in mitotic chromosomes structure is cohesin. It has been stated that most of the cohesin is removed from mitotic chromosomes during prophase, only a small percentage (up to 15%) remained and is localized at the centromere in metaphase. During the metaphase-anaphase transition cohesin is removed from metaphase chromosomes by the separin protein allowing the sister chromatids to be separated by mitotic spindle (Waizenegger et al., 2000).

Most studies of mitotic chromosome structure are performed using microscopy, chromosome conformation capture techniques (e.g High Chromosome Contact (Hi-C)) that quantifies the interaction of the compacted chromatin (here mitotic chromosomes) genome wide and mathematical modelling to understand the higher order organisation of mitotic chromosomes. Recent advances in microscopy have drastically improved the resolution limit. More specifically, over the past couple of years cryo-EM achieved a near atomic resolution (up to 2 Ångström). This is mostly due to an improvement in sample preparation technique and better detectors (direct electron detectors). Recent studies have been able to shed some light on

mitotic chromosomes structure in mitotic cells using CLEM microscopy (Booth et al., 2016) and ChromEMT (Ou et al., 2017). CLEM microscopy takes advantages of new generation microscopes combining both EM and light microscopy while ChromEMT uses photooxidation of a fluorescent dye (DRAQ5) to enhance DNA contrast in EM. Despite the recent discoveries regarding mitotic chromosomes structure, how mitotic chromosomes are condensed and what substructure lies underneath mitotic chromosomes remains unclear.

In this study, I re-established flow karyotyping to isolate mouse mitotic chromosomes (Ng and Carter, 2006). To demonstrate that the flow karyotyping setup implemented in my host institute worked, I successfully isolated the mouse mitotic chromosomes 19. I present that structural analysis of sorted mouse mitotic chromosomes 19 is achieved by super-resolution microscopy (Structured Illumination Microscopy (SIM) and cryo-EM). To demonstrate the applications of these techniques, I investigate the effect of loss of cohesin in mouse mitotic chromosomes 19, which is the easiest chromosome to isolate with our setup and to image by cryo-EM since it is the smallest mouse chromosome.

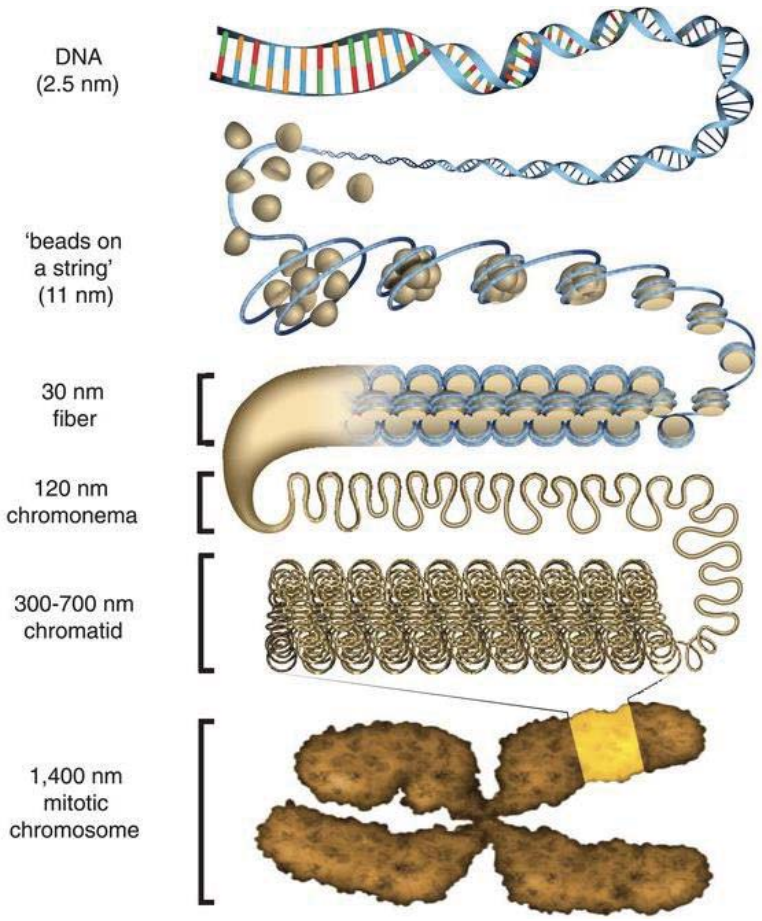

Figure 5-1:Hierarchical model of mitotic chromosome folding.

DNA wrapped itself around nucleosomes to form the bead on a string model which then fold into 30nm fibers that condensed even more into chromonema. All this level of compactions forms then mitotic chromosomes. (Ou et al., 2017)

5.2 Isolation of mouse mitotic chromosomes by FACS

Several techniques have previously been developed to isolate mitotic chromosomes in solution (Fan et al., 2011). With them it is however not possible to isolate a specific subset of chromosomes. Isolation of chromosomes can be achieved by fluorescence-activated cell sorting (FACS) of chromosomes. Chromosomes sorting have been used for the past 30 years (Gray et al., 1986). Isolation of chromosomes takes advantage of DNA specific binding dyes that preferentially bind to AT rich regions and GC rich regions. This specificity in binding allows the generation of a bivariate plot where chromosomes are separated based on their AT and CG content and chromosomes size. Flow karyotyping has been used to generate chromosome-specific probes that can be used for DNA FISH (Langford et al., 1996). It is also used for several

clinical applications including detection of chromosomal abnormalities, gene mapping and variation between human chromosomes (Arkesteijn et al., 1988; Ferguson-Smith et al., 1998; Gray et al., 1988). However, it has never been done as a tool to isolate and study the structure of mitotic chromosomes after sorting certainly because unfixed chromosomes are thought to be fragile and therefore their structural integrity might be altered.

To obtain specific mouse mitotic chromosomes, cells need to be synchronized and harvested at a specific cell cycle stage. Once the cells (here mouse B cell line) reached a 70 % confluency, colcemid is added to the media for a maximum of 6 hours to enrich for mitotic cells (Figure 5-2.A). Colcemid is a drug that inhibits microtubule assembly and therefore blocking the cells in metaphase (Rieder and Palazzo, 1992). The short colcemid incubation time prevents alteration of the mitotic chromosome structure. After colcemid incubation the chromosomes are released from the cells into a polyamine buffer (PAB), that protects the chromosomes from degradation, by mechanical stress after a hypotonic shock (Figure 5-2.A). To distinguish one set of mitotic chromosomes from another, two DNA binding dyes that specifically bind to AT and GC rich (Hoechst and Chromomycin A3 respectively) regions are incorporated to chromosomes in solution prior to sorting. This DNA binding preference generates a bivariate plot where each cluster corresponds to a specific chromosomes population (Figure 5-2.A).

The bivariate plot obtained with our flow cytometer was similar to the one obtained by Bee Ling Ng et al (Figure 5-2.A and B) (Ng and Carter, 2006). To validate this technique, I sorted chromosome 19 as it is nicely separated from the rest of the chromosomes on the flow karyotype (Figure 5-2.B).

Two different techniques were used to validate the enrichment of chromosome 19 after FACS in the collected samples. The first one consists of amplifying the sorted chromosomes by Degenerated Oligonucleotide Primers-PCR (DOP-PCR), using a mouse specific universal primer, to generate a test probe by incorporation of fluorescent dUTP. The test probe (Figure 5-2.B, red signal) is then compared with a reference probe specific for chromosome 19 (Figure 5-2.B green signal) by DNA FISH on metaphase spread cells. The test probe (Figure 5-2.B red signal)

marked only two chromosomes (Figure 5-2.B, validation one middle panel). The same two chromosomes were also tagged with the reference probe (Figure 5-2.B, validation 1 left panel). This suggests that chromosome 19 was accurately sorted with an enrichment superior to 95%.

The other technique used to assess the enrichment of collected chromosomes after sorting is by directly labelling the sorted chromosomes with a reference paint by DNA FISH (Figure 5-2.B, validation 2). FACS chromosomes were marked with the reference paint for chromosome 19 confirming that the sorted chromosomes were the 19. Both of the techniques gave an enrichment superior to 95% (n=20).

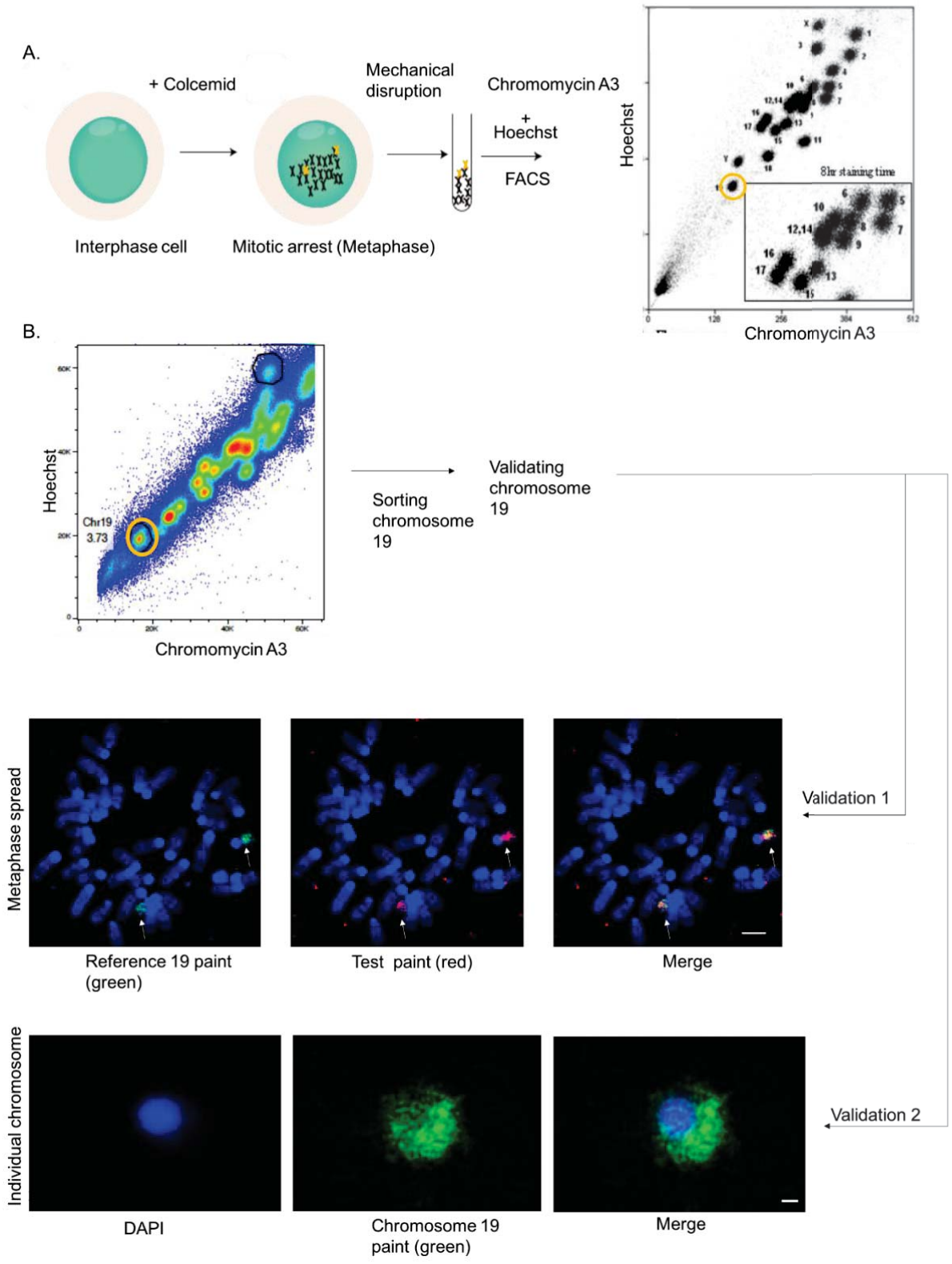

(Legend next page)

Figure 5-2: Isolation of mouse mitotic chromosome 19 by FACS.

(A) Schematic representation of the experimental protocol for isolating mitotic chromosomes by FACS. Chromosomes highlighted in orange represent the chromosomes 19. Hoechst and Chromomycin A3 dyes allowed us to obtain a bivariate plot (B) similar to the one obtained by Bee Ling Ng et al, 2006 (A). Chromosomes 19 was sorted and the purity of the sort was assessed using two different methods. Validation 1 consists of amplifying sorted chromosome 19 preparations and using this a probe (test paint, red) for DNA FISH on mouse metaphase samples. Labelling of the test (red) and a commercial probe for mouse chromosome 19 (Reference paint, green). In Validation 2, sorted chromosome 19 were fixed and labelled with reference paint for mouse chromosome 19 with assistance from Karen Brown. Scale bar =10 µm.

5.3 Visualizing mitotic chromosomes

To date, chromosomes isolated by FACS have not been used to study the structure of mitotic chromosomes. Isolation of chromosomes by FACS involves high pressure sheath flow and encapsulation of mitotic chromosomes within droplets that were then collected. Therefore, chromosome sorting may alter the structure of sorted mitotic chromosomes, thus chromosome shape has to be assessed prior further analysis. Once the enrichment of mitotic chromosomes isolated by FACS was confirmed, we imaged by high-resolution light microscopy and by cryo-EM unfixed mouse mitotic chromosomes before and after sorting.

Unlike human mitotic chromosomes, which possess a typical X shape, mouse mitotic chromosomes are acrocentric and possess two long arms visible by microscopy and two short arms. Structured Illumination Microscopy (SIM) pictures of mouse mitotic chromosome before sorting showed a DAPI stained (Figure 5-3.A, left) mitotic chromosome imaged in solution, where two arms could be seen as well as a stronger DAPI signal corresponding to the centromere.

After sorting, chromosomes 19 still possess two visible arms and a centromere corresponding to the bright DAPI signal (Figure 5-3. B, left). Immunofluorescence of Centromere Protein A (CENPA) revealed two foci (green signal) localized at centromere. CENPA is a histone-like nucleosomal protein that specifically binds to the centromeric region during mitosis (Kunitoku et al., 2003; Zeitlin et al., 2001).

Cryo-EM technique consists of imaging samples, here unfixed chromosomes, in a frozen-hydrated state with a resolution that cannot be achieved by light microscopy (up to 2 Å).

Sample preparations for cryo-EM is relatively simple. Briefly, two to three µl of chromosomes in solution was placed onto a copper grid. The excess of liquid was removed so that only a thin layer of buffer remained (Performed by T.Bharat). The grid is then plunged into liquid ethane which instantaneously freeze the sample allowing us to preserve samples without any chemical fixation. The rapid drop in temperature prevented crystal formation that are deleterious for imaging.

To my knowledge, larger structures such as mitotic chromosomes, have never been imaged using cryo-EM. Figure 5-3.A, right, represents a cryo-EM image of what is assumed to be a mitotic chromosome before sorting, where DNA is the electron dense matter (dark region in Figure 5-3.A, right). Two arms could be seen with a gap in between. Also we assumed that there is a putative centromere indicated by the red arrow in the picture on the right in figure 5-3.A. Fibrous materials coming from the chromosome was visible by cryo-EM, which could be chromatin fibers. This indicates that mitotic chromosomes can be imaged by cryo-EM.

After sorting, cryo-EM data revealed a highly electron dense region corresponding to a potential sorted chromosome 19. The protrusion arising from the electron dense region in this picture represents a putative centromere and the two red arrows indicate the localization of the chromosomes arms. Figure 5-3.C shows chromosomes 19, the shape of the chromosome varies according to the way the mitotic chromosomes 19 are facing the EM-grid.

Area and Aspect Ratio (AR) were calculated from SIM and EM data to assess the degree of compaction of mitotic chromosome 19 after sorting (Figure 5-3.D, left). Boxplots in figure 5-3.D indicated that surface and aspect ratio of mitotic chromosome 19 were consistent in between samples with an average chromosome area obtained by cryo-EM of approximately three μm^2 and an aspect ratio of 1.3. SIM data indicates that the area was around five μm^2 with a large variation in between chromosomes indicated by the minimum and maximum (whiskers in the boxplot) from the boxplot. The high amplitude of the variation for the SIM data in both area and AR could be explained by the difference in sample preparation. Taken together these data suggests that sorted mitotic chromosomes maintained a certain degree of compaction and that some mitotic specific proteins such as CENPA remained attached to mitotic chromosomes.

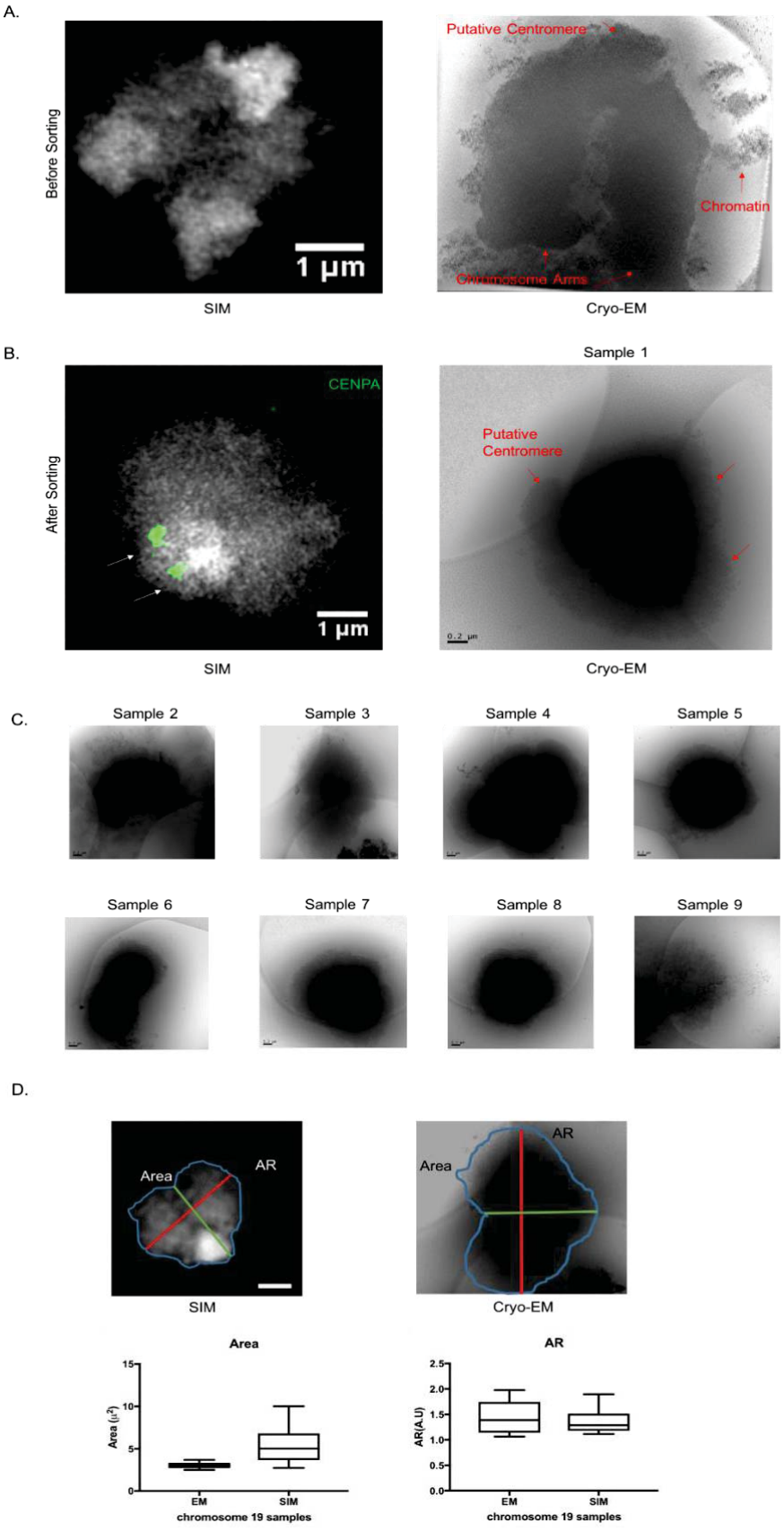

(Legend on the next page)

Figure 5-3: Visualizing by SIM and cryo-EM of mouse mitotic chromosomes 19 isolated by FACS enriched mitotic samples.

(A) Representative images of unsorted and unfixed mitotic chromosomes. Chromosomes imaged by SIM were stained with DAPI (Grey), where the strong DAPI signal correspond to the centromere (Left). Scale bar =1µm. Two chromosome arms could be distinguished on this picture. The overall shape of mitotic chromosomes imaged by cryo-EM (Right) is similar to the shape observed by SIM. Chromosomes imaged by cryo-EM where not stained. Arrows indicate putative chromosomes arms and the putative centromeric region of mouse mitotic chromosome 19. We hypothesized that these were the chromosome arms and centromere based on the information collected from SIM pictures. (B) Representative image of sorted and fixed mouse mitotic chromosome 19 taken with SIM stained with DAPI (Grey) and CENPA (Green foci) detected by immunofluorescence. White arrows indicate the position of CENPA proteins. The bright DAPI signal is specific for the centromere. Scale bar=1µm. Right, Representative image of sorted unfixed and unstained mitotic chromosome 19 taken by cryo-EM. Arrows indicate putative centromere and chromosome arms. Arrowed were placed based on the SIM data. (C) Chromosomes 19 sample used for the area and aspect ratio analysis (D)The electrons dense areas represent the chromosome 19, onto a cryo-EM grid. Differences in shapes are caused by the way chromosomes are dropped onto the grid. (D) Surface area and Aspect Ratio (AR) were calculated from cryo-EM data with n=10. The boxplots represent the surface area and AR of chromosomes 19, where the whiskers are the extrema (i.e minimum and maximum values) and the box edges are the first and last quartiles. Cryo-EM pictures were taken by Tanmay Bharat.

5.4 Cryo-EM tomogram and 3D reconstruction of mouse mitotic chromosomes

Cryo-EM tomography (cryo-EMT) have previously been used to image bacteria or viruses at high-resolution (Bharat et al., 2015). Tomogram acquisition gives access to volumetric data and 3D reconstruction. Here, I am using cryo-EMT to obtain the 3D structure of mitotic chromosomes.

To obtain a tomogram the sample was rotated with an angle of 60 ± degree with an increment of 1 degree, while electrons went through the sample and collected by a detector (Figure 5-4.A). The collected images were then aligned using gold fiducial markers. 3D reconstruction could then be performed using a weighted backprojection algorithm (IMOD software performed by Tanmay Bharat) (Figure 5-4.A). The reason why weighted backprojection was used here is to reduce the blurriness that happened when using normal backprojection leading to better 3D structure. Besides weighted backprojection are efficient compared to other reconstruction algorithms. Represented in figure 5-4.B is a serie of 2D pictures taken from a tomogram at various angles. While the stage is being tilted some part of the chromosome became in focus while others went out of focus were not.

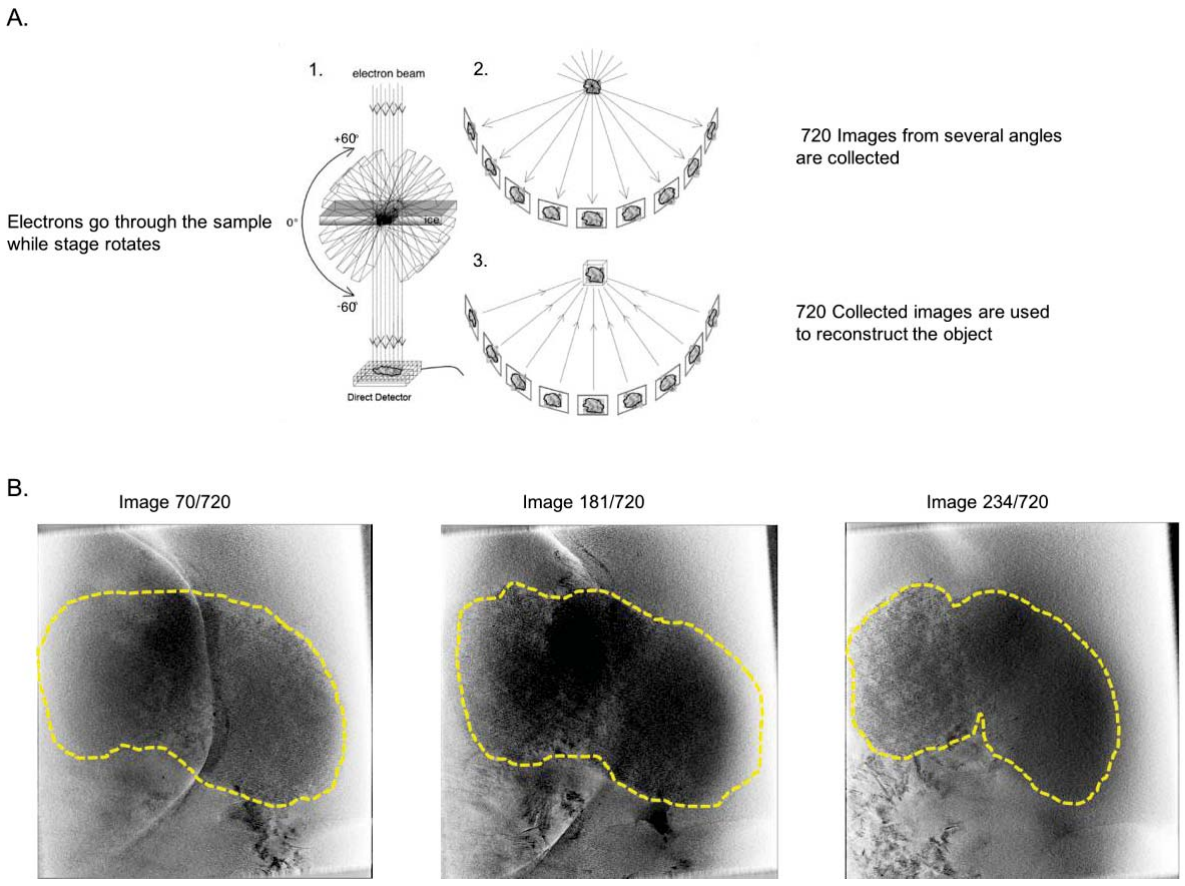

Figure 5-4: Principle of cryo-EM tomography and reconstruction.

(A) Schematic representation of imaging specimen (here chromosomes) by cryo-EM tomography. First, electrons go through the sample while the stage is being tilted from an angle varying between + 70° to -70°. The electrons that go through the samples are collected and for each angle an image is generated (2). After collection, data are processed by Fourier transform to generate a tomogram and ultimately a 3D reconstruction of the specimen. (B) Representative images of a chromosome 19 at different angle. The yellow dashed lines indicates the border of the chromosome. Tomogram were taken by Tanmay Bharat.

Once the tomogram was acquired, 3D reconstruction was performed from which volume could be estimated. The workflow to obtain the volume of mouse mitotic chromosome 19 was indicated in Figure 5-5.B. First the images were reconstructed to form a tomogram, then 3D reconstruction was performed. Here, green represented a reconstruction of a mouse mitotic chromosome 19 on top of a 2D picture. The reconstruction possessed a typical shape of a mouse mitotic chromosome. Volumetric analysis revealed that the volume was consistent between different samples of chromosomes 19 with an average volume of 1.3×10^{12} Å (Figure 5-5.A, right).

It is worth noting that in the tomogram the sub-areas of the mitotic chromosome in figure 5-5.A are more electron dense than others. For example, the putative centromere in figure 5-5.A seems to have a higher electron density compared to the hypothetical chromosome arms. To confirm this hypothesis, pixel intensity analysis was performed on mitotic chromosomes. The histogram revealed that the tomogram could be separated into two distinct regions with high and low pixel intensity corresponding to low electron density and high electron density respectively (Figure 5-5.C). Electron density is inversely proportional to pixel intensity. The low pixel intensity region corresponded to the chromosome whereas the high pixel intensity represented the empty copper grid (background). The tomogram was then divided into regions from which pixel intensity was calculated for each region (Figure 5-5.B). The pixel values of the regions was then plotted as a heatmap (Figure 5-5.D) with, in red the electron dense region and in purple/blue the regions with low electron density. This heatmap was performed to confirm the presence of an electron dense area located at the center of the chromosome. The heatmap data suggests a core electron dense region that could correspond to the centromere. Figure 5-5.E represents a 3D model of a mitotic chromosome in green with the centromere in purple. Taken together these data demonstrated the elaboration of a set of techniques, from the isolation of mitotic chromosomes to the imaging by cryo-EM that allow the study of mouse mitotic chromosome structure in their native state.

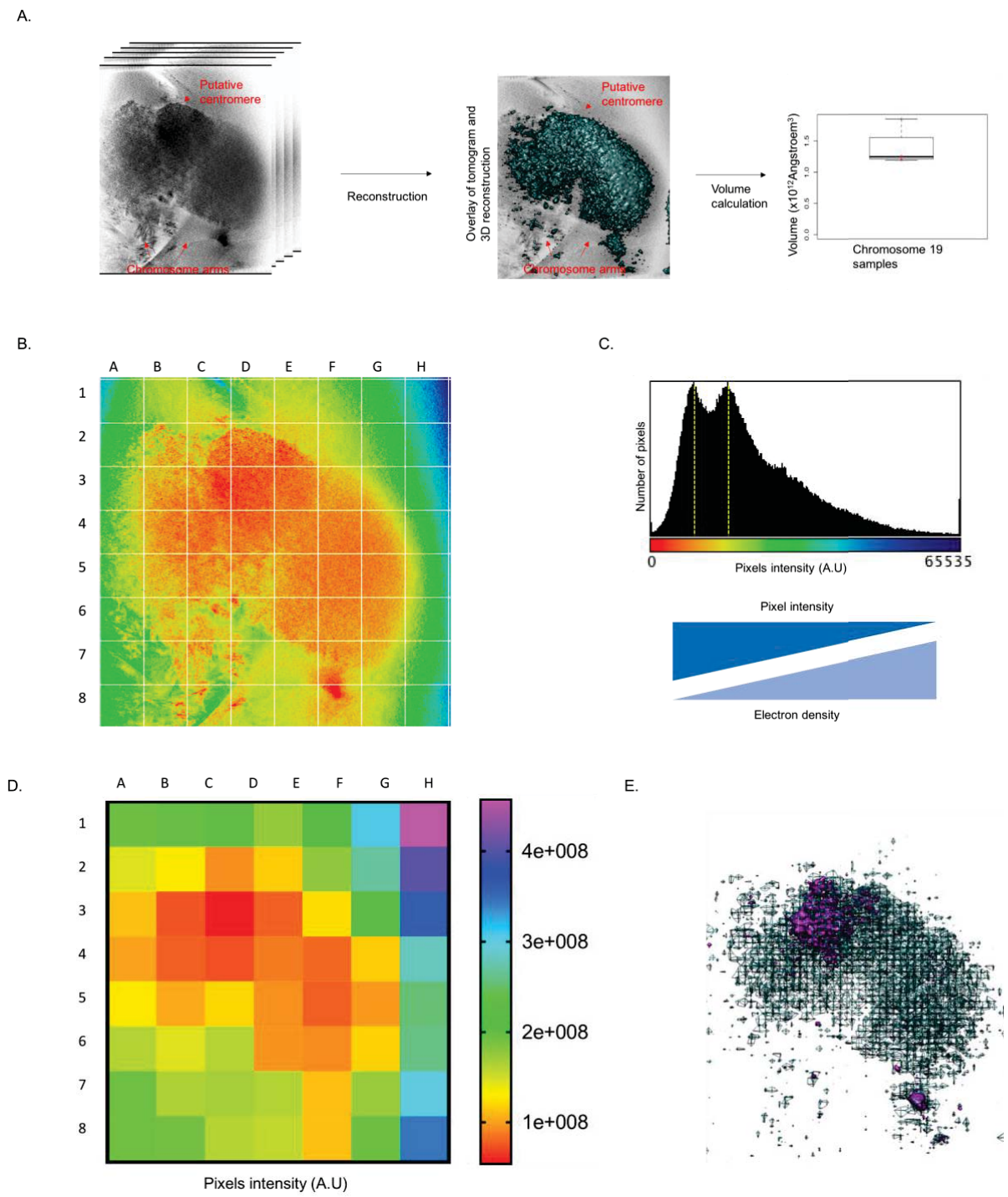

Figure 5-5: Tomographic Reconstruction of mouse mitotic chromosome 19.

(A) Representative workflow of a tomogram to calculate the volume of a mitotic chromosome. Arrows indicate putative centromere and chromosomes arms based on its morphology and electron density. Green represents the 3D reconstruction of mitotic chromosome. (B) 2D picture of a cryo-EM tomogram where the colors indicate the pixel intensity. (D) Histogram representing the pixel intensity of the picture obtained in B. 0 to 65535 indicate the pixel intensity values where blue corresponds to high intensity pixels and red low intensity pixels. Intensity of the pixels are inversely proportional to electron density. (D) Heatmap from the picture in B where each square correspond to the average pixel intensity value correspond to the square represented in B. (E) Model of mouse mitotic chromosome 19 where purple corresponds to electron dense region.

5.5 Cohesin depletion in mitotic chromosomes

Next, I decided to use this set of techniques to investigate the role of cohesin in the structure of metaphase chromosomes. Waizenegger et al., have shown that cohesin is removed from mitotic chromosomes by two distinct pathways. First most of cohesin was removed between the prophase and metaphase steps, this step does not involve cleavage of Rad21 subunit of the cohesin complex. This lead to the removal of most the cohesin, only a small percentage is left and localized at the centromere. During the metaphase-anaphase transition, Rad21 is cleaved by the separin protein and cohesin is released from mitotic chromosomes (Figure 5-6).

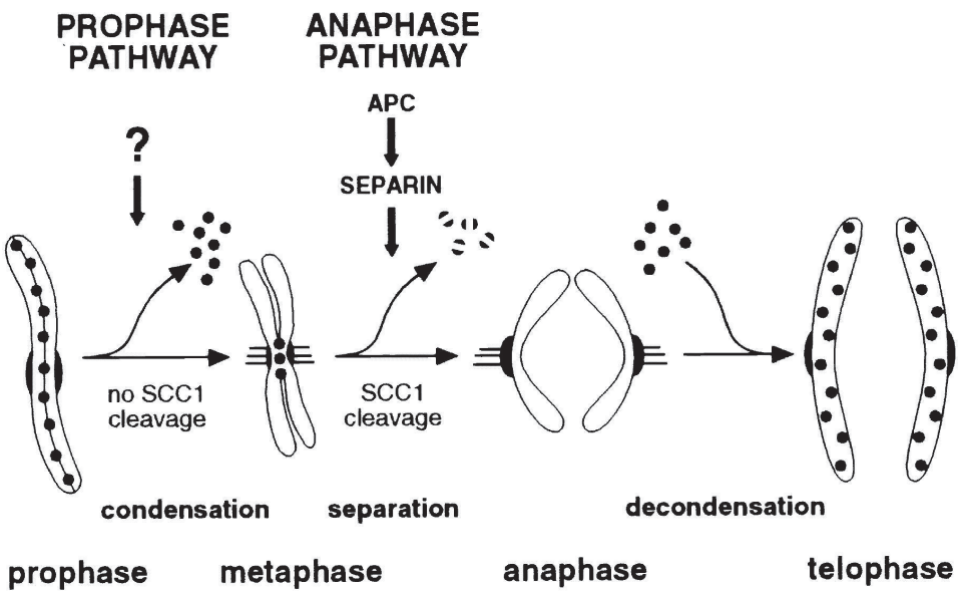

Figure 5-6:Dynamics of cohesin in mitosis.

Most of the cohesin complex is removed from mitotic chromosomes during prophase to metaphase transition. The remaining of cohesin, localized at the centromere, is cleaved by the separin enzyme between metaphase and anaphase. Cohesin is depicted with black dots. (Waizenegger et al., 2000).

To study the effect of Rad21 depletion on mitotic chromosomes, I took advantage of a Rad21 cleavable pre B cell line previously established in the laboratory. Rad21 has been genetically modified to contain a TEV cleavage site and a c-terminal myc-tag to facilitate the detection of Rad21 fragments (Figure 5-7.A). Cleavage of Rad21 lead to removal of cohesin from mitotic chromosome 19. This allowed me to study the role of cohesin on mitotic chromosome structure. I first isolated mouse mitotic chromosomes 19 by FACS using the same protocol as before (Figure 5-7.B). Once chromosome 19 was isolated, the Rad21 subunit was cleaved in the presence of TEV-protease creating two fragments (Figure 5-7.C).

The same number of sorted chromosomes 19 was treated with and without TEV-protease, both samples contained the exact same buffer condition. After an overnight incubation half of the chromosomes were cryo-preserved on an EM grid to image them, while the other half was used to assess the efficiency of the cleavage (Figure 5-7.D). To detect the cleaved and uncleaved band, c-myc tag antibody was used. As expected, western blot analysis on sorted chromosomes 19 showed that the uncleaved sample possess only one band around 180kDa (expected uncleaved band size 165kDa). The sample treated with TEV protease also possessed only one band with a different molecular weight (65kDa), which was consistent with the length of the tagged fragment, and no band around 180kDa indicating that the cleavage of Rad21 by TEV protease was successful. Quantitative analysis confirmed the efficiency superior to 95% (Figure 5-7.D).

Once it has been confirmed that Rad21 can be cleaved in solution on sorted mitotic chromosomes 19 by TEV-protease, cryo-EM was used to image in 2D and by tomogram (3D) mitotic chromosomes 19 treated and non-treated with TEV-protease (+ and – TEV respectively). To determine if loss of cohesin affects the chromatin compaction of mitotic chromosome 19, chromosomal area was assessed from 2D cryo-EM images for both conditions. Chromosomal volume would have most likely given us similar information. Tomography is quite time consuming therefore we did not obtain enough 3D tomogram of chromosomes to have a robust analysis of chromatin compaction compared to 2D pictures. Without TEV-protease treatment, the average area of chromosome 19 was around 6 μm^2 whereas with TEV protease treatment, the average area of chromosomes 19 is around 8 μm^2

with a maximum of 19 μm^2 for some chromosomes. This data indicates that chromosomes 19 treated with TEV-protease increase in area compared to chromosomes 19 non-treated with TEV-protease. Statistical analysis revealed that the difference in area was significant (Figure 5-7.F). Additionally, cryo-EM tomogram revealed that non-treated chromosome 19 (-TEV) possess a shape consistent with the shape of mouse mitotic chromosomes with two distinct arms visible (Figure 5-7. E, left). However, mitotic chromosomes 19 treated with TEV-protease (+TEV) no arms could be seen, only chromatin without any specific arrangement (Figure 5-7.E, right). Besides, the treated chromosomes (+TEV) appeared to occupy a larger volume and chromatin seemed more loose compared with the untreated sample. This result was unexpected as cohesin is thought to be localized at the centromere in metaphase chromosomes, therefore its depletion should not affect the compaction of the chromatin located on the chromosome arms. The area and volume measurement of the mitotic chromosomes could not be affected by non-mitotic chromosomes due to stringent gates performed during sorting, where non-mitotic chromosomes would have been considered as debris. A control experiment was performed on WT chromosomes to verify if TEV protease was specifically cleaving TEV chromosomes. This experiment was carried out on WT unsorted chromosomes and revealed no difference in shape or structure between treated and untreated TEV samples (data not shown). This experiment will have to be performed using sorted mitotic chromosomes and analyzed by cryo-EM to confirm these preliminary results.

Taken together these results indicate that the removal of cohesin from mouse mitotic chromosomes increases the size of mitotic chromosomes suggesting a decondensation of the mitotic chromatin fibres. Further analysis needs to be performed in order to confirm this unexpected finding.

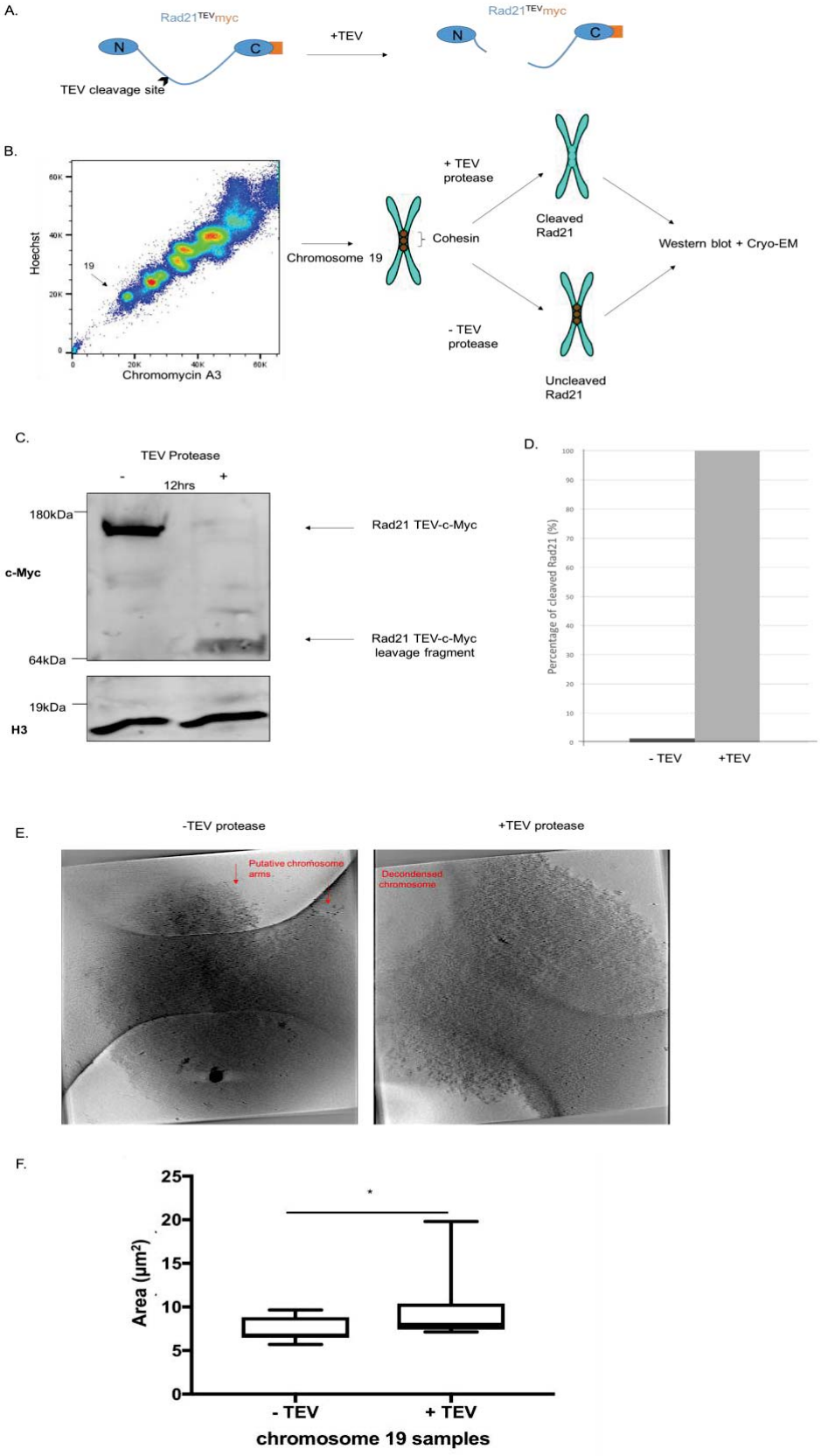

(Legend on the next page)

Figure 5-7: Depletion of Rad21 on mitotic chromosomes leads to decondensation of the chromatin fibers.

(A) Schematic representation of Rad21 cleavage principle. (B) Schematic representation of the experimental system. Mitotic chromosomes 19 were isolated by FACS using Hoechst (HO) and Chromomycin A3 (CA3). After isolation, chromosomes were treated with (+) and without (-) TEV protease. The enzyme will cleave Rad21 cohesin subunit; and cryo-EM and Western blot analysis was performed on both samples (+ and - TEV). The efficiency of the cleavage of Rad21 was detected by western blot analysis and quantify after an overnight incubation (12 hours) (C). H3 was used as a loading control for western blot analysis. (D) Quantitative analysis of Western blots to assess the cleavage efficiency with n=2. (E) Representative images taken from a tomogram of chromosome 19 treated with (+TEV) and without TEV (-TEV). (F) Chromosomal area of treated (+TEV) and untreated (-TEV) mitotic chromosome 19 with n=19. Two tails Student's t-test was performed with $p<0.05$. Cryo-EM performed by Tanmay Bharat.

5.6 Discussion and future work

In this chapter, I have used FACS and DNA binding specific dyes to isolate specifically mouse mitotic chromosome 19. I chose chromosome 19 because it is well separated by Flow karyotyping. I confirmed the identity of the chromosomes 19 in two different ways. First, I used the sorted chromosomes to create a fluorescent probes and used it on metaphase spread chromosomes combined with DNA FISH. The fluorescent signal from the probe originated from the sorted chromosomes was compared with a commercially available probe that specifically stains chromosome 19 (reference probe). The other validation technique consisted of directly staining the sorted chromosomes with the reference probe (Figure 5-2). My data suggest that other chromosomes, such as the X chromosome can be sorted and analyzed using analogous approaches. The validation techniques allowed us to see whether samples are contaminated by other mitotic chromosomes.

Flow karyotyping has previously been used to generate fluorescent probes or to sequence an entire chromosome (Rabbitts et al., 1995). However, for these previous applications verifying the integrity of sorted chromosomes was not important. Here, the aim of my study was to study the structure of mitotic chromosomes, thus I had to verify the structure after sorting of mitotic chromosomes by visualizing them using SIM and cryo-EM. SIM imaging revealed that after sorting, chromosome shape is consistent with mouse mitotic chromosomes and retain some proteins specific for mitotic chromosomes such as CENPA. To further confirm the integrity of mitotic chromosomes isolated by FACS, telomere proteins should have been verified as well. Unfortunately, proteins from the sheltering complex are hard to visualized in mouse mitotic chromosomes particularly on the chromosome 19 which is the smallest one. Generation of a cell line containing a fluorescent tag for a protein from the sheltering complex is currently being made in my host laboratory to overcome this issue.

I also confirmed that mitotic chromosomes could be imaged without any chemical fixation, avoiding any artefact from the fixation step, using cryo-EM (Kellenberger et al., 1992). The area and aspect ratio of mitotic chromosomes 19 variation is low indicating an overall intact structure in between chromosomes 19 (Figure 5-3). Chromosomes were preserved by plunge freezing and no staining visible in EM was performed, thus it was difficult to distinguish specific

features of mitotic chromosomes such as the centromere or telomeres. Cryo-EM can be used to take tomograms, which can then be used to create a three-dimension model of mitotic chromosomes. However, since chromosomes were extremely electron dense, little can be extracted regarding the structure of mitotic chromosomes from the 3D reconstruction. Volumetric analysis of 3D reconstructed chromosomes revealed a volume constant in between chromosomes. Pixel density revealed a higher density in one specific area, which could correspond to the centromere of mitotic chromosome (Figure 5-5). To confirm the localization of the centromere gold immunostaining for CENPA was performed on mitotic chromosomes. Gold nanoparticles were too large (10 nm) to allow the antibody to bind to CENPA (data not shown). This phenomenon named steric hindrance explain why CENPA immunolabeling worked with fluorescence but not with gold nanoparticle (Ribrioux et al., 1996). Since mitotic chromosomes are large and condensed entities to image with cryo-EM smaller gold nanoparticles would be harder to distinguish by cryo-EM.

In this first part, I have been able to establish a set of tool that allowed me to isolate a specific subset of chromosomes. Chromosomes can be further imaged unfixed using cryo-EM, which allow us to obtain surface and volumetric measurement from mitotic chromosomes in their native state. As a proof of concept, I decided to study the impact on mouse mitotic chromosomes of cohesion depletion. Rad21 cleavage was successfully performed using TEV protease on sorted chromosomes and assessed by western blot analysis (Figure 5-7.C and D) suggesting that cohesin was removed from mitotic chromosomes. Loss of cohesin increased the surface area of chromosomes (Figure 5-7.F) and cryo-EM tomograms showed an unraveled chromatin structure in mitotic chromosomes 19 without cohesin (Figure 5-7.E). This suggests that some cohesin remained attached to mitotic chromosomes throughout the transition between prophase to metaphase and that it could play a role in chromatin condensation during mitosis. Another potential explanation for the loss of compaction in mitotic chromosomes 19 could be that cohesin loss triggers centromere decondensation. This in turn affects the compaction of the chromosomes arms. This suggests a crucial role for centromere in chromosomes structure.

FUTURE WORK

Isolation of mitotic chromosomes by FACS requires staining of chromosomes which may alter the structure of mitotic chromosomes by disrupting DNA interaction (Chatterjee et al., 2001; Durand and Olive, 1982; Nayak et al., 1975). Besides FACS is a relatively harsh process on cells and can cause damages to the cells (Emre et al., 2010).

To avoid DNA damage from the DNA dyes and potential damages due to sorting, microfluidics chip could be used to isolate mitotic chromosomes based on their size. To do this, a device could be design to extract mitotic chromosomes from cells, then separate and isolate mitotic chromosomes based on their size. With this technique mitotic chromosomes could then be imaged without dyes or fixations avoiding the potential artefacts.

Chapter 6 : GENERAL DISCUSSION AND FUTURE WORK

Reprogramming is a process in which one cell type is converted to another one. An example of reprogramming was performed by Choi et al., where fibroblasts became myoblast using MyoD (Choi et al., 1990). Reprogramming towards pluripotency is the transformation of a differentiated cell towards a pluripotent cell such as ES cells. Reprogramming towards pluripotency can be achieved experimentally using three different approaches. In 1962 John Gurdon developed SNCT where one somatic cell nucleus is inserted inside an enucleated oocyte (Gurdon, 1962). In 2006 Yamanaka developed a new method to obtain pluripotent cell (iPS) using four ectopic transcription factors (OSKM) (Takahashi and Yamanaka, 2006). Finally, the third method to reprogram somatic cells towards pluripotency is cell fusion where a somatic cell is fused with a pluripotent cell (Harris and Watkins, 1965). Cell fusion based reprogramming is the least well-known technique and allow us to study earliest molecular event in reprogramming and its requirements (Piccolo et al., 2013). In this thesis chapters 3 and 4 were aiming at obtaining a better understanding on reprogramming towards pluripotency mediated by cell fusion. This was done by investigating new potential factors crucial for reprogramming, or by studying the epigenetic remodeling of one chromosome upon reprogramming.

This last chapter will be divided into three parts. The first part will be focused on the importance of ploidy in reprogramming towards pluripotency, the second part will be focused on X chromosome reactivation and finally the third part will describe future works that could be done using chromosome sorting and cryo-EM to visualize chromatin structural changes under different conditions.

6.1 Ploidy: an important factor for reprogramming somatic cells towards pluripotency?

In Chapter 4, I assessed the reprogramming potential of haploid ES cells compared to diploid ES cells. I showed that haploid ES cells are able to reprogram with a much lower potential compared to diploid ES cells (Figure 6-1. Top). The low induction of human pluripotent genes in haploid ES cells could be due to several reasons. The concept of dominance in reprogramming one cell type towards another, means that one of the two cell type (dominant) will trigger a nuclear reprogramming on the other cell which lead to the erasure of repressive epigenetic marks to induce expression of genes from the dominant cells (Soza-Ried and Fisher, 2012). This lead the non-dominant cell to a radical change in both transcriptome and phenotype. In this specific case of reprogramming towards pluripotency, the ES cells dominantly reprogram the somatic cells (Miller and Ruddle, 1976). However, the reprogramming efficiency is low (up to 1%). Haploid ES cells reprogramming potential was even lower than the diploid ES cells reprogramming potential. One possible explanation could be that ploidy plays an important role in reprogramming towards pluripotency. In other words, the cells with a higher number of chromosomes dominantly reprogram ES cells. Ploidy is defined as the number of chromosome sets within a cell. Most mammalian cells possess two sets of chromosomes. Gametes possess only one set of chromosomes. Recently, haploid ES cells were derived from gametes and possess also one set of chromosome. Ploidy is often associated with cell size where haploid cells tend to be smaller than diploid cells, tri or tetraploid cells are larger than diploid ES cells. It has been suggested that to maintain a similar concentration in haploid, diploid, tri and tetraploid cells, the absolute number of RNA varies (Padovan-Merhar et al., 2015). Larger cells contain more absolute number of RNA molecules, whereas smaller cells have less total number of RNA. In the case of the experiments performed addressed in this thesis, haploid ES cells were smaller than diploid ES cells, as it could be seen on FACS profile (data not shown) and the total RNA and protein content were also less in haploid than in diploid cells. Whether the ploidy number is directly linked to RNA and protein level in a linear fashion is not quite clear. Therefore, it is difficult to assess whether it is the ploidy itself or the cell size that could affect the reprogramming potential of haploid ES cells. Ideally, if haploid somatic cells were available, an additional experiment could confirm that ploidy itself and no other factors inherent to ploidy affect cell fusion reprogramming. This

experiment would consist of fusion haploid ES cells with haploid somatic cells. The efficiency of reprogramming should be comparable to the one from a fusion between two diploid cells (Figure 6-1.B top). A more representative experiment could be to fuse either haploid or diploid ES cells with a tri or tetraploid somatic cells. Here, the expected results would be a low reprogramming potential comparable to the one from haploid ES cells with diploid somatic cells (Figure 6-1 bottom).

In the chapter 3 of this thesis, I demonstrated that the fibroblasts used for reprogramming had a near tetraploid karyotype that led to karyotypically unstable hybrid cells. I also suspected that the low reprogramming potential could be due to this tetraploid karyotype and evoke previous publication to support this theory. 4n fibroblasts fusion with 2n ES cells would tend to generate more fibroblasts like hybrid cells than ES cell-like hybrids. Indeed, during hybrid clone isolation, I noticed fibroblasts 10 to 13 days after fusion despite drug selection. Those fibroblasts had multiple nuclei compared to fibroblasts prior to fusion, suggesting that they were fused with ES cells but instead of reprogramming towards ES cells the fibroblasts dominantly reprogrammed the diploid ES cells. Taken together, these results suggest that ploidy plays an important role in the direction of reprogramming. It suggests that cells with higher number of chromosomes dominantly reprogram the other cells partner.

Another explanation for the low reprogramming potential of haploid ES cells could be linked to the somatic cell fusion partner. Several hypotheses have been proposed to explain why specific type of somatic cells have a lower reprogramming potential. Terminally differentiated cells are less efficient to reprogram towards pluripotency compared to less differentiated cells (Piccolo et al., 2011b). As an example, neural stem cells (NS) have a higher reprogramming potential compared to fibroblasts or B cells (Silva et al., 2006). In the case of haploid ES cells, the fusion was performed with B cells. B cells are non-adherent cells, during the fusion experiment it was difficult to assess by light microscopy whether hybrid cells were generated with a B cell like phenotype. To verify the assumption that haploid ES cells fused with diploid somatic cells dominantly reprogram towards diploid somatic cells, a fusion experiment should be performed with adherent somatic cells such as fibroblast. Indeed, a recent study from 2017 showed that ES cells fused with fibroblast generated two types of hybrids: ES cells like and fibroblast like hybrids (Matveeva et al., 2017).

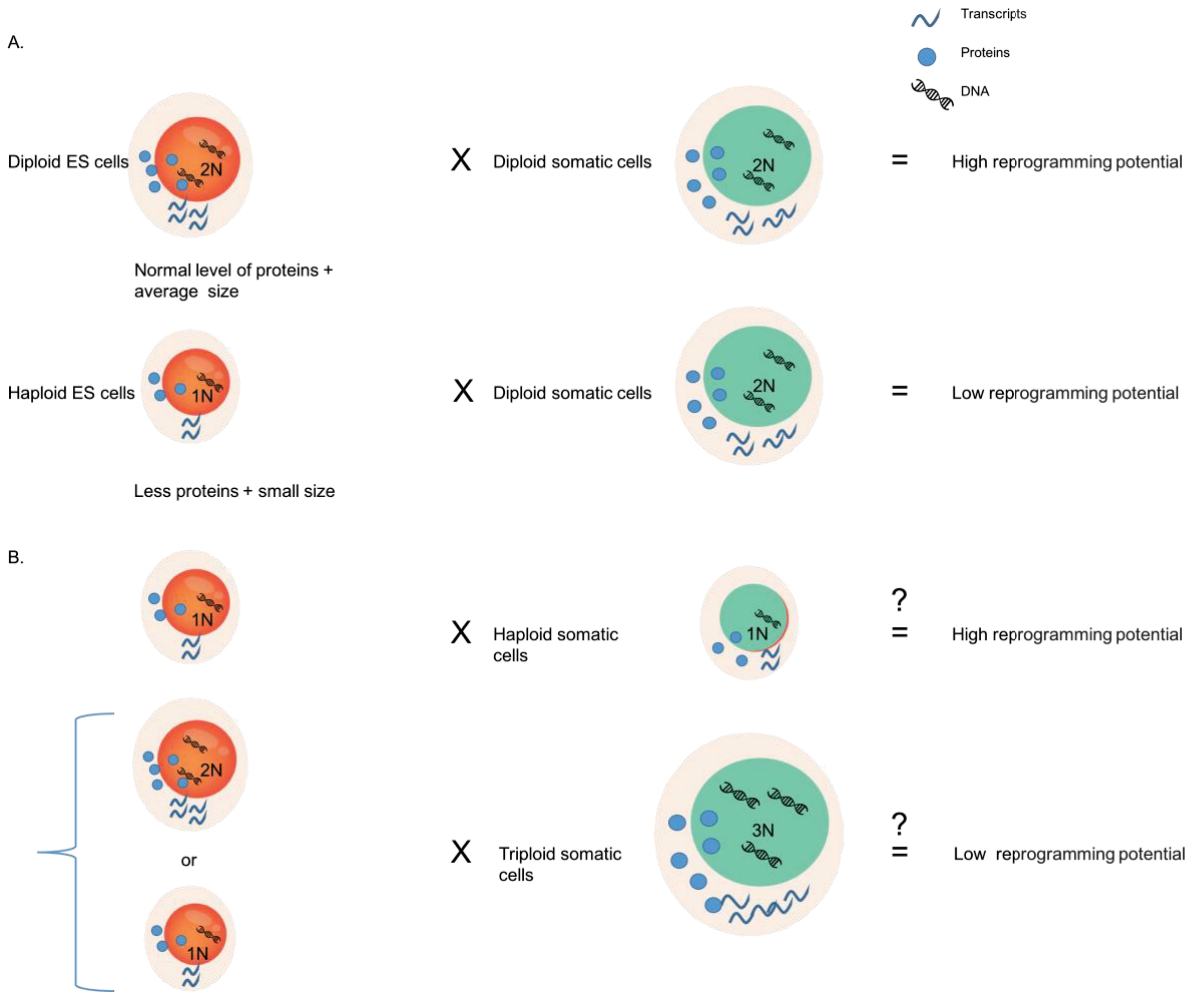

Figure 6-1: Role of ploidy in reprogramming towards pluripotency.

(A) Schematic representation of the experimental results obtained in chapter 4 in which I demonstrated that haploid ES cells had a lower reprogramming potential than diploid ES cells. This could be due to lower amount of proteins present in the haploid ES cells. The reason behind the lower amount of proteins is hard to determine whether it is a direct consequence of DNA copy number or to other factors such as the size of the cells. (B) Schematic representation of the hypothetic outcome of fusion between cells with different ploidy. If the both cell types were haploid, the reprogramming efficiency should be similar to the one obtained from a fusion between two diploid cell types. On the other hand, if cell fusion is performed between haploid or diploid ES cells and tri or tetraploid ES cells, the outcome should be a low reprogramming potential.

6.2 X chromosome reactivation

A pertinent example of epigenetic remodeling is the reactivation of the Xi in female somatic cell upon reprogramming. Understanding how the epigenetic remodeling occurs and whether the is also physical or architectural changes regarding the Xi reactivation could allow a better understanding of epigenetic erasure. In the chapter 3 of this thesis, I demonstrated that it was possible to reactivate some genes from the previously inactive X chromosome. This process of reactivation is a hallmark of reprogramming towards pluripotency. However, other mechanism exist that reactivates Xi genes. As an example some cancer cells (breast and ovarian cancers) harbor two active X chromosomes (Chaligné and Heard, 2014). Another way of reactivating some X-linked genes is the pharmaceutical approach that uses molecule such as TSA, VPA or 5-AzaC to modify the chromatin environment of somatic cells. This could be used to understand the mechanism of Xi reactivation prior to cell fusion. Drugs that either promote histone acetylation or demethylate DNA may make DNA more accessible to transcription factors and cells more prone to reprogramming (Fisher and Cantone, 2017). This is important for cell fusion as promoting a better access of pluripotency associated factors from the ES cell to somatic cell DNA, may enhance erasure of the epigenetic memory and in this case promote Xi reactivation. Furthermore, Cantone et al., have recently demonstrated that the use of 5-AzaC increase the number of X-linked genes reactivated upon reprogramming (Cantone et al., 2017). Very recently Lee and colleagues published an early report showing the reactivation of the Xi as a potential treatment for the Rhett syndrome (Carrette et al., 2018). This highlight the importance of studying Xi reactivation.

6.3 Future work

As previously mentioned in the introduction chapter, in female mammals one of the two X chromosomes is silenced. This silencing of an entire chromosome involves several epigenetic mechanisms leading to a more compact inactive X chromosome in interphase cells. Recently Hi-C data and mathematical modeling showed that the inactive and the active X chromosome have a different 3D structure (Nora et al., 2012). Indeed, the inactive X chromosomes possess two distinct (Topologically Associating Domain) TAD. Mitotic active and inactive X chromosomes may behave differently compared to interphase chromosomes. In human XIST does not remain on the mitotic inactive X chromosomes (Duthie et al., 1999). Therefore, it might be interesting to investigate the differences in structure of active and inactive mitotic X chromosomes. The structural difference between mitotic active and inactive X chromosomes would most likely be difficult to detect with light microscopy due to the diffraction limits. As mentioned in the introduction, EM allows a resolution better than the one achieved by light microscopy (up to 10 nm). The set of techniques that I developed in my last thesis chapter could be used to assess the potential differences between the active and the inactive chromosomes. Both X chromosomes would be isolated by flow cytometry. The active and inactive X chromosomes could be distinguished by either flow karyotyping using a fluorescently tagged protein enriched on the inactive X chromosomes such as the histone variant macroH2A which remains on the inactive X chromosomes during mitosis (Mermoud et al., 1999). This would allow us, by gating the entire X chromosomes population, to sort two distinct populations macroH2A high and low corresponding to inactive and active X chromosomes respectively. The recent CRISPR/cas9 technology could be used to insert a tag to the endogenous locus. The tag could be one of those recent clip/Snap technology. Another way of separating the active from the inactive X chromosomes would be by native immunolabeling which has already been implemented for EM and showed promising results (Yi et al., 2015). Steric hindrance can affect the binding of the antibodies to its epitope, this is mostly due to the size of the gold nanoparticle. As an alternative, the area and volume of the active X chromosomes could be experimentally obtained by sorting the unique active X chromosomes from the female haploid ES cells. Then using advanced data processing the volume and area of the inactive and active X chromosomes could be distinguished.

Another application for cryo-EM would be to follow over time the structural changes that happens during reactivation of Xi upon reprogramming towards pluripotency. Indeed, previous studies suggested that complete reactivation of the Xi happens through a series of steps. Arresting hybrid cells, arising from cell fusion between mouse ES cells and female somatic cells, in mitosis would be one way of obtaining Xi at different stages of the Xi reactivation. Hybrid cells have the advantage of undergoing mitosis contrary to heterokaryons. Besides, this will allow us to study X reactivation architectural changes throughout the reprogramming towards pluripotency process. Compared to human iPS, generation of mouse hybrid cells have the advantages of not suffering from the erosion of the X chromosome already characterized in various studies (Kim et al., 2014; Vallot et al., 2015). This type of analysis wouldn't necessary need the use of flow karyotyping to isolate the X chromosomes. Other high resolution microscopy technique could be used as well to characterize the potential structural changes happening to the Xi during its reactivation. However, none of the light super resolution microscopy techniques are able to reach a resolution similar to cryo-EM. Never the less for a preliminary study, assessing an increase in area on the inactive Xi would be ideal. This could be performed by SIM for example were reactivation of the Xi would be determined by loss of a Xi specific mark such as macroH2A or H3K27me3.

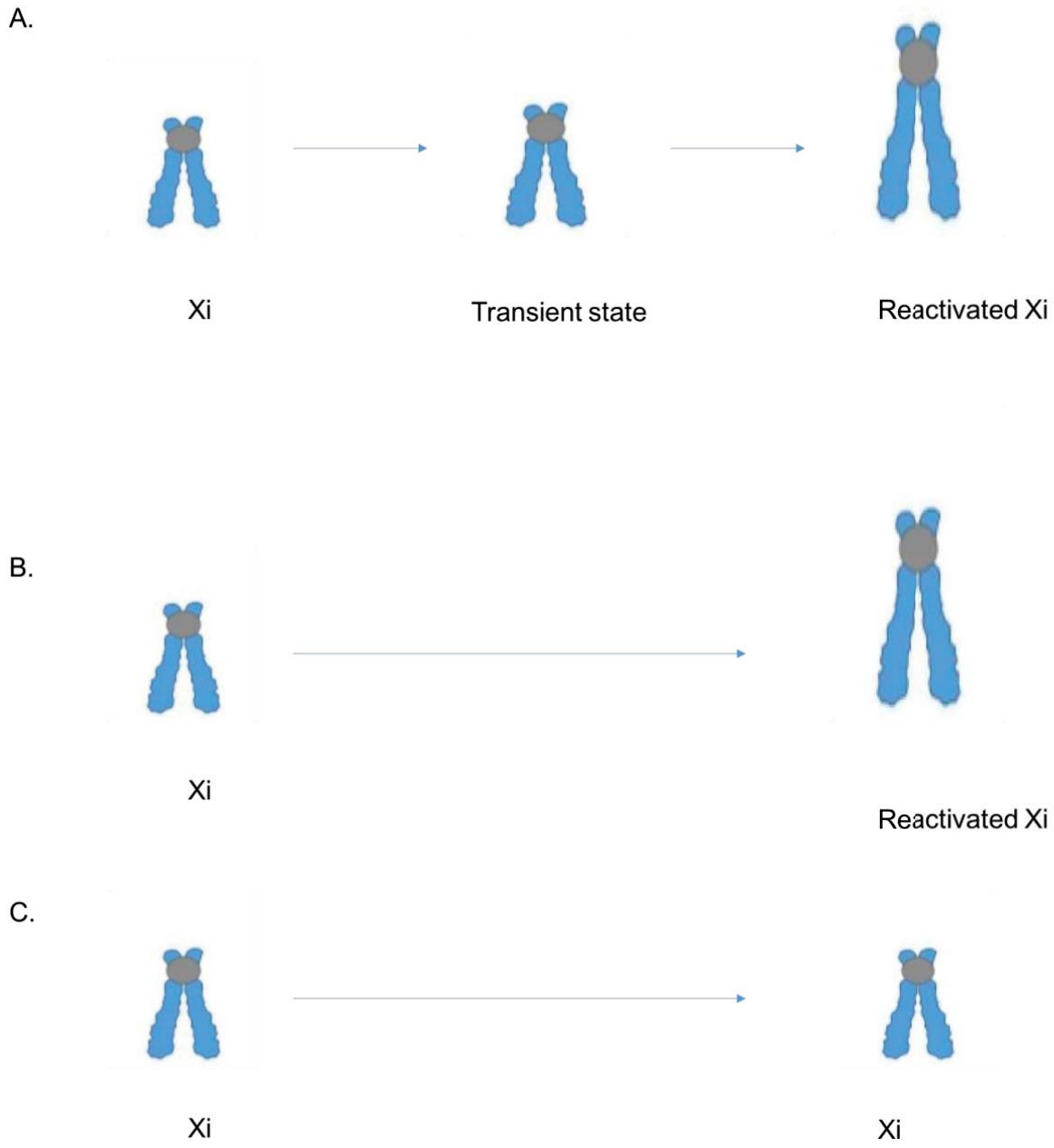

Figure 6-2: Structural changes during Xi reactivation.

Schematic representation of the hypothetical structural changes happening during Xi reactivation. During the reactivation Xi goes through a progressive unravelling until it reaches a shape similar to the Xa with a potential distinctive transient state (A) or without a transient state (B). Another possibility would be that no noticeable changes occur (C).

In the last couple of years, the field of structural biology reached a breakthrough with the technical improvements of cryo-EM. However, the use of cryo-EM in epigenetic remains quite sporadic. This is most likely due to the technical challenges of imaging an entire mammalian cells and DNA within the cell. In this thesis and with the examples mentioned above I presented a technique to study epigenetic differences characterized by the variations of mitotic chromosome structure. The new development of algorithms to obtain better data with a lower signal to noise ratio combined with better detectors will make cryo-EM an excellent tool to study structural modifications of DNA within the cell during epigenetic reprogramming. This will allow us a deeper understanding of the molecular mechanisms of reprogramming towards pluripotency.

BIBLIOGRAPHY

Arkesteijn, G., Martens, A., and Hagenbeek, A. (1988). Bivariate flow karyotyping in human Philadelphia-positive chronic myelocytic leukemia. Blood *72*.

Avilion, A.A., Nicolis, S.K., Pevny, L.H., Perez, L., Vivian, N., and Lovell-Badge, R. (2003). Multipotent cell lineages in early mouse development depend on SOX2 function. Genes Dev. *17*, 126–140.

Azuara, V., Perry, P., Sauer, S., Spivakov, M., Jørgensen, H.F., John, R.M., Gouti, M., Casanova, M., Warnes, G., Merkenschlager, M., et al. (2006). Chromatin signatures of pluripotent cell lines. Nat. Cell Biol. *8*, 532–538.

Barakat, T.S., Gunhanlar, N., Pardo, C.G., Achame, E.M., Ghazvini, M., Boers, R., Kenter, A., Rentmeester, E., Grootegoed, J.A., and Gribnau, J. (2011). RNF12 activates Xist and is essential for X chromosome inactivation. PLoS Genet. *7*, e1002001.

BARR, M.L., and MOORE, K.L. (1957). Chromosomes, sex chromatin, and cancer. *2*, 3–16.

Barr, M.L. & Bertram, E.G. (1949). A morphological distinction between neurones of the male and female, and the behaviour of the nucleolar satellite during accelerated nucleoprotein synthesis. Nature *163*, 676.

Belmont, A.S., Sedat, J.W., and Agard, D.A. (1987). A three-dimensional approach to mitotic chromosome structure: evidence for a complex hierarchical organization. J. Cell Biol. *105*, 77–92.

van den Berg, D.L.C., Zhang, W., Yates, A., Engelen, E., Takacs, K., Bezstarosti, K., Demmers, J., Chambers, I., and Poot, R.A. (2008). Estrogen-related receptor beta interacts with Oct4 to positively regulate Nanog gene expression. Mol. Cell. Biol. *28*, 5986–5995.

Bernstein, B.E., Mikkelsen, T.S., Xie, X., Kamal, M., Huebert, D.J., Cuff, J., Fry, B., Meissner, A., Wernig, M., Plath, K., et al. (2006). A Bivalent Chromatin Structure Marks Key Developmental Genes in Embryonic Stem Cells. Cell *125*, 315–326.

Bestor, T.H. (2000). The DNA methyltransferases of mammals. Hum. Mol. Genet. *9*, 2395–2402.

Bestor, T., Laudano, A., Mattaliano, R., and Ingram, V. (1988). Cloning and sequencing of a

cDNA encoding DNA methyltransferase of mouse cells. The carboxyl-terminal domain of the mammalian enzymes is related to bacterial restriction methyltransferases. J. Mol. Biol. *203*, 971–983.

Bharat, T.A.M., Murshudov, G.N., Sachse, C., and Löwe, J. (2015). Structures of actin-like ParM filaments show architecture of plasmid-segregating spindles. Nature *523*, 106–110.

Bhutani, N., Brady, J.J., Damian, M., Sacco, A., Corbel, S.Y., and Blau, H.M. (2010). Reprogramming towards pluripotency requires AID-dependent DNA demethylation. Nature *463*, 1042–1047.

Blewitt, M.E., Gendrel, A.-V., Pang, Z., Sparrow, D.B., Whitelaw, N., Craig, J.M., Apedaile, A., Hilton, D.J., Dunwoodie, S.L., Brockdorff, N., et al. (2008). SmcHD1, containing a structural-maintenance-of-chromosomes hinge domain, has a critical role in X inactivation. Nat. Genet. *40*, 663–669.

Booth, D.G., Beckett, A.J., Molina, O., Samejima, I., Masumoto, H., Kouprina, N., Larionov, V., Prior, I.A., and Earnshaw, W.C. (2016). 3D-CLEM Reveals that a Major Portion of Mitotic Chromosomes Is Not Chromatin. Mol. Cell *64*, 790–802.

Brambrink, T., Foreman, R., Welstead, G.G., Lengner, C.J., Wernig, M., Suh, H., and Jaenisch, R. (2008). Sequential Expression of Pluripotency Markers during Direct Reprogramming of Mouse Somatic Cells. Cell Stem Cell *2*, 151–159.

Busslinger, M., Nutt, S.L., Heavey, B., and Rolink, A.G. (1999). Commitment to the B-lymphoid lineage depends on the transcription factor Pax5. Nature *401*, 556–562.

Cantone, I., and Fisher, A.G. (2017). Human X chromosome inactivation and reactivation: implications for cell reprogramming and disease. Philos. Trans. R. Soc. B Biol. Sci. *372*, 20160358.

Cantone, I., Bagci, H., Dormann, D., Dharmalingam, G., Nesterova, T., Brockdorff, N., Rougeulle, C., Vallot, C., Heard, E., Chaligne, R., et al. (2016). Ordered chromatin changes and human X chromosome reactivation by cell fusion-mediated pluripotent reprogramming. Nat. Commun. *7*, 12354.

Cantone, I., Dharmalingam, G., Chan, Y.-W., Kohler, A.-C., Lenhard, B., Merkenschlager, M., and Fisher, A.G. (2017). Allele-specific analysis of cell fusion- mediated pluripotent reprograming reveals distinct and predictive susceptibilities of human X-linked genes to

reactivation. Genome Biol. 2017 182.

Carrette, L.L.G., Wang, C.-Y., Wei, C., Press, W., Ma, W., Kelleher, R.J., and Lee, J.T. (2018). A mixed modality approach towards Xi reactivation for Rett syndrome and other X-linked disorders. Proc. Natl. Acad. Sci. U. S. A. *115*, E668–E675.

De Carvalho, D.D., You, J.S., and Jones, P.A. (2010). DNA methylation and cellular reprogramming. Trends Cell Biol. *20*, 609–617.

Castillo, F.J., Mullen, L.J., Grant, B.C., DeLeon, J., Thrift, J.C., Chang, L.W., Irving, J.M., and Burke, D.J. (1994). Hybridoma stability. Dev. Biol. Stand. *83*, 55–64.

Catez, F., Ueda, T., and Bustin, M. (2006). Determinants of histone H1 mobility and chromatin binding in living cells. Nat. Struct. Mol. Biol. *13*, 305–310.

Cedar, H., and Bergman, Y. (2009). Linking DNA methylation and histone modification: patterns and paradigms. Nat. Rev. Genet. *10*, 295–304.

Cesana, M., Cacchiarelli, D., Legnini, I., Santini, T., Sthandier, O., Chinappi, M., Tramontano, A., and Bozzoni, I. (2011). A Long Noncoding RNA Controls Muscle Differentiation by Functioning as a Competing Endogenous RNA. Cell *147*, 358–369.

Chaligné, R., and Heard, E. (2014). X-chromosome inactivation in development and cancer. FEBS Lett. *588*, 2514–2522.

Chatterjee, S., Zaman, K., Ryu, H., Conforto, A., and Ratan, R.R. (2001). Sequence-selective DNA binding drugs mithramycin A and chromomycin A3 are potent inhibitors of neuronal apoptosis induced by oxidative stress and DNA damage in cortical neurons. Ann. Neurol. *49*, 345–354.

Chaumeil, J. (2006). A novel role for Xist RNA in the formation of a repressive nuclear compartment into which genes are recruited when silenced. Genes Dev. *20*, 2223–2237.

Cheng, X., and Blumenthal, R.M. (2008). Mammalian DNA Methyltransferases: A Structural Perspective. Structure *16*, 341–350.

Choi, J., Costa, M.L., Mermelstein, C.S., Chagas, C., Holtzer, S., and Holtzer, H. (1990). MyoD converts primary dermal fibroblasts, chondroblasts, smooth muscle, and retinal pigmented epithelial cells into striated mononucleated myoblasts and multinucleated myotubes. Proc. Natl. Acad. Sci. U. S. A. *87*, 7988–7992.

Chow, J., and Heard, E. (2009). X inactivation and the complexities of silencing a sex chromosome. Curr. Opin. Cell Biol. *21*, 359–366.

Costanzi, C., and Pehrson, J.R. (1998). histone macroH2A1 is concentrated in the inactive X chromosome of female mammals. *628*, 1997–1999.

Cowan, C.A., Atienza, J., Melton, D.A., and Eggan, K. (2005). Nuclear Reprogramming of Somatic Cells After Fusion with Human Embryonic Stem Cells. Science (80-.). *309*.

Croce, C.M. (1976). Loss of mouse chromosomes in somatic cell hybrids between HT-1080 human fibrosarcoma cells and mouse peritoneal macrophages (chromosome segregation/isozymes/transformed fibroblasts). Genetics *73*, 3248–3252.

Csankovszki, G., Panning, B., Bates, B., Pehrson, J.R., and Jaenisch, R. (1999). Conditional deletion of Xist disrupts histone macroH2A localization but not maintenance of X inactivation. Nat. Genet. *22*, 323–324.

Csankovszki, G., Nagy, a, and Jaenisch, R. (2001). Synergism of Xist RNA, DNA methylation, and histone hypoacetylation in maintaining X chromosome inactivation. J. Cell Biol. *153*, 773–784.

Cuvier, O., and Hirano, T. (2003). A role of topoisomerase II in linking DNA replication to chromosome condensation. J. Cell Biol. *364511*, 21–9525.

Daban, J.-R. (2015). Stacked thin layers of metaphase chromatin explain the geometry of chromosome rearrangements and banding. Sci. Rep. *5*, 14891.

Davis, R.L., Weintraub, H., and Lassar, A.B. (1987). Expression of a single transfected cDNA converts fibroblasts to myoblasts. Cell *51*, 987–1000.

Deluz, C., Friman, E.T., Strebinger, D., Benke, A., Raccaud, M., Callegari, A., Leleu, M., Manley, S., and Suter, D.M. (2016). A role for mitotic bookmarking of SOX2 in pluripotency and differentiation. Genes Dev. *30*, 2538–2550.

Do, J.T., and Schöler, H.R. (2004). Nuclei of Embryonic Stem Cells Reprogram Somatic Cells. Stem Cells *22*, 941–949.

Dong, B., Almassalha, L.M., Stypula-Cyrus, Y., Urban, B.E., Chandler, J.E., Nguyen, T.-Q., Sun, C., Zhang, H.F., and Backman, V. (2016). Superresolution intrinsic fluorescence imaging of chromatin utilizing native, unmodified nucleic acids for contrast. Proc. Natl.

Acad. Sci. U. S. A. *113*, 9716–9721.

Durand, R.E., and Olive, P.L. (1982). Cytotoxicity, Mutagenicity and DNA damage by Hoechst 33342. J. Histochem. Cytochem. *30*, 111–116.

Duthie, S., Nesterova, T.B., Formstone, E.J., Keohane, A.M., Turner, B.M., Zakian, S.M., and Brockdorff, N. (1999). Xist RNA exhibits a banded localization on the inactive X chromosome and is excluded from autosomal material in cis. Hum. Mol. Genet. *8*, 195–204.

Earnshaw, W.C., and Heck, M.M. (1985). Localization of topoisomerase II in mitotic chromosomes. J. Cell Biol. *100*.

Earnshaw, W.C., and Laemmli, U.K. (1983). Architecture of metaphase chromosomes and chromosome scaffolds. J. Cell Biol. *96*, 84–93.

Eggan, K., Akutsu, H., Hochedlinger, K., Iii, W.R., Yanagimachi, R., and Jaenisch, R. (2000). X-Chromosome Inactivation in Cloned Mouse Embryos. *290*, 1578–1582.

Elhamamsy, A.R. (2017). Role of DNA methylation in imprinting disorders: an updated review. J. Assist. Reprod. Genet. *34*, 549–562.

Elling, U., Taubenschmid, J., Wirnsberger, G., O'Malley, R., Demers, S.P., Vanhaelen, Q., Shukalyuk, A.I., Schmauss, G., Schramek, D., Schnuetgen, F., et al. (2011). Forward and reverse genetics through derivation of haploid mouse embryonic stem cells. Cell Stem Cell *9*, 563–574.

Eltsov, M., Maclellan, K.M., Maeshima, K., Frangakis, A.S., and Dubochet, J. (2008). Analysis of cryo-electron microscopy images does not support the existence of 30-nm chromatin fibers in mitotic chromosomes in situ. Proc. Natl. Acad. Sci. U. S. A. *105*, 19732–19737.

Emre, N., Vidal, J.G., Elia, J., O'Connor, E.D., Paramban, R.I., Hefferan, M.P., Navarro, R., Goldberg, D.S., Varki, N.M., Marsala, M., et al. (2010). The ROCK inhibitor Y-27632 improves recovery of human embryonic stem cells after fluorescence-activated cell sorting with multiple cell surface markers. PLoS One *5*, e12148.

Fan, H.C., Wang, J., Potanina, A., and Quake, S.R. (2011). Whole-genome molecular haplotyping of single cells. Nat. Biotechnol. *29*, 51–57.

Fang, J., Chen, T., Chadwick, B., Li, E., and Zhang, Y. (2004). Ring1b-mediated H2A

ubiquitination associates with inactive X chromosomes and is involved in initiation of X inactivation. J. Biol. Chem. *279*, 52812–52815.

Farr, C.J., Antoniou-Kourounioti, M., Mimmack, M.L., Volkov, A., and Porter, A.C.G. (2014). The isoform of topoisomerase II is required for hypercompaction of mitotic chromosomes in human cells. Nucleic Acids Res. *42*, 4414–4426.

Ferguson-Smith, M.A., Yang, F., O'Brien, P.C.M., E, B., CC, L., MA, F.-S., MA, F.S., A, C., A, C., L, C., et al. (1998). Comparative Mapping Using Chromosome Sorting and Painting. ILAR J. *39*, 68–76.

Festuccia, N., Osorno, R., Halbritter, F., Karwacki-Neisius, V., Navarro, P., Colby, D., Wong, F., Yates, A., Tomlinson, S.R., and Chambers, I. (2012). Esrrb Is a Direct Nanog Target Gene that Can Substitute for Nanog Function in Pluripotent Cells. Cell Stem Cell *11*, 477–490.

Festuccia, N., Dubois, A., Vandormael-Pournin, S., Gallego Tejeda, E., Mouren, A., Bessonnard, S., Mueller, F., Proux, C., Cohen-Tannoudji, M., and Navarro, P. (2016). Mitotic binding of Esrrb marks key regulatory regions of the pluripotency network. Nat. Cell Biol. *18*, 1139–1148.

Filipczyk, A., Marr, C., Hastreiter, S., Feigelman, J., Schwarzfischer, M., Hoppe, P.S., Loeffler, D., Kokkaliaris, K.D., Endele, M., Schauberger, B., et al. (2015). Network plasticity of pluripotency transcription factors in embryonic stem cells. Nat. Cell Biol. *17*, 1235–1246.

Filipowicz, W., Jaskiewicz, L., Kolb, F.A., Pillai, R.S., Patel, D.J., and Westhof, E. (2005). Post-transcriptional gene silencing by siRNAs and miRNAs This review comes from a themed issue on Nucleic acids Edited. Curr. Opin. Struct. Biol. *15*, 331–341.

Fischle, W., Tseng, B.S., Dormann, H.L., Ueberheide, B.M., Garcia, B.A., Shabanowitz, J., Hunt, D.F., Funabiki, H., and Allis, D. (2005). Regulation of HP1–chromatin binding by histone H3 methylation and phosphorylation. Nature *438*, 22–29.

Frazer, K. a, Eskin, E., Kang, H.M., Bogue, M. a, Hinds, D. a, Beilharz, E.J., Gupta, R. V, Montgomery, J., Morenzoni, M.M., Nilsen, G.B., et al. (2007). A sequence-based variation map of 8.27 million SNPs in inbred mouse strains. Nature *448*, 1050–1053.

Fukuda, A., Tomikawa, J., Miura, T., Hata, K., Nakabayashi, K., Eggan, K., Akutsu, H., and Umezawa, A. (2014). The role of maternal-specific H3K9me3 modification in establishing

imprinted X-chromosome inactivation and embryogenesis in mice. Nat. Commun. *5*, 5464.

Gascoigne, K.E., Takeuchi, K., Suzuki, A., Hori, T., Fukagawa, T., and Cheeseman, I.M. (2011). Induced Ectopic Kinetochore Assembly Bypasses the Requirement for CENP-A Nucleosomes. Cell *145*, 410–422.

Gasser, S.M., Laroche, T., Falquet, J., Boy de la Tour, E., and Laemmli, U.K. (1986). Metaphase chromosome structure. Involvement of topoisomerase II. J. Mol. Biol. *188*, 613–629.

Gentile, F., Moretti, M., Limongi, T., Falqui, A., Bertoni, G., Scarpellini, A., Santoriello, S., Maragliano, L., Proietti Zaccaria, R., and di Fabrizio, E. (2012). Direct Imaging of DNA Fibers: The Visage of Double Helix. Nano Lett. *12*, 6453–6458.

Goll, M.G., Kirpekar, F., Maggert, K.A., Yoder, J.A., Hsieh, C.-L., Zhang, X., Golic, K.G., Jacobsen, S.E., and Bestor, T.H. (2006). Methylation of tRNAAsp by the DNA Methyltransferase Homolog Dnmt2. Science (80-.). *311*, 395–398.

Gopalakrishnan, S., Sullivan, B.A., Trazzi, S., Della Valle, G., and Robertson, K.D. (2009). DNMT3B interacts with constitutive centromere protein CENP-C to modulate DNA methylation and the histone code at centromeric regions. Hum. Mol. Genet. *18*, 3178–3193.

Grant, S.G., and Worton, R.G. (1989). Differential activation of the hprt gene on the inactive X chromosome in primary and transformed Chinese hamster cells. Mol. Cell. Biol. *9*, 1635–1641.

Gray, J.W., Lucas, J., Peters, D., Pinkel, D., Trask, B., van den Engh, G., and Van Dilla, M. (1986). Flow karyotyping and sorting of human chromosomes. Cold Spring Harb. Symp. Quant. Biol. *51 Pt 1*, 141–149.

Gray, J.W., Trask, B., van den Engh, G., Silva, A., Lozes, C., Grell, S., Schonberg, S., Yu, L.C., and Golbus, M.S. (1988). Application of flow karyotyping in prenatal detection of chromosome aberrations. Am. J. Hum. Genet. *42*, 49–59.

Green, L.C., Kalitsis, P., Chang, T.M., Cipetic, M., Kim, J.H., Marshall, O., Turnbull, L., Whitchurch, C.B., Vagnarelli, P., Samejima, K., et al (2012). Contrasting roles of condensin I and condensin II in mitotic chromosome formation. J. Cell Sci. *125*, 1591–1604.

Gridina, M.M., and Serov, O.L. (2010). Bidirectional reprogramming of mouse embryonic stem cell/fibroblast hybrid cells is initiated at the heterokaryon stage. Cell Tissue Res. *342*,

377–389.

Grunstein, M. (1997). Histone acetylation in chromatin structure and transcription. Nature *389*, 349–352.

Guacci, V., Koshland, D., Strunnikov, A., Miyauchi, T., Muramatsu, H., Muramatsu, T., Yanagida, M., Kawarabayasi, Y., Ishikawa, K., and Tabata, S. (1997). A direct link between sister chromatid cohesion and chromosome condensation revealed through the analysis of MCD1 in S. cerevisiae. Cell *91*, 47–57.

Guo, A., Huang, S., Yu, J., Wang, H., Li, H., Pei, G., and Shen, L. (2017). Single-Cell Dynamic Analysis of Mitosis in Haploid Embryonic Stem Cells Shows the Prolonged Metaphase and Its Association with Self-diploidization. Stem Cell Reports *8*, 1124–1134.

Gurdon, J.B. (1962). The Developmental Capacity of Nuclei taken from Intestinal Epithelium Cells of Feeding Tadpoles. Development *10*.

HARRIS, H., and WATKINS, J.F. (1965). HYBRID CELLS DERIVED FROM MOUSE AND MAN: ARTIFICIAL HETEROKARYONS OF MAMMALIAN CELLS FROM DIFFERENT SPECIES. Nature *205*, 640–646.

HARRIS, H., MILLER, O.J., KLEIN, G., WORST, P., and TACHIBANA, T. (1969). Suppression of Malignancy by Cell Fusion. Nature *223*, 363–368.

Hasegawa, K., Zhang, P., Wei, Z., Pomeroy, J.E., Lu, W., and Pera, M.F. (2010). Comparison of Reprogramming Efficiency Between Transduction of Reprogramming Factors, Cell-Cell Fusion, and Cytoplast Fusion. Stem Cells *28*, 1338–1348.

Hay, D.C., Sutherland, L., Clark, J., and Burdon, T. (2004). Oct-4 Knockdown Induces Similar Patterns of Endoderm and Trophoblast Differentiation Markers in Human and Mouse Embryonic Stem Cells. Stem Cells *22*, 225–235.

Heard, E., Rougeulle, C., Arnaud, D., Avner, P., Allis, C.D., and Spector, D.L. (2001). Methylation of Histone H3 at Lys-9 Is an Early Mark on the X Chromosome during X Inactivation University of Virginia Health System. *107*, 727–738.

Hermann, A., Goyal, R., and Jeltsch, A. (2004). The Dnmt1 DNA-(cytosine-C5)-methyltransferase Methylates DNA Processively with High Preference for Hemimethylated Target Sites. J. Biol. Chem. *279*, 48350–48359.

Hiromi, Y., and Gehring, W.J. (1987). Regulation and function of the Drosophila segmentation gene fushi tarazu. Cell *50*, 963–974.

Hochedlinger, K., and Plath, K. (2009). Epigenetic reprogramming and induced pluripotency. Development *136*, 509–523.

Holliday, R., and Pugh, J.E. (1975). DNA modification mechanisms and gene activity during development. Science *187*, 226–232.

Hotchkiss, R.D. (1948). The quantitative separation of purines pyrimidines, and nucleosides by paper chromatography. J. Biol. Chem. *175*, 315–332.

Hu, N., Zhang, X., Yang, J., Joo, S.W., and Qian, S. (2013). A cell electrofusion microfluidic chip with micro-cavity microelectrode array. Microfluid. Nanofluidics *15*, 151–160.

Hudson, D.F., Vagnarelli, P., Gassmann, R., and Earnshaw, W.C. (2003). Condensin Is Required for Nonhistone Protein Assembly and Structural Integrity of Vertebrate Mitotic Chromosomes. Dev. Cell *5*, 323–336.

Huynh, V.A.T., Robinson, P.J.J., and Rhodes, D. (2005). A Method for the In Vitro Reconstitution of a Defined "30nm" Chromatin Fibre Containing Stoichiometric Amounts of the Linker Histone. J. Mol. Biol. *345*, 957–968.

Inoue, K., Kohda, T., Sugimoto, M., Sado, T., Ogonuki, N., Matoba, S., Shiura, H., Ikeda, R., Mochida, K., Fujii, T., et al. (2010). Impeding Xist Expression from the Active X Chromosome Improves Mouse Somatic Cell Nuclear Transfer. Science (80-.). *330*, 496–499.

Issa, J.-P. (2004). CpG island methylator phenotype in cancer. Nat. Rev. Cancer *4*, 988–993.

JOHNSON, R.T., and RAO, P.N. (1970). Mammalian Cell Fusion : Induction of Premature Chromosome Condensation in Interphase Nuclei. Nature *226*, 717–722.

Jonkers, I., Barakat, T.S., Achame, E.M., Monkhorst, K., Kenter, A., Rentmeester, E., Grosveld, F., Grootegoed, J.A., and Gribnau, J. (2009). RNF12 is an X-Encoded dose-dependent activator of X chromosome inactivation. Cell *139*, 999–1011.

Kaslow, D.C., and Migeon, B.R. (1987). DNA methylation stabilizes X chromosome inactivation in eutherians but not in marsupials: evidence for multistep maintenance of mammalian X dosage compensation. Proc. Natl. Acad. Sci. U. S. A. *84*, 6210–6214.

Kellenberger, E., Johansen, R., Maeder, M., Bohrmann, B., Stauffer, E., and Villiger, W.

(1992). Artefacts and morphological changes during chemical fixation. J. Microsc. *168*, 181–201.

Kim, J., Chu, J., Shen, X., Wang, J., and Orkin, S.H. (2008). An extended transcriptional network for pluripotency of embryonic stem cells. Cell *132*, 1049–1061.

Kim, K.-Y., Hysolli, E., Tanaka, Y., Wang, B., Jung, Y.-W., Pan, X., Weissman, S.M., and Park, I.-H. (2014). X Chromosome of Female Cells Shows Dynamic Changes in Status during Human Somatic Cell Reprogramming. Stem Cell Reports *2*, 896–909.

Kimura, H., Tada, M., Nakatsuji, N., and Tada, T. (2004). Histone code modifications on pluripotential nuclei of reprogrammed somatic cells. Mol. Cell. Biol. *24*, 5710–5720.

KÖHLER, G., and MILSTEIN, C. (1975). Continuous cultures of fused cells secreting antibody of predefined specificity. Nature *256*, 495–497.

Kopp, J.L., Ormsbee, B.D., Desler, M., and Rizzino, A. (2008). Small Increases in the Level of Sox2 Trigger the Differentiation of Mouse Embryonic Stem Cells. Stem Cells *26*, 903–911.

Kornberg, R.D. (1974). Chromatin structure: a repeating unit of histones and DNA. Science *184*, 868–871.

Kornberg, R.D., and Thonmas, J.O. (1974). Chromatin Structure: Oligomers of the Histones. Science (80-.). *184*.

Kruglova, A.A., Matveeva, N.M., Gridina, M.M., Battulin, N.R., Karpov, A., Kiseleva, E. V., Morozova, K.N., and Serov, O.L. (2010). Dominance of parental genomes in embryonic stem cell/fibroblast hybrid cells depends on the ploidy of the somatic partner. Cell Tissue Res. *340*, 437–450.

Kunitoku, N., Sasayama, T., Marumoto, T., Zhang, D., Honda, S., Kobayashi, O., Hatakeyama, K., Ushio, Y., Saya, H., and Hirota, T. (2003). CENP-A Phosphorylation by Aurora-A in Prophase Is Required for Enrichment of Aurora-B at Inner Centromeres and for Kinetochore Function. Dev. Cell *5*, 853–864.

de Lange, T. (2005). Shelterin: the protein complex that shapes and safeguards human telomeres. Genes Dev. *19*, 2100–2110.

Langford, C.F., Fischer, P.E., Binns, M.M., Holmes, N.G., and Carter, N.P. (1996).

Chromosome-specific paints from a high-resolution flow karyotype of the dog. Chromosom. Res. *4*, 115–123.

Langmore, J.P., Paulson, J.R., and JR (1983). Low angle x-ray diffraction studies of chromatin structure in vivo and in isolated nuclei and metaphase chromosomes. J. Cell Biol. *96*, 1120–1131.

Lee, J.T., Strauss, W.M., Dausman, J.A., and Jaenisch, R. (1996). A 450 kb transgene displays properties of the mammalian X-inactivation center. Cell *86*, 83–94.

Lee, J.T., Davidow, L.S., and Warshawsky, D. (1999). Tsix, a gene antisense to Xist at the X-inactivation centre. Nat. Genet. *21*, 400–404.

Lee, J.T., Bartolomei, M.S., Kung, J.T., Ogawa, Y., Grau, D.J., Sarma, K., Song, J.J., Kingston, R.E., Borowsky, M., Lee, J.T., et al. (2013). X-Inactivation, Imprinting, and Long Noncoding RNAs in Health and Disease. Cell *152*, 1308–1323.

Leeb, M., and Wutz, A. (2011). Derivation of haploid embryonic stem cells from mouse embryos. Nature *479*, 131–134.

Lei, H., Oh, S.P., Okano, M., Juttermann, R., Goss, K.A., Jaenisch, R., and Li, E. (1996). De novo DNA cytosine methyltransferase activities in mouse embryonic stem cells. Development *122*.

Luni, C., Giulitti, S., Serena, E., Ferrari, L., Zambon, A., Gagliano, O., Giobbe, G.G., Michielin, F., Knöbel, S., Bosio, A., et al. (2016). High-efficiency cellular reprogramming with microfluidics. Nat. Methods *13*, 446–452.

Lyon, M.F. (1962). Sex chromatin and gene action in the mammalian X-chromosome. Am. J. Hum. Genet. *14*, 135–148.

Lyst, M.J., and Bird, A. (2015). Rett syndrome: a complex disorder with simple roots. Nat. Publ. Gr. *16*.

Maeshima, K., and Laemmli, U.K. (2003). A Two-Step Scaffolding Model for Mitotic Chromosome Assembly. Dev. Cell *4*, 467–480.

Maherali, N., Sridharan, R., Xie, W., Utikal, J., Eminli, S., Arnold, K., Stadtfeld, M., Yachechko, R., Tchieu, J., Jaenisch, R., et al. (2007). Directly reprogrammed fibroblasts show global epigenetic remodeling and widespread tissue contribution. Cell Stem Cell *1*, 55–

70.

Mak, W., Nesterova, T.B., de Napoles, M., Appanah, R., Yamanaka, S., Otte, A.P., and Brockdorff, N. (2004). Reactivation of the paternal X chromosome in early mouse embryos. Science *303*, 666–669.

Marchese, F.P., and Huarte, M. (2014). Long non-coding RNAs and chromatin modifiers. 21–26.

Marguerat, S., and Bähler, J. (2012). Coordinating genome expression with cell size. Trends Genet. *28*, 560–565.

Margueron, R., Justin, N., Ohno, K., Sharpe, M.L., Son, J., Drury, W.J., Voigt, P., Martin, S.R., Taylor, W.R., De Marco, V., et al. (2009). Role of the polycomb protein EED in the propagation of repressive histone marks. Nature *461*, 762–767.

Marks, H., Chow, J.C., Denissov, S., Franc, K., Brockdorff, N., Heard, E., and Stunnenberg, H.G. (2009). High-resolution analysis of epigenetic changes associated with X inactivation. *3*, 1361–1373.

Marks, H., Kalkan, T., Menafra, R., Denissov, S., Jones, K., Hofemeister, H., Nichols, J., Kranz, A., Francis Stewart, A., Smith, A., et al. (2012). The transcriptional and epigenomic foundations of ground state pluripotency. Cell *149*, 590–604.

Marks, P.A., Rifkind, R.A., Richon, V.M., Breslow, R., Miller, T., and Kelly, W.K. (2001). Histone deacetylases and cancer: causes and therapies. Nat. Rev. Cancer *1*, 194–202.

Matsuda, A., Shao, L., Boulanger, J., Kervrann, C., Carlton, P.M., Kner, P., Agard, D., and Sedat, J.W. (2010). Condensed Mitotic Chromosome Structure at Nanometer Resolution Using PALM and EGFP-Histones. PLoS One *5*.

Matveeva, N.M., Fishman, V.S., Zakharova, I.S., Shevchenko, A.I., Pristyazhnyuk, I.E., Menzorov, A.G., and Serov, O.L. (2017). Alternative dominance of the parental genomes in hybrid cells generated through the fusion of mouse embryonic stem cells with fibroblasts. Sci. Rep. *7*, 18094.

Mermoud, J.E., Costanzi, C., Pehrson, J.R., and Brockdorff, N. (1999). Histone MacroH2A1 . 2 Relocates to the Inactive X Chromosome after Initiation and Propagation of X-Inactivation. *147*, 1399–1408.

Michaelis, C., Ciosk, R., Nasmyth, K., Obermaier, B., Nasmyth, K., Mizuno, T., Ruderman, J.V., and Hershko, A. (1997). Cohesins: chromosomal proteins that prevent premature separation of sister chromatids. Cell *91*, 35–45.

Miller, R.A., and Ruddle, F.H. (1976). Pluripotent teratocarcinoma-thymus somatic cell hybrids. Cell *9*, 45–55.

Mitsui, K., Tokuzawa, Y., Itoh, H., Segawa, K., Murakami, M., Takahashi, K., Maruyama, M., Maeda, M., and Yamanaka, S. (2003). The homeoprotein Nanog is required for maintenance of pluripotency in mouse epiblast and ES cells. Cell *113*, 631–642.

Monfort, A., Di Minin, G., Postlmayr, A., Freimann, R., Arieti, F., Thore, S., and Wutz, A. (2015). Identification of Spen as a Crucial Factor for Xist Function through Forward Genetic Screening in Haploid Embryonic Stem Cells. Cell Rep. *12*, 554–561.

Nagasaka, K., Hossain, M.J., Roberti, M.J., Ellenberg, J., and Hirota, T. (2016). Sister chromatid resolution is an intrinsic part of chromosome organization in prophase. Nat. Cell Biol. *18*, 692–699.

de Napoles, M., Nesterova, T., and Brockdorff, N. (2007). Early loss of Xist RNA expression and inactive X chromosome associated chromatin modification in developing primordial germ cells. PLoS One *2*, e860.

Nasmyth, K., Tanaka, T., Fuchs, J., and Loidl, J. (2000). Cohesin ensures bipolar attachment of microtubules to sister centromeres and resists their precocious separation. Nat. Cell Biol. *2*, 492–499.

Nayak, R., Sirsi, M., and Podder, S.K. (1975). Mode of action of antitumour antibiotics. Biochim. Biophys. Acta - Nucleic Acids Protein Synth. *378*, 195–204.

Ng, B.L., and Carter, N.P. (2006). Factors Affecting Flow Karyotype Resolution. *1036*, 1028–1036.

Nichols, J., Zevnik, B., Anastassiadis, K., Niwa, H., Klewe-Nebenius, D., Chambers, I., Schöler, H., and Smith, A. (1998). Formation of pluripotent stem cells in the mammalian embryo depends on the POU transcription factor Oct4. Cell *95*, 379–391.

Nishino, Y., Eltsov, M., Joti, Y., Ito, K., Takata, H., Takahashi, Y., Hihara, S., Frangakis, A.S., Imamoto, N., Ishikawa, T., et al. (2012). Human mitotic chromosomes consist predominantly of irregularly folded nucleosome fibres without a 30-nm chromatin structure.

EMBO J. *31*, 1644–1653.

Nora, E.P., Lajoie, B.R., Schulz, E.G., Giorgetti, L., Okamoto, I., Servant, N., Piolot, T., van Berkum, N.L., Meisig, J., Sedat, J., et al. (2012). Spatial partitioning of the regulatory landscape of the X-inactivation centre. Nature *485*, 381–385.

Ohhata, T., and Wutz, A. (2013). Reactivation of the inactive X chromosome in development and reprogramming. Cell. Mol. Life Sci. *70*, 2443–2461.

Okamoto, I., Otte, A.P., Allis, C.D., Reinberg, D., and Heard, E. (2004). Epigenetic Dynamics of Imprinted. *303*, 644–650.

Okano, M., Bell, D.W., Haber, D.A., and Li, E. (1999). DNA Methyltransferases Dnmt3a and Dnmt3b Are Essential for De Novo Methylation and Mammalian Development. Cell *99*, 247–257.

Ono, T., Losada, A., Hirano, M., Myers, M.P., Neuwald, A.F., and Hirano, T. (2003). Differential Contributions of Condensin I and Condensin II to Mitotic Chromosome Architecture in Vertebrate Cells. Cell *115*, 109–121.

Ooi, S.K.T., Qiu, C., Bernstein, E., Li, K., Jia, D., Yang, Z., Erdjument-Bromage, H., Tempst, P., Lin, S.-P., Allis, C.D., et al. (2007). DNMT3L connects unmethylated lysine 4 of histone H3 to de novo methylation of DNA. Nature *448*, 714–717.

Orkin, S.H., Wang, J., Kim, J., Chu, J., Rao, S., Theunissen, T.W., Shen, X., and Levasseur, D.N. (2008). The Transcriptional Network Controlling Pluripotency in ES Cells. Cold Spring Harb. Symp. Quant. Biol. *73*, 195–202.

Ou, H.D., Phan, S., Deerinck, T.J., Thor, A., Ellisman, M.H., and O'Shea, C.C. (2017). ChromEMT: Visualizing 3D chromatin structure and compaction in interphase and mitotic cells. Science (80-.). *357*.

Padovan-Merhar, O., Nair, G.P., Biaesch, A.G., Mayer, A., Scarfone, S., Foley, S.W., Wu, A.R., Churchman, L.S., Singh, A., Raj, A., et al. (2015). Single Mammalian Cells Compensate for Differences in Cellular Volume and DNA Copy Number through Independent Global Transcriptional Mechanisms. Mol. Cell *58*, 339–352.

Panning, B., Dausman, J., and Jaenisch, R. (1997). X chromosome inactivation is mediated by Xist RNA stabilization. Cell *90*, 907–916.

Pasque, V., Tchieu, J., Karnik, R., Uyeda, M., Sadhu Dimashkie, A., Case, D., Papp, B., Bonora, G., Patel, S., Ho, R., et al. (2014). X chromosome reactivation dynamics reveal stages of reprogramming to pluripotency. Cell *159*, 1681–1697.

Paulson, J.R., and Laemmli, U.K. (1977). The structure of histone-depleted metaphase chromosomes. Cell *12*, 817–828.

Pereira, C.F., Terranova, R., Ryan, N.K., Santos, J., Morris, K.J., Cui, W., Merkenschlager, M., and Fisher, A.G. (2008). Heterokaryon-based reprogramming of human B lymphocytes for pluripotency requires Oct4 but not Sox2. PLoS Genet. *4*, e1000170.

Pereira, C.F., Piccolo, F.M., Tsubouchi, T., Sauer, S., Ryan, N.K., Bruno, L., Landeira, D., Santos, J., Banito, A., Gil, J., et al. (2010). ESCs Require PRC2 to Direct the Successful Reprogramming of Differentiated Cells toward Pluripotency. Cell Stem Cell *6*, 547–556.

Piccolo, F.M., Pereira, C.F., Cantone, I., Brown, K., Tsubouchi, T., Soza-Ried, J., Merkenschlager, M., and Fisher, A.G. (2011a). Using heterokaryons to understand pluripotency and reprogramming. Philos. Trans. R. Soc. B Biol. Sci. *366*.

Piccolo, F.M., Pereira, C.F., Cantone, I., Brown, K., Tsubouchi, T., Soza-Ried, J., Merkenschlager, M., and Fisher, A.G. (2011b). Using heterokaryons to understand pluripotency and reprogramming. Philos. Trans. R. Soc. London B Biol. Sci. *366*.

Piccolo, F.M., Bagci, H., Brown, K.E., Landeira, D., Soza-Ried, J., Feytout, A., Mooijman, D., Hajkova, P., Leitch, H.G., Tada, T., et al. (2013). Different Roles for Tet1 and Tet2 Proteins in Reprogramming-Mediated Erasure of Imprints Induced by EGC Fusion. Mol. Cell *49*, 1023–1033.

Plath, K., and Lowry, W.E. (2011). Progress in understanding reprogramming to the induced pluripotent state. Nat. Rev. Genet. *12*, 253–265.

Plath, K., Fang, J., Mlynarczyk-Evans, S.K., Cao, R., Worringer, K. a, Wang, H., de la Cruz, C.C., Otte, A.P., Panning, B., and Zhang, Y. (2003). Role of histone H3 lysine 27 methylation in X inactivation. Science *300*, 131–135.

Poirier, M.G., and Marko, J.F. (2002). Mitotic chromosomes are chromatin networks without a mechanically contiguous protein scaffold. Proc. Natl. Acad. Sci. U. S. A. *99*, 15393–15397.

Polo, J.M., Anderssen, E., Walsh, R.M., Schwarz, B.A., Nefzger, C.M., Lim, S.M., Borkent, M., Apostolou, E., Alaei, S., Cloutier, J., et al. (2012). A molecular roadmap of

reprogramming somatic cells into iPS cells. Cell *151*, 1617–1632.

Raab, S., Klingenstein, M., Liebau, S., and Linta, L. (2014). A Comparative View on Human Somatic Cell Sources for iPSC Generation. Stem Cells Int. *2014*, 768391.

Rabbitts, P., Impey, H., Heppell-Parton, A., Langford, C., Tease, C., Lowe, N., Bailey, D., Ferguson-Smith, M., and Carter, N. (1995). Chromosome specific paints from a high resolution flow karyotype of the mouse. Nat. Genet. *9*, 369–375.

RAO, P.N., and JOHNSON, R.T. (1970). Mammalian Cell Fusion : Studies on the Regulation of DNA Synthesis and Mitosis. Nature *225*, 159–164.

Rastan, B.S. (1982). Timing of X-chromosome inactivation in postimplantation mouse embryos. *71*, 11–24.

Ribrioux, S., Kleymann, G., Haase, W., Heitmann, K., Ostermeier, C., and Michel3, H. (1996). Use of Nanogold-and Fluorescent-labeled Antibody Fv Fragments in Immunocytochemistry'. *44*, 207–213.

Rieder, C., and Palazzo, R. (1992). Colcemid and the mitotic cycle. J. Cell Sci. *102*.

Robertson, K.D. (2005). DNA methylation and human disease. Nat. Rev. Genet. *6*, 597–610.

Rodda, D.J., Chew, J.-L., Lim, L.-H., Loh, Y.-H., Wang, B., Ng, H.-H., and Robson, P. (2005). Transcriptional regulation of nanog by OCT4 and SOX2. J. Biol. Chem. *280*, 24731–24737.

Rongeat, N., Ledroit, S., Chauvet, L., Cremien, D., Urankar, A., Couderc, V., and Nérin, P. (2011). Automatic cytometric device using multiple wavelength excitations. J. Biomed. Opt. *16*, 57006.

Sado, T., Fenner, M.H., Tan, S.S., Tam, P., Shioda, T., and Li, E. (2000). X inactivation in the mouse embryo deficient for Dnmt1: distinct effect of hypomethylation on imprinted and random X inactivation. Dev. Biol. *225*, 294–303.

Saitoh, Y., and Laemmli, U.K. (1994). Metaphase chromosome structure: Bands arise from a differential folding path of the highly AT-rich scaffold. Cell *76*, 609–622.

Saksouk, N., Simboeck, E., Déjardin, J., Song, I., Sullivan, B., and Plotnikova, O. (2015). Constitutive heterochromatin formation and transcription in mammals. Epigenetics Chromatin *8*, 3.

Schmitges, F.W., Prusty, A.B., Faty, M., Stützer, A., Lingaraju, G.M., Aiwazian, J., Sack, R., Hess, D., Li, L., Zhou, S., et al. (2011). Histone Methylation by PRC2 Is Inhibited by Active Chromatin Marks. Mol. Cell *42*, 330–341.

Schroeder-Reiter, E., Pérez-Willard, F., Zeile, U., and Wanner, G. (2009). Focused ion beam (FIB) combined with high resolution scanning electron microscopy: A promising tool for 3D analysis of chromosome architecture. J. Struct. Biol. *165*, 97–106.

Silva, J., Mak, W., Zvetkova, I., Appanah, R., Nesterova, T.B., Webster, Z., Peters, A.H.F.M., Jenuwein, T., Otte, A.P., and Brockdorff, N. (2003). Establishment of histone h3 methylation on the inactive X chromosome requires transient recruitment of Eed-Enx1 polycomb group complexes. Dev. Cell *4*, 481–495.

Silva, J., Chambers, I., Pollard, S., and Smith, A. (2006). Nanog promotes transfer of pluripotency after cell fusion. Nature *441*, 997–1001.

Silva, J., Nichols, J., Theunissen, T.W., Guo, G., van Oosten, A.L., Barrandon, O., Wray, J., Yamanaka, S., Chambers, I., and Smith, A. (2009). Nanog Is the Gateway to the Pluripotent Ground State. Cell *138*, 722–737.

Singh, A.M., Hamazaki, T., Hankowski, K.E., and Terada, N. (2007). A Heterogeneous Expression Pattern for Nanog in Embryonic Stem Cells. Stem Cells *25*, 2534–2542.

Siomi, M.C., Sato, K., Pezic, D., and Aravin, A.A. (2011). PIWI-interacting small RNAs: the vanguard of genome defence. Nat. Rev. Mol. Cell Biol. *12*, 246–258.

Soza-Ried, J., and Fisher, A.G. (2012). Reprogramming somatic cells towards pluripotency by cellular fusion. Curr. Opin. Genet. Dev. *22*, 459–465.

Spencer, C.A., Kruhlak, M.J., Jenkins, H.L., Sun, X., and Bazett-Jones, D.P. (2000). Mitotic transcription repression in vivo in the absence of nucleosomal chromatin condensation. J. Cell Biol. *150*, 13–26.

Sridharan, R., Tchieu, J., Mason, M.J., Yachechko, R., Kuoy, E., Horvath, S., Zhou, Q., and Plath, K. (2009). Role of the Murine Reprogramming Factors in the Induction of Pluripotency. Cell *136*, 364–377.

Stadtfeld, M., Maherali, N., Breault, D.T., and Hochedlinger, K. (2008). Defining Molecular Cornerstones during Fibroblast to iPS Cell Reprogramming in Mouse. Cell Stem Cell *2*, 230–240.

Sugimoto, M., and Abe, K. (2007). X chromosome reactivation initiates in nascent primordial germ cells in mice. PLoS Genet. *3*, e116.

Sun, S., Del Rosario, B.C., Szanto, A., Ogawa, Y., Jeon, Y., and Lee, J.T. (2013). Jpx RNA activates Xist by evicting CTCF. Cell *153*, 1537–1551.

Tachibana, M., Amato, P., Sparman, M., Gutierrez, N.M., Tippner-Hedges, R., Ma, H., Kang, E., Fulati, A., Lee, H.-S., Sritanaudomchai, H., et al. (2013). Human embryonic stem cells derived by somatic cell nuclear transfer. Cell *153*, 1228–1238.

Tada, M., Tada, T., Lefebvre, L., Barton, S.C., and Surani, M.A. (1997). Embryonic germ cells induce epigenetic reprogramming of somatic nucleus in hybrid cells. EMBO J. *16*, 6510–6520.

Tada, M., Takahama, Y., Abe, K., Nakatsuji, N., and Tada, T. (2001). Nuclear reprogramming of somatic cells by in vitro hybridization with ES cells. Curr. Biol. *11*, 1553–1558.

Takagi, N., and Sasaki, M. (1975). Preferential inactivation of the paternally derived X chromosome in the extraembryonic membranes of the mouse. Nature *256*, 640–642.

Takagi, N., Sugawara, O., and Sasaki, M. (1982). Regional and Temporal Changes in the Pattern of X-Chromosome Replication During the Early Post-Implantation Development of the Female Mouse. *286*, 275–286.

Takagi, N., Yoshida, M.A., Sugawara, O., and Sasaki, M. (1983). Reversal of X-inactivation in female mouse somatic cells hybridized with murine teratocarcinoma stem cells in vitro. Cell *34*, 1053–1062.

Takahashi, K., and Yamanaka, S. (2006). Induction of Pluripotent Stem Cells from Mouse Embryonic and Adult Fibroblast Cultures by Defined Factors. Cell *126*, 663–676.

Tanaka, Y., Nureki, O., Kurumizaka, H., Fukai, S., Kawaguchi, S., Ikuta, M., Iwahara, J., Okazaki, T., and Yokoyama, S. (2001). Crystal structure of the CENP-B protein-DNA complex: the DNA-binding domains of CENP-B induce kinks in the CENP-B box DNA. EMBO J. *20*, 6612–6618.

Tang, Y.A., Huntley, D., Montana, G., Cerase, A., Nesterova, T.B., and Brockdorff, N. (2010). Efficiency of Xist-mediated silencing on autosomes is linked to chromosomal domain organisation. Epigenetics Chromatin *3:10*.

Theunissen, T.W., van Oosten, A.L., Castelo-Branco, G., Hall, J., Smith, A., and Silva, J.C.R. (2011). Nanog overcomes reprogramming barriers and induces pluripotency in minimal conditions. Curr. Biol. *21*, 65–71.

Thoma, F., Koller, T., and Klug, A. (1979). Involvement of histone H1 in the organization of the nucleosome and of the salt-dependent superstructures of chromatin. J. Cell Biol. *83*.

Thomas, J. 0 (1999). Histone Hl: location and role. Curr. Opin. Cell Biol. *11*, 312–317.

Tian, D., Sun, S., and Lee, J.T. (2010). The long noncoding RNA, Jpx, is a molecular switch for X chromosome inactivation. Cell *143*, 390–403.

Tiemann, U., Sgodda, M., Warlich, E., Ballmaier, M., Schöler, H.R., Schambach, A., and Cantz, T. (2011). Optimal reprogramming factor stoichiometry increases colony numbers and affects molecular characteristics of murine induced pluripotent stem cells. Cytom. Part A *79A*, 426–435.

Tsubouchi, T., Soza-Ried, J., Brown, K., Piccolo, F.M., Cantone, I., Landeira, D., Bagci, H., Hochegger, H., Merkenschlager, M., and Fisher, A.G. (2013). DNA synthesis is required for reprogramming mediated by stem cell fusion. Cell *152*, 873–883.

Vallot, C., Ouimette, J.-F., Makhlouf, M., Féraud, O., Pontis, J., Côme, J., Martinat, C., Bennaceur-Griscelli, A., Lalande, M., and Rougeulle, C. (2015). Erosion of X Chromosome Inactivation in Human Pluripotent Cells Initiates with XACT Coating and Depends on a Specific Heterochromatin Landscape. Cell Stem Cell *16*, 533–546.

Waizenegger, I.C., Hauf, S., Meinke, A., and Peters, J.M. (2000). Two distinct pathways remove mammalian cohesin from chromosome arms in prophase and from centromeres in anaphase. Cell *103*, 399–410.

Wakayama, T., Perry, A.C.F., Zuccotti, M., Johnson, K.R., and Yanagimachi, R. (1998). Full-term development of mice from enucleated oocytes injected with cumulus cell nuclei. Nature *394*, 369–374.

Wang, Y., Xu, Z., Jiang, J., Xu, C., Kang, J., Xiao, L., Wu, M., Xiong, J., Guo, X., Liu, H., et al. (2013). Endogenous miRNA Sponge lincRNA-RoR Regulates Oct4, Nanog, and Sox2 in Human Embryonic Stem Cell Self-Renewal. Dev. Cell *25*, 69–80.

Weiss, R.L., Kukora, J.R., and Adams, J. (1975). The relationship between enzyme activity, cell geometry, and fitness in Saccharomyces cerevisiae. Proc. Natl. Acad. Sci. U. S. A. *72*,

794–798.

Williams, L.H., Kalantry, S., Starmer, J., and Magnuson, T. (2011). Transcription precedes loss of Xist coating and depletion of H3K27me3 during X-chromosome reprogramming in the mouse inner cell mass. Development *138*.

Wilmut, I., Schnieke, A.E., McWhir, J., Kind, A.J., and Campbell, K.H.S. (1997). Viable offspring derived from fetal and adult mammalian cells. Nature *385*, 810–813.

Wiśniewski, J.R., Zougman, A., Krüger, S., and Mann, M. (2007). Mass Spectrometric Mapping of Linker Histone H1 Variants Reveals Multiple Acetylations, Methylations, and Phosphorylation as Well as Differences between Cell Culture and Tissue. Mol. Cell. Proteomics *6*, 72–87.

Yamanaka, S., and Blau, H.M. (2010). Nuclear reprogramming to a pluripotent state by three approaches. Nature *465*, 704–712.

Yang, H., Wang, H., Shivalila, C.S., Cheng, A.W., Shi, L., and Jaenisch, R. (2013). One-step generation of mice carrying reporter and conditional alleles by CRISPR/Cas-mediated genome engineering. Cell *154*, 1370–1379.

Yeom, Y.I., Fuhrmann, G., Ovitt, C.E., Brehm, A., Ohbo, K., Gross, M., Hübner, K., and Schöler, H.R. (1996). Germline regulatory element of Oct-4 specific for the totipotent cycle of embryonal cells. Development *122*, 881–894.

Yi, H., Strauss, J.D., Ke, Z., Alonas, E., Dillard, R.S., Hampton, C.M., Lamb, K.M., Hammonds, J.E., Santangelo, P.J., Spearman, P.W., et al. (2015). Native Immunogold Labeling of Cell Surface Proteins and Viral Glycoproteins for Cryo-Electron Microscopy and Cryo-Electron Tomography Applications. J. Histochem. Cytochem.

Ying, Q., Nichols, J., Evans, E.P., and Smith, A.G. (2002). Changing potency by spontaneous fusion. Nature *416*, 545–548.

Ying, Q.-L., Wray, J., Nichols, J., Batlle-Morera, L., Doble, B., Woodgett, J., Cohen, P., and Smith, A. (2008). The ground state of embryonic stem cell self-renewal. Nature *453*, 519–523.

Zaidi, S.K., Young, D.W., Montecino, M.A., Lian, J.B., van Wijnen, A.J., Stein, J.L., and Stein, G.S. (2010). Mitotic bookmarking of genes: a novel dimension to epigenetic control. Nat. Rev. Genet. *11*, 583–589.

Zaidi, S.K., Grandy, R.A., Lopez-Camacho, C., Montecino, M., van Wijnen, A.J., Lian, J.B., Stein, J.L., and Stein, G.S. (2014). Bookmarking Target Genes in Mitosis: A Shared Epigenetic Trait of Phenotypic Transcription Factors and Oncogenes? Cancer Res. *74*.

Zeitlin, S.G., Shelby, R.D., and Sullivan, K.F. (2001). CENP-A is phosphorylated by Aurora B kinase and plays an unexpected role in completion of cytokinesis. J. Cell Biol. *155*, 1147–1158.

Zhang, X., Zhang, J., Wang, T., Esteban, M.A., and Pei, D. (2008). *Esrrb* Activates *Oct4* Transcription and Sustains Self-renewal and Pluripotency in Embryonic Stem Cells. J. Biol. Chem. *283*, 35825–35833.